

Review

Advances and Challenges in Palaeoenvironmental Studies Based on Oxygen Isotope Composition of Skeletal Carbonates and Phosphates

Hubert Wierzbowski 

Polish Geological Institute—National Research Institute, Rakowiecka 4, 00-975 Warszawa, Poland; hubert.wierzbowski@pgi.gov.pl

Abstract: Oxygen isotopes are widely used in palaeoenvironmental and palaeoclimatic studies as they record variations in the precipitation temperature of biogenic carbonates and phosphates. Problems associated with the preservation state of fossils, selection of the proper temperature equation, vital effects occurring during biomineralization, habitat effects of organisms as well as salinity, bathymetry and water circulation changes limit, however, the applicability of oxygen isotopes to reconstruction of ancient environmental settings. The progress of oxygen isotope studies, temperature calculations and ambiguities of the isotope record are discussed in this paper. The same applies to the methods of retrieving reliable temperature signals and the record of water chemistry changes based on well-preserved calcareous and phosphatic fossils. Sometimes neglected importance of sedimentological and faunistic data associated with sea-level changes and salinity variations is emphasised as an important tool for refinement of the temperature trends of epeiric sedimentary basins. In addition, published case datasets and new laboratory techniques, including micro-area and clumped isotope analyses, are presented to demonstrate examples and prospective ways of extension of the scope of palaeoenvironmental research. The provided information may be used in discussion and a critical review of published oxygen isotope data and their palaeoenvironmental interpretations.

Keywords: oxygen isotopes; carbonate and phosphate fossils; diagenetic alteration; temperature equations; vital effects; water depth and salinity; microsampling; clumped isotopes



Citation: Wierzbowski, H. Advances and Challenges in Palaeoenvironmental Studies Based on Oxygen Isotope Composition of Skeletal Carbonates and Phosphates. *Geosciences* **2021**, *11*, 419. <https://doi.org/10.3390/geosciences11100419>

Academic Editors: Tadeusz Peryt, Marek Jasionowski and Jesus Martinez-Frias

Received: 15 September 2021

Accepted: 5 October 2021

Published: 9 October 2021

Publisher's Note: MDPI stays neutral with regard to jurisdictional claims in published maps and institutional affiliations.



Copyright: © 2021 by the author. Licensee MDPI, Basel, Switzerland. This article is an open access article distributed under the terms and conditions of the Creative Commons Attribution (CC BY) license (<https://creativecommons.org/licenses/by/4.0/>).

1. Introduction

Oxygen isotope studies of biogenic (and non-biogenic) carbonates and phosphates are one of the most widely applied methods of reconstruction of temperature and environmental settings of ancient marine or restricted-marine environments. The palaeoceanographic investigations are possible due to significant temperature dependence of the oxygen isotope fractionation between carbonates or phosphates and ambient water. This dependence was initially recognized for carbonates, by H. Urey and his co-workers [1–5], and successively for phosphates, by A. Longinelli, Y. Kolodny and their colleagues [6,7]. In the next decades both methods were improved, and new precise laboratory techniques were developed. Both methods have become a basis for the publication of numerous scientific articles devoted to the $\delta^{18}\text{O}$ record of marine sedimentary rocks and fossils as well as reconstructions of palaeotemperature, palaeosalinity, thermal stratification of water column, animal habitats or temporal climatic variations.

The aim of the present contribution is not to duplicate information on basic principles, laboratory methods or precipitation patterns and temporal $\delta^{18}\text{O}$ trends of biogenic carbonates and phosphates given in numerous review papers (cf. [8–21]) but to focus on the most important practical aspects and controversies associated with the interpretation of the oxygen isotope composition of marine fossils. They mostly arise because of a need for the selection of proper and comparable methods of screening for diagenetic alteration, an appropriate oxygen isotope equation, vital effects, often forgotten effects of animal habits or

migrations and palaeoceanographic factors such as changes in the bathymetry, circulation pattern and salinity of ancient epicontinental seas. The critical approach to some published oxygen isotope results seems necessary, taking into account the appearance of numerous conflicting data and interpretations along with the increasing number of isotope studies. Many factors such as a lack of scrutiny in the determination of the state of preservation of studied fossils, erroneous sedimentological background or wrong chronostratigraphical correlations of results used for the construction of temporal temperature trends may also be a serious problem. In addition, the gradually increasing use of new laboratory methods such as microsampling techniques or clumped isotope analysis offers new instrumental possibilities, which may be used to filter the available data and retrieve the original temperature signal recorded in $\delta^{18}\text{O}$ values of skeletal carbonates or phosphates. This paper offers a practical compendium of information on up-to-date methods of palaeoenvironmental reconstructions based on oxygen isotope ratios of marine carbonate and phosphate fossils.

2. Diagenetic Alteration

Post-depositional alterations of sedimentary rocks and fossils usually induce changes in their oxygen isotope ratios. They are related to re-equilibration of the isotope composition of carbonate or phosphate with diagenetic fluids or the precipitation of secondary mineral phases, which may occur during multi-step dissolution and re-precipitation processes. Carbonate $\delta^{18}\text{O}$ values equilibrate with diagenetic fluids at much lower water-rock ratios than $\delta^{13}\text{C}$ values owing to high concentrations of oxygen in water (cf. [22]); therefore, pronounced negative shifts in both values may be assigned to diagenetic alteration. Although oxygen isotope composition of phosphates is regarded as more resistant to late diagenetic alteration, owing to a strong binding of oxygen atoms in PO_4^{3-} ion group, early diagenetic enzymatic activity of microbes or degradation of organic matter may lead to isotope exchange and the precipitation of secondary apatite [23–25].

It is noteworthy that compilations of skeletal carbonate and phosphate data show a long-term increase in published $\delta^{18}\text{O}$ values throughout the Phanerozoic Eon, which is usually regarded as a result of elevated surface temperatures or a gradual change in the composition of seawater linked to variations in the global rate of chemical weathering and seafloor hydrothermal activity [26–29]. Rigorous screening of the shell material could remove only a part of the low, early Palaeozoic $\delta^{18}\text{O}$ values [16,17] and a negative shift, at least to -6‰ , is observed in the oldest data from the Phanerozoic dataset [30,31]. The temporal evolution of oxygen isotope composition of seawater is, nevertheless, still a matter of debate. This is due to some contradictory data derived from clumped isotope analyses of Palaeozoic carbonate fossils or oxygen isotope studies of Neoproterozoic hydrothermal deposits [32,33].

2.1. Calcareous Fossils

Low-Mg calcite is a relatively stable carbonate mineral that possesses high potential for the preservation of primary oxygen isotope composition [10,12]. Diagenetic alteration of low-Mg calcite macro- and microfossils (e.g., belemnite rostra, oyster, inoceramid, pinnid and brachiopod shells as well as foraminifera tests) can be screened using geochemical tracers or by the examination of the shell microstructure.

Minor and trace element contents of marine calcitic shells are mostly close to chemical equilibrium with ambient seawater. Post-depositional alteration usually causes an increase in Fe and Mn concentrations and a decrease in Sr (and sometimes Na) concentrations as diagenetic fluids in reduced and freshwater environments are strongly enriched in iron and manganese and depleted in strontium and sodium, respectively [9,10,12,34–36]. In addition, distribution coefficients of strontium are much higher in many calcitic shells than in inorganic calcite, which contributes to higher probability of diagenetic loss of this element [36,37]. Mn^{2+} ions are also an activator of the orange-red cathodoluminescence typical of altered calcites [10,38].

Screening of fossil preservation states should be preceded by their textural and optical inspection for possible mineral replacement, fracturing, recrystallization of primary structure and the presence of dark and clouded areas [16,36]. Staining of thin sections with Evamy's solution (a mixture of alizarin red-S and potassium ferricyanide, cf. [39]) is sometimes postulated to visualize Fe-rich areas [40,41]. Cathodoluminescence as well as minor and trace element studies are well-established methods for screening of the preservation state of calcitic marine macrofossils (cf. [9,10]). Relatively fast cold cathode cathodoluminescence analysis can be used for the selection of well-preserved areas of the shells, which may, in turn, be cleaned mechanically from altered rims or diagenetically cemented zones. Although non-luminescent calcite is usually regarded as pristine, it is worth noting that dull to moderate luminescence intensities or bright luminescent bands are observed within modern calcitic shells of bivalves and benthic foraminifera [42–44]. Such cathodoluminescence can be induced by low admixtures of Mn^{2+} ions incorporated into calcite lattice during slow growth periods in bottom or intra-sediment settings [42,44]. On the other hand, elevated concentrations of Fe^{2+} can quench the luminescence of calcite [38,45]. The combination of cathodoluminescence studies with chemical analyses of the calcite shell material is, therefore, recommended.

It is important to note that isotope geochemists use certain threshold limits of element concentrations as diagnostic of well-preserved fossils. They should be in agreement with Fe, Mn and Sr concentrations in modern shells, including counterparts or relatives of extinct organisms, or concentrations calculated for inorganic calcites precipitated in chemical equilibrium with seawater. Different authors use, actually, various cut-off limits of minor and trace elements concentrations, as characteristic of well-preserved low-Mg calcite, for the same sorts of fossils. As a result, some of them differ by more than two times in absolute concentrations of elements (Tables 1–3). In addition, many authors do not measure or do not take into consideration the limits of concentrations of some chemical elements.

Table 1. Published threshold limits of element concentrations in well-preserved belemnite rostra.

	Mn (ppm)	Fe (ppm)	Sr (ppm)
Veizer et al. [26]	<500	-	≥800
Anderson et al. [46]	<100	<1000	-
Jones et al. [47]	<50	<150	-
Price et al. [48]	<100	<250	-
Rosales et al. [49]	<32	<250	>950
Gröcke et al. [50]	<100	<200	-
Rosales et al. [51]	-	<250	≥900
Voigt et al. [52]	<100	<500	-
Price and Mutterlose [53], Price and Rogov [54], Nunn and Price [40]	<100	<150	-
Wierzbowski et al. [55]	<100	<200	≥800
Alberti et al. [56]	<50	<300	≥800
Alberti et al. [57]	<100	<300	>800
Wierzbowski [58], Arabas [59]	<100	<200	≥900
Korte and Hesselbo [60]	<250	-	≥400
Žak et al. [61]	<150	-	≥900

Table 2. Published threshold limits of element concentrations in well-preserved brachiopod shells.

	Mn (ppm)	Fe (ppm)	Sr (ppm)
Joachimski et al. [62], van Geldern et al. [63]	<100	<400	>500
Korte et al. [64,65], Korte and Hesselbo [60]	<250	-	>400
Armendáriz et al. [66]	<60	<300	-
Voigt et al. [52]	<100	<500	-
Bruckschen and Veizer [67]	<350	-	>600
Bruckschen et al. [68]	<200	-	-
Zuo et al. [69]	<100	<800	>700
Korte et al. [65]	<250	-	>400
Angiolini et al. [70]	<200	-	-
Wierzbowski [58]	<100	<300	>340

Sr content of fossils may vary due to temporal variations of the strontium concentration in seawater and noticeable biofractionation effects (cf. [37]), but the full range of reported Mn and Fe contents in modern brachiopod and bivalve shells is also significant [71,72]. It is well-documented that the total range of Mn and Fe concentrations in modern brachiopods is high due to the presence of few specimens enriched in these elements (up to 330 ppm of Mn, 1169 ppm of Fe), whereas most brachiopod shells have Mn and Fe concentrations of less than 80 ppm and 140 ppm, respectively [72]. This seems to be caused by a specific habitat of some modern brachiopods. As it is difficult to state with certainty that a particular fossil grew in a specific environment of decreased oxygenation or under the influence of pore waters enriched in manganese and iron, some reported elemental cut-off limits seem to be set too liberally. The same applies to the abandonment of measuring Sr concentrations, which can be a good proxy for diagenetic alteration under oxidizing conditions as this element has diagenetic behaviour other than that of manganese and iron.

The diagenetic behaviour of sodium is difficult to predict due to a complex process of Na co-precipitation with calcite and the possibility of its presence in interstitial sites (cf. [73]), but in the case of the existence of a clear diagenetic trend, sodium concentrations can be helpful as supporting evidence of chemical alteration of low-Mg calcites and used for finding the best-preserved part of the sample set [58,74,75].

The applicability of cold cathode cathodoluminescence analyses to screening of the preservation state of calcitic foraminifera tests is problematic due to their small size and preparation difficulties. In addition, orange-red luminescence of modern or well-preserved benthic foraminifera tests, which have secreted calcite in a specific microhabitat within the sediment column, is commonly observed [42–44]. A cathodoluminescence study of co-occurring planktonic foraminifera or spectroscopic analysis of the intensity of cathodoluminescence emission bands can be used for the evaluation of the degree of diagenetic alteration of such fossils [44,76,77].

Table 3. Published threshold limits of element concentrations in well-preserved oyster shells.

	Mn (ppm)	Fe (ppm)	Sr (ppm)
Anderson et al. [46]	<100	<1000	-
Jones et al. [47]	<50	<150	-
Wierzbowski and Joachimski [78], Wierzbowski [79]	<100	<250	>490
Korte and Hesselbo [60]	<250	-	>400
Zuo et al. [69]	<100	<700	>600
Danise et al. [80]	<250	<250	>350

Instead of challenging chemical analyses of small foraminifera tests, investigations of their micro- or nanostructure can be applied. It is generally accepted that pristine

foraminifera tests are glassy (translucent), with well-preserved microstructural details and microgranular texture, as opposed to frosty specimens, which show diagenetic calcite overgrowths. Various stages of microstructure preservation of foraminifera tests have been described by Sexton et al. [81]. However, the magnification of images presented by numerous authors (cf. [76,82–87]) is too low to show important structural details of the surfaces of foraminifera tests. Minor diagenetic alteration can be demonstrated by the occurrence of a few micron-large aggregates of neomorphic calcite microcrystals (Figure 1; see also [18,77,81]). Many elements such as ~1 μm blade-like “minitowers” with smooth surfaces observed within muricae (mount-like appendices) of morozovellid foraminiferal genera can, however, be difficult to distinguish from primary microstructural features (cf. [88]).

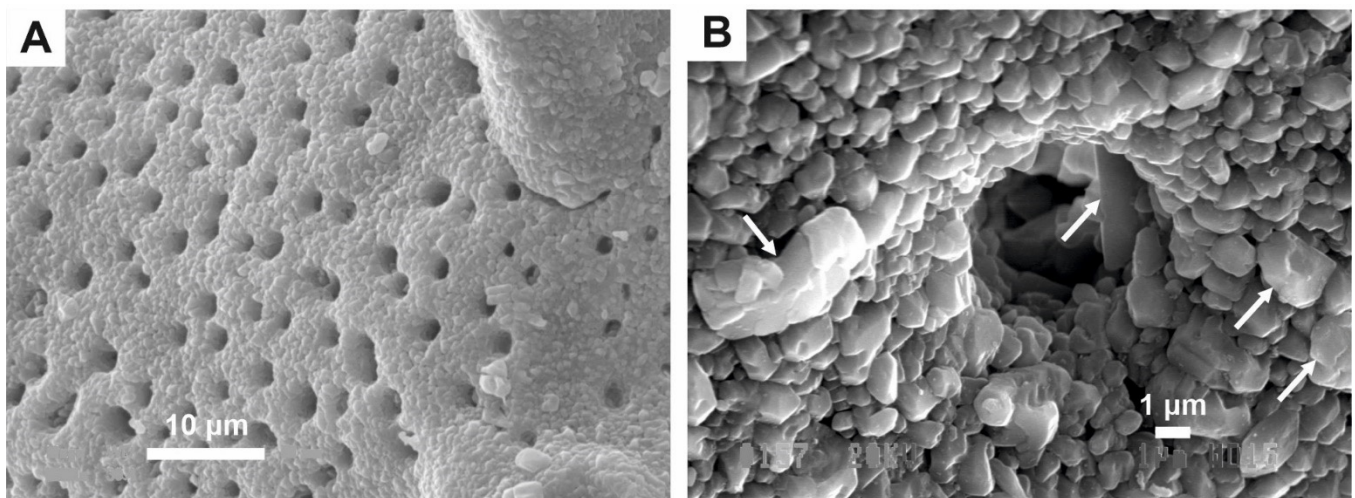


Figure 1. SEM photomicrographs of the microstructure of foraminifera tests from Campanian–Maastrichtian (Upper Cretaceous) chalk of Mielnik (Eastern Poland; cf. [77]). (A) Well-preserved microgranular texture of *Bolivinoides giganteus* foraminifera test. (B) Merged second-order aggregates (arrowed) indicate minor diagenetic alteration of *Gavelinella* sp. foraminifera test.

Insufficient screening for diagenetic alteration of foraminifera tests is likely a reason for the well-known “cool tropic” paradox of the Cretaceous and the Palaeogene related to the recrystallization of tropical planktonic foraminifera in the cold, deep-ocean floor [81,89]. Studies of exceptionally well-preserved foraminifera from oceanic sites show, as opposed to earlier data, high sea-surface temperatures of the Late Cretaceous and Palaeogene tropical oceans, which is consistent with a greenhouse climatic mode predicted for these epochs [88,90–93]. Nevertheless, it is possible that the process of prolonged solid-state diffusion may affect isotope composition of minute foraminifera tests with little (or no) impact on their microstructure [88,94]. Although it is not clear if published isotope values of apparently well-preserved foraminifera tests can really be affected by such a process (cf. [95,96]), care should be taken while handling with new foraminiferal samples, especially from localities, where comparative stable isotope data are lacking.

In certain cases, stable isotope composition of well-preserved aragonite fossils may be used as a proxy for ancient water temperatures and chemistry. Although the preservation of metastable aragonite is exceptional within ancient sediments, it may be fully preserved in impermeable clay or asphalt of low degree of thermal alteration. Previous authors assumed that the presence of pure aragonite in fossils, as documented by X-ray analyses, could be evidence of their good preservation [46,97,98]. However, diagenetic alteration of the microstructure of purely aragonitic fossils (Figure 2; [99–101]) and its impact on stable isotope ratios are well-documented [78,102,103]. A visual scale of the alteration of the ammonite microstructure consisting of nacreous tablets or crossed lamellar microstructure of gastropods and bivalves has been established by Cochran et al. [102] and Knoll et al. [103].

The alteration is visualized by a gradual passage from microstructure characterized by clean crystal surfaces and regular and distinct tablet (or bundle) boundaries into that with etched surfaces showing fusion of adjacent structural elements. Isotope exchange reactions with diagenetic fluids seem to be responsible for oxygen (and strontium) isotope shifts observed in partially dissolved or re-crystallized biogenic aragonite samples [102]. In addition, Raman spectroscopy, along with spot measurements of Mn/Ca ratios, may be used to demonstrate aragonite preservation or spatial distribution of aragonite and calcite phases in micro-samples (cf. [104,105]).

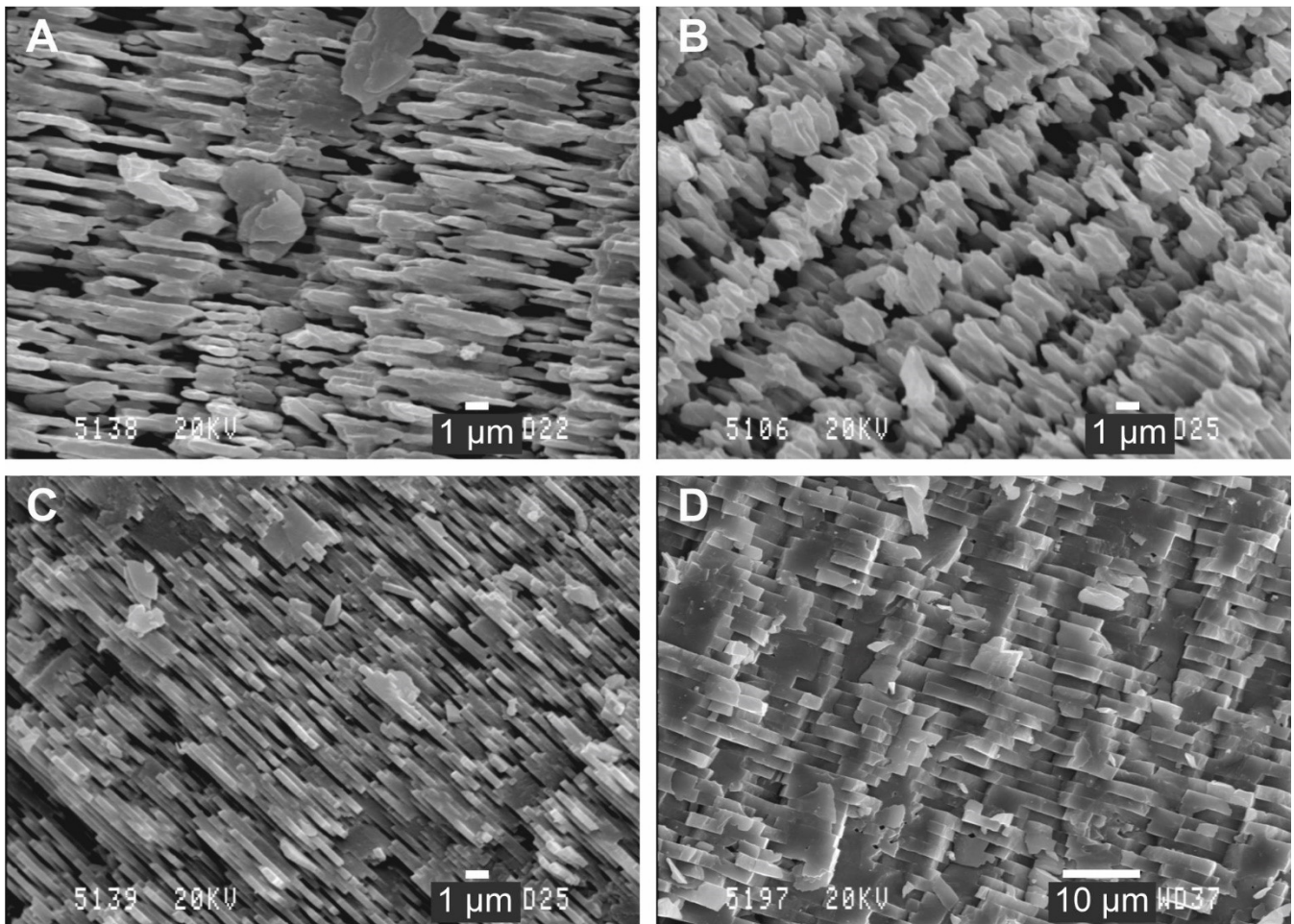


Figure 2. SEM photomicrographs of the microstructure of nacreous layer of Middle Bathonian (Middle Jurassic) aragonitic shells from central Poland (studied for stable isotopes by Wierzbowski and Joachimski [78]). (A) Partially dissolved ammonite shell. (B) Strongly dissolved ammonite shell. (C) Well-preserved ammonite shell. (D) Well-preserved bivalve (*Trigonia*) shell.

Despite general agreement concerning the necessity of using well-preserved fossil material, its selection is not always possible. Good examples are terebratulid and orthid brachiopod shells (cf. [106]) possessing perforated shell structure with minute punctae, which are usually filled with diagenetic calcite showing red to orange cathodoluminescence (Figure 3). Such shell material cannot be fully cleaned during manual preparation and always contains admixtures of calcite cements. The impact of the puncta-filling cement on oxygen isotope composition of the entire brachiopod shells may be considerable, providing that its $\delta^{18}\text{O}$ values are at least one order of magnitude lower than those of the surrounding shell, which is possible in the case of freshwater alteration [107]. Due to the lack of other fossils in certain intervals or locations, terebratulid oxygen isotope data are, however, taken into account in many cases (e.g. [56,69,108–110]).

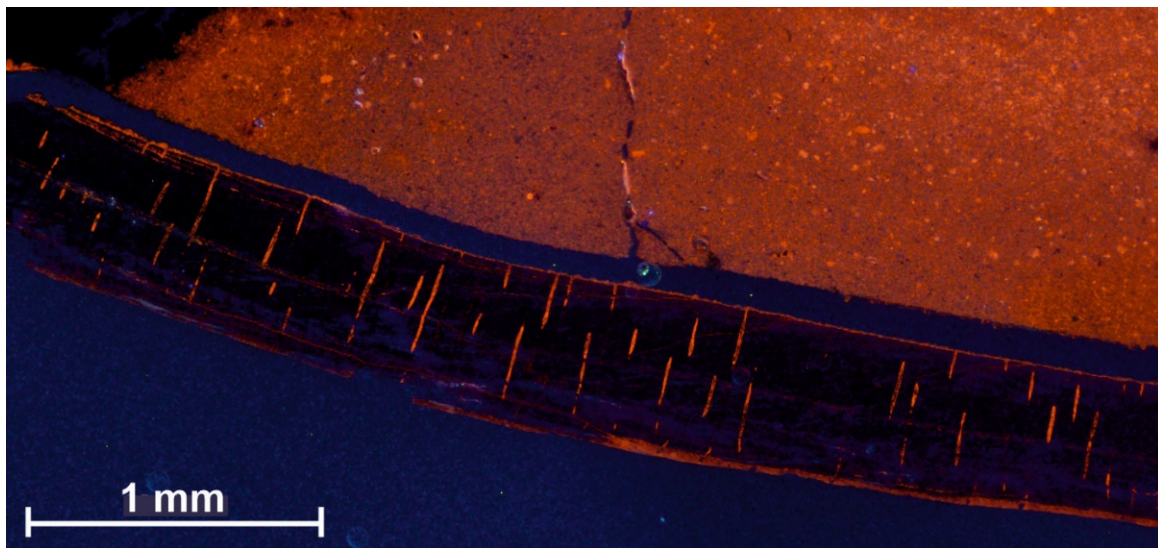


Figure 3. Cold cathodoluminescent image of an Upper Maastrichtian (Upper Cretaceous) terebratulid brachiopod shell from Chełm quarry (eastern Poland; cf. [111]). Puncta of the originally perforated shell are filled with luminescent diagenetic cements.

2.2. Apatite Fossils

Highly mineralized parts of phosphate skeletons of marine organisms such as tooth enamel(oid) or conodont crown tissue have great potential for preservation of the original oxygen isotope signal but, in opposition to calcium carbonate shells, there is no well-established screening method for detection of the preservation state of bioapatites. This results in many ambiguities concerning the selection of well-preserved bioapatites for oxygen isotope analyses.

Many authors simply assume that the studied phosphate material is well-preserved, focus on highly mineralized parts of apatite skeletons or check if the measured $\delta^{18}\text{O}_{\text{phosphate}}$ values are within the expected range of values for particular fossils and locations (cf. [13,62,112–119]). Although some indirect methods of the evaluation of the preservation state of phosphate fossils based on a comparison between enamel and bulk teeth $\delta^{18}\text{O}_{\text{phosphate}}$ values [24], determination of phosphate concentration in a sample [120], differentiation of $\delta^{18}\text{O}$ values between carbonate and phosphate components of bioapatites [121], crystallinity index [122,123] or Raman spectral shifts [124] were proposed, their practical use is hampered by methodological and interpretational difficulties.

Commonly applied is, on the other hand, a method for the visual inspection of conodont elements for thermal alteration, which is based on a change in their colour [125,126]. The scale of colours of conodont elements, from pale yellow through brown into final colourless—a so-called conodont colour-alteration index (CAI) is directly related to the temperature and time of the alteration and correlated to other thermal indices such as vitrinite reflectance (R_o) and palynomorph thermal alteration index (TAI; [127]). There is, however, no consensus about the effect of CAI value on oxygen isotope ratios, as Joachimski et al. [128] and Trotter et al. [129] show that conodont elements with $\text{CAI} \leq 5$ preserve their original $\delta^{18}\text{O}$ values, whereas Wheeley et al. [130] demonstrate decreased $\delta^{18}\text{O}$ values, with positively skewed value distribution, in conodont elements with $\text{CAI} > 1$. Enhanced freshwater diagenesis or visible recrystallization may, on the other hand, be connected with no or only a little change in conodont colour (Figure 4; see also [131,132]). The CAI index is, thus, helpful in screening of conodont elements but cannot be used as a definite proof for their good state of preservation.

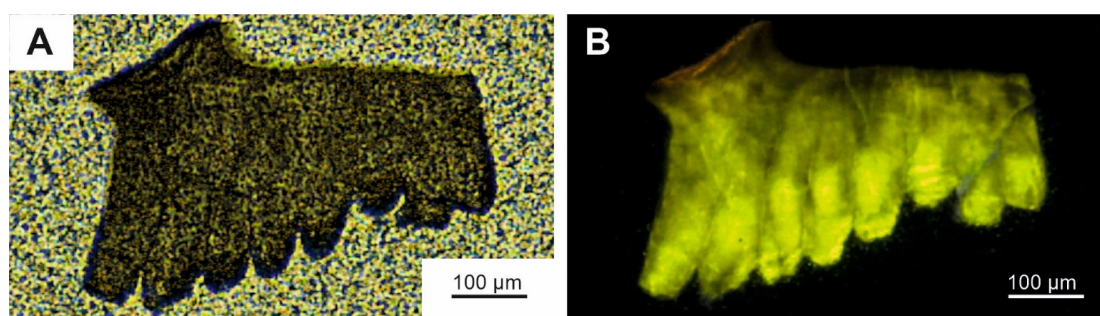


Figure 4. Lower Triassic (Dienerian) *Neospathodus* conodont element from Spitsbergen (studied for elemental and isotope composition by Wierzbowski et al. [132]), characterized by the low conodont colour-alteration index (CAI = 1). (A) Transmitted light image of the crown. (B) Intensive, yellow luminescence of the same area observed during the hot cathodoluminescence study.

The impact of diagenetic alteration on chemical composition of bioapatites is noticeable. Increases in concentrations of several minor and trace elements including Fe, S, Mn, V, Si, Al, Ba, U, Th, F, and rare-earth elements (REE)—particularly so called “middle REE”, are observed in altered vertebrate teeth and conodont elements ([41,133–139]. They are mostly related to the precipitation of secondary mineral phases such as oxyhydroxides and silicates [134] but also to mineralogical alteration such as the transformation of hydroxyapatites into fluorapatites (cf. [140–142]). Enrichments in “middle REE”, Fe and possibly S contents seems to be of particular importance for assessment of the preservation state of bioapatites. The “bell-shaped” REE pattern, which results from the preferential incorporation of the middle REE, is recognized as a valuable indicator of apatite alteration [115,135,137,143]. Fe and S enrichments in apatites occur during recrystallization in varying redox (micro)environmental conditions associated with the microbial activity (cf. [41,132,134,139]). Concentrations of these elements can be easily measured using an electron microprobe (EMP) analyser and compared to the concentrations found in apatite skeletons of modern organisms or well-preserved fossil parts (Figure 5; see also [41,132]).

Another valuable screening method of the preservation state of skeletal phosphates is hot cathode cathodoluminescence microscopy. Elevated Mn and REE concentrations induce orange to violet cathodoluminescence of skeletal apatites [144]. The cathodoluminescence analysis has been successfully used for the assessment of the preservation state of vertebrate teeth (cf. [41,145,146]) and conodont elements ([132]; Figure 4). Cathodoluminescence and elemental concentration analyses seem, thus, to be crucial for correct evaluation of the preservation state of fossil skeletal apatites.

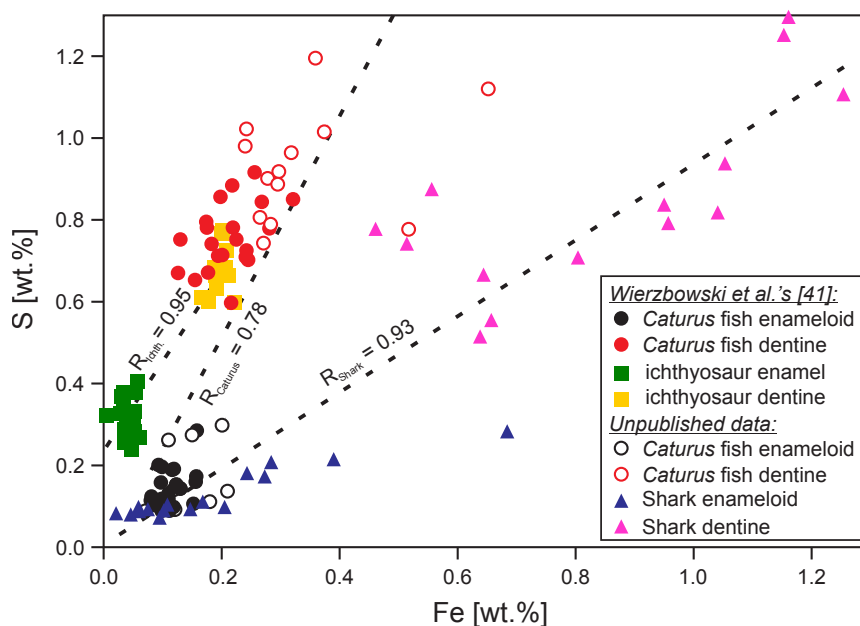


Figure 5. Fe and S concentrations in uppermost Jurassic *Cryopterygius kielanae* ichthyosaur and *Caturus* fish teeth from central Poland as well as Eocene *Striatolamia* shark teeth from Seymour Island (Antarctica). All measurements were conducted using an electron microprobe (Cameca SX100). Fe and S concentrations are relatively low in enamel(oid) and high in dentine. Diagenetic incorporation of both elements is revealed by strong, positive correlation of their concentrations; the linear relationships have slightly different slope in three groups in studied teeth (unpublished data and data from Wierzbowski et al. [41]).

3. Temperature Equations

3.1. Calcium Carbonate

Although a well-known carbonate temperature oxygen isotope Equation (1) presented by Epstein et al. [5] is based on aragonite-calcitic mollusc shells, it is traditionally used for calcites. A similarity of this equation to other equations established for calcite is likely due to helium stream roasting applied by Epstein's team as a pre-treatment, which induced negative $\delta^{18}\text{O}$ shifts in studied samples (see discussion in Wierzbowski [147]). Water and calcium carbonate isotope values are reported in Epstein et al.'s [5] Equation (1) as $\delta^{18}\text{O}$ values of CO_2 equilibrated with water and $\delta^{18}\text{O}$ values of acid-liberated CO_2 , respectively, and have to be re-calculated for (V)SMOW and (V)PDB scales.

$$T(^{\circ}\text{C}) = 16.5 - 4.3 \times (\delta^{18}\text{O}_{\text{calcite}} - \delta^{18}\text{O}_{\text{water}}) + 0.14 \times (\delta^{18}\text{O}_{\text{calcite}} - \delta^{18}\text{O}_{\text{water}})^2 \quad (1)$$

Craig [148] has introduced some instrumental corrections to the original equation of Epstein et al. [5]. Anderson and Arthur [8] have recalculated the equation of Craig [148] to express the $\delta^{18}\text{O}$ values of water and calcium carbonate relative to SMOW and PDB scales. Anderson and Arthur's [8] Equation (2) is given as follows:

$$T(^{\circ}\text{C}) = 16.0 - 4.14 \times (\delta^{18}\text{O}_{\text{calcite}} - \delta^{18}\text{O}_{\text{water}}) + 0.13 \times (\delta^{18}\text{O}_{\text{calcite}} - \delta^{18}\text{O}_{\text{water}})^2 \quad (2)$$

where $\delta^{18}\text{O}_{\text{calcite}}$ is the oxygen isotope composition of carbonate on the PDB scale and $\delta^{18}\text{O}_{\text{water}}$ is the oxygen isotope composition of water on the SMOW scale. The Equation (2) is widely used in palaeoclimatic studies for calcites, although it might further be corrected for a new relationship between VSMOW and VPDB scales established by Coplen et al. [149]. The latter correction gives, however, a negligible shift of ca. -0.2°C in the temperatures calculated.

Another experimental calibration of the oxygen isotope temperature scale (3) of Friedman and O'Neil [150], based on inorganic calcite, is very similar to the relationships

of Craig [148] and Anderson and Arthur ([8]; Figure 6). It is a corrected version of the equation previously given by O'Neil et al. [151].

$$10^3 \ln \alpha_{\text{calcite-water}} = 2.78 \times 10^6 / T^2 - 2.89 \quad (3)$$

where $\alpha_{\text{calcite-water}}$ is equilibrium fractionation factor between calcite and water, and T is the temperature in Kelvin. It is noteworthy that for the calculation of calcite SMOW values, used in this equation, the conversion between PDB and SMOW scales given by Friedman and O'Neil [150] should be applied.

A quadratic approximation of Friedman and O'Neil's [150] equation, shown as a temperature dependence of $\delta^{18}\text{O}_{\text{calcite}}$ and $\delta^{18}\text{O}_{\text{water}}$ values, has been given by Hays and Grossman [152]. Some confusion may arise because of incorrect information given in the study of Hays and Grossman [152] that it is a recalculated form of the original equation of O'Neil et al. [151]. This has been clarified by Grossman [16], who notified that Hay and Grossman's [152] equation is a recalculated version of O'Neil et al.'s [151] equation with correction of Friedman and O'Neil [148]. The Hays and Grossman [152] Equation (4) can be easily used in palaeotemperature studies based on skeletal calcites.

$$T(^{\circ}\text{C}) = 15.7 - 4.36 \times (\delta^{18}\text{O}_{\text{calcite}} - \delta^{18}\text{O}_{\text{water}}) + 0.12 \times (\delta^{18}\text{O}_{\text{calcite}} - \delta^{18}\text{O}_{\text{water}})^2 \quad (4)$$

where $\delta^{18}\text{O}_{\text{calcite}}$ is the oxygen isotope composition of carbonate on the PDB scale and $\delta^{18}\text{O}_{\text{water}}$ is the oxygen isotope composition of water on the SMOW scale.

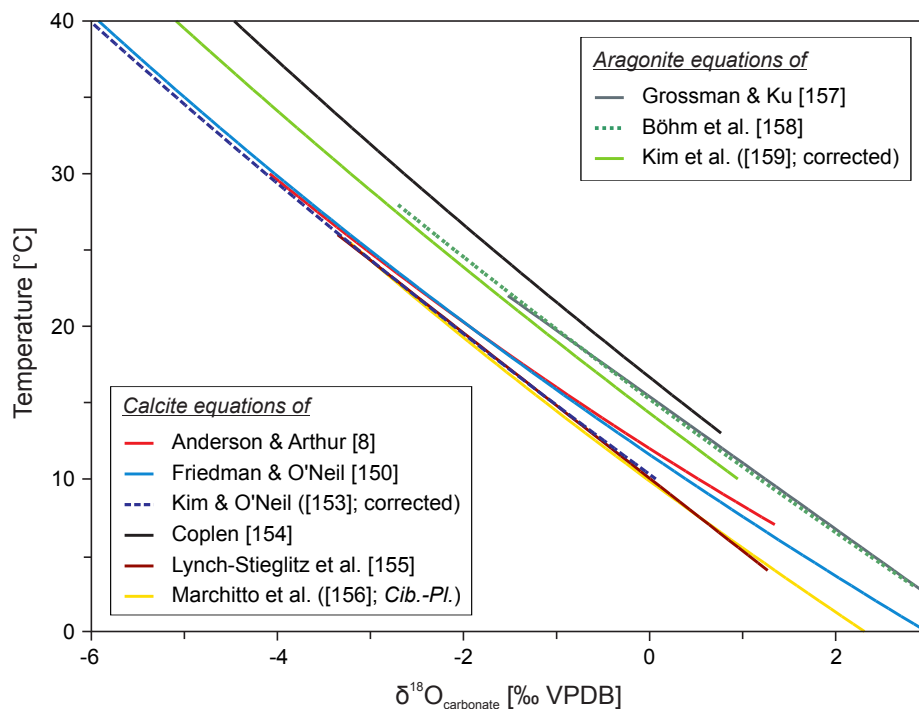


Figure 6. Comparison between published oxygen isotope temperature scales [8,150,153–159] comprising calcite-water and aragonite-water fractionation for $\delta^{18}\text{O}_{\text{water}}$ value = -1‰ VSMOW, which is usually assumed as characteristic of an ice-free world (cf. [160]).

There is a newer calibration of the oxygen isotope temperature scale for inorganic calcites by Kim and O'Neil [153]. The authors have used for calculation of $\delta^{18}\text{O}_{\text{calcite}}$ values a non-conventional CO_2 -calcite acid fractionation factor of 1.01050, and their equation has to be re-calculated for an acid fractionation factor of 1.01025, which is traditionally applied for calcite (see [150]). This correction is, unfortunately, not employed by many authors who use the original version of Kim and O'Neil's [153] equation. It causes an offset of ca. $-1.1\text{ }^{\circ}\text{C}$ in the temperature calculated compared to the corrected version of this equation.

The corrected version (5) of Kim and O’Neil’s [153] equation, as reported in a study of Zhou and Zheng [161], is given as follows:

$$10^3 \ln \alpha_{\text{calcite-water}} = 18.03 \times 10^3 / T - 32.17 \quad (5)$$

where $\alpha_{\text{calcite-water}}$ is equilibrium fractionation factor between calcite and water, and T is the temperature in Kelvin. The equation, even after a correction for the non-conventional acid fractionation factors, gives ca. 1.4 °C lower temperatures than those calculated using more traditional equations of Friedman and O’Neil [150] and Anderson and Arthur [8].

Numerous studies have shown that oxygen isotope composition of skeletal calcites, which are not significantly affected by vital effects, like the inner portion of the secondary layer of brachiopods (cf. [72,162–164]) or foliated and chalky layers of oyster shells (cf. [165–170]), approach oxygen isotope equilibrium predicted in the temperature equations of Friedman and O’Neil [150] or Anderson and Arthur [8]. The same applies to most representatives of *Bolivina*, *Bulimina*, *Gyroidina*, *Oridorsalis*, *Pullenia* and *Uvigerina* genera of benthic foraminifera, which are regarded as exerting minor vital effects (cf. [77,171–182]). However, 0.5–1.0‰ lower $\delta^{18}\text{O}$ values of *Cibicidoides* benthic foraminifera, compared to higher values of previously mentioned taxa, are also occasionally claimed to represent equilibrium fractionation [18,155,156,183]. This is likely due to the application of the non-corrected version of Kim and O’Neil’s [153] equation, which gives slightly lower temperatures than the Friedman and O’Neil [150] and Anderson and Arthur [8] equations (cf. Figure 6).

Oxygen temperature equations determined for many taxa of calcitic planktonic foraminifera have slopes similar to the traditional equations established for molluscs or inorganic calcite but deviate in absolute values (cf. [155,156,184–187]). This can be assigned to negative $\delta^{18}\text{O}$ shifts induced by vital effects related to the activity of photosynthetic symbionts or speciation of inorganic carbon sources (CO_2 , HCO_3^- , CO_3^{2-}) at varying pH (cf. [18]).

Some bias in oxygen isotope temperatures calculated for calcite samples may arise because of the effect of substitution of Mg ions in crystal lattice. The $\delta^{18}\text{O}$ value effect has been estimated by Jiménez-López et al. [188] to be +0.17‰ for each MgCO_3 mol%, which is three times higher than its previous estimate of Taratuni et al. [189]. An adjustment to the MgCO_3 effect is applied in the temperature Equation (6) of Brand et al. [190] established for modern brachiopod shell results. According to its authors, it results in better agreement between calculated and measured precipitation temperatures.

$$T(^{\circ}\text{C}) = 16.192 - 3.468 \times (\delta^{18}\text{O}_{\text{calcite}} - \delta^{18}\text{O}_{\text{water}} - \delta^{18}\text{O}_{\text{Mg-adjust}}) \quad (6)$$

where $\delta^{18}\text{O}_{\text{calcite}}$ is the oxygen isotope composition of carbonate on the PDB scale, $\delta^{18}\text{O}_{\text{water}}$ is the oxygen isotope composition of water on the SMOW scale and $\delta^{18}\text{O}_{\text{Mg-adjust}}$ is an adjustment for the change of $\delta^{18}\text{O}_{\text{calcite}}$ by +0.17‰ for each MgCO_3 mol%.

Importantly, Coplen [154], Day and Henderson [191], Dietzel et al. [192], Gabitov et al. [193], and Watkins et al. [194,195] have recently shown, based on precipitation studies in specific natural and experimental laboratory conditions, that the oxygen isotope fractionation in calcite is significantly affected by crystal growth rate and pH variations at the site of calcification. Therefore, oxygen isotope equilibrium is not maintained during spontaneous calcite precipitation, characterized by a relatively high rate of crystal growth, typical of many natural or laboratory settings. Coplen [154] has, therefore, argued that previously published oxygen isotope temperature equations are biased by 1.4‰, due to kinetic factors, but may still work well for most skeletal calcites, which are precipitated under ubiquitous, relatively constant isotope disequilibria. Equation (7) of Coplen [154], corroborated by the data of Gabitov et al. [193] and Watkins et al. [194], gives 5–6 °C higher temperatures than traditional oxygen isotope temperature equations for calcite (Figure 6) and can possibly

be applied for certain fossils such as calcitic rostra of the Jurassic and Cretaceous Boreal belemnite families (see discussion in the next section).

$$10^3 \ln \alpha_{\text{calcite-water}} = 17.4 \times 10^3 / T - 28.6 \quad (7)$$

where $\alpha_{\text{calcite-water}}$ is the equilibrium fractionation factor between calcite and water, and T is the temperature in Kelvin.

Aragonite precipitated in equilibrium with ambient water is assumed and reported to be enriched by 0.6 to 1‰ in ^{18}O compared to calcite (cf. [158]). However, the difference between $\delta^{18}\text{O}$ values of aragonite and calcite layers of modern mollusc shells is found to be lower (ca. 0.4‰) and related to the disparity in accepted acid fractionation factors [196]. Biogenic aragonite-water oxygen isotope fractionation was investigated by Grossman and Ku [157] who presented two equations “for molluscs” and “all (skeletal) data”. These equations must be corrected for water $\delta^{18}\text{O}$ value as the values reported by the authors are lower by 0.2‰ compared to the SMOW scale (cf. [16]). The corrected “all (skeletal) data” Equation (8) is given as follows:

$$T(^{\circ}\text{C}) = 20.6 - 4.34 \times (\delta^{18}\text{O}_{\text{aragonite}} - \delta^{18}\text{O}_{\text{water}} + 0.2) \quad (8)$$

where $\delta^{18}\text{O}_{\text{aragonite}}$ is the oxygen isotope composition of carbonate on the PDB scale and $\delta^{18}\text{O}_{\text{water}}$ is the oxygen isotope composition of water on the SMOW scale.

Böhm et al. [158] have compiled the newly obtained oxygen isotope data of aragonitic coralline sponges with published data to calculate revised aragonite temperature dependence given both as linear regression and fractionation factor formula—see Equation (9). Their dependence shows reduced error limits compared to the original equations of Grossman and Ku [157].

$$10^3 \ln \alpha_{\text{aragonite-water}} = 18.45 \times 10^3 / T - 32.54 \quad (9)$$

where $\alpha_{\text{aragonite-water}}$ is the equilibrium fractionation factor between aragonite and water, and T is the temperature in Kelvin.

Since both Grossman and Ku [157] and Böhm et al. [158] calibrated aragonite oxygen isotope composition relative to calcite NBS19 standard, at the temperature range of 50–75 °C, no specific CO_2 -aragonite acid fractionation factor should be applied while calculating the precipitation temperature using these formulas (this is in accordance with the presently most widely used method of reporting aragonite isotope values without a specific correction for the aragonite acid fractionation). Similar aragonite temperature scales have been established for fish otoliths [197–199] and freshwater molluscs [200]. These authors also do not take into account the specific acid fractionation factor for aragonite.

A new equation established for inorganic aragonite has been presented by Kim et al. [159]. Unfortunately, most people do not notice that Kim et al.’s [159] temperature dependence is based on a new, unconventional CO_2 -aragonite acid fractionation factor of 1.01063 and needs to be re-calculated for a CO_2 -calcite acid fractionation factor of 1.01025 (given after Friedman and O’Neil [150]), to be consistent with other aragonite formulas. The corrected version (10) of Kim et al.’s [159] equation is given as follows:

$$10^3 \ln \alpha_{\text{aragonite-water}} = 17.88 \times 10^3 / T - 30.76 \quad (10)$$

where $\alpha_{\text{aragonite-water}}$ is the equilibrium fractionation factor between calcite and water, and T is the temperature in Kelvin.

All the discrepancies and required corrections can lead to misunderstandings and biases in palaeotemperature calculations based on oxygen isotope composition of skeletal calcium carbonate. A choice of an appropriate temperature equation is not a trivial point and should be made, as a rule of thumb, based on similar sort of the investigated material or data confirming the reliability of a certain equation to oxygen isotope fractionation in skeletons of selected groups of marine calcareous organisms or their modern relatives.

Temperatures calculated using various oxygen isotope equations for calcium carbonate can be easily compared using a calculator available in Supplementary Materials to this article (Table S1, List S1). The temperature formulas, in the calculator, have been standardized to VSMOW-VPDB scales and the CO₂-calcite acid fractionation factor of 1.01025.

3.2. Calcium Phosphate

There is some confusion regarding phosphate oxygen isotope temperature scales owing to a gradual change in laboratory techniques (BiPO₄ and Ag₃PO₄ precipitation techniques, analysing CO or CO₂ gases obtained by total fluorination of phosphates or their partial reduction with graphite) and adoption of different values of apatite NBS120b and NBS120c standards (cf. [201–204]).

The appropriate corrections include a reported 1.4‰ offset between δ¹⁸O values of NBS 120b reference measured using an older BiPO₄ precipitation technique and a newer Ag₃PO₄ precipitation technique (cf. [201,202,205]). This correction should be applied in Longinelli and Nuti's [6] and Kolodny et al.'s [7] equations. Nowadays, an NBS 120c value of 21.7‰ VSMOW is usually accepted, and this also imposes a 0.9‰ correction, which is already predicted in the equation presented by Pucéat et al. [201] for all published data (see Equation (11)).

$$T(^{\circ}\text{C}) = 118.7 - 4.22 \times (\delta^{18}\text{O}_{\text{phosphate}} - \delta^{18}\text{O}_{\text{water}} + 0.9) \quad (11)$$

where δ¹⁸O_{phosphate} is the oxygen isotope composition of carbonate and δ¹⁸O_{water} is the oxygen isotope composition of water, both reported versus the VSMOW scale.

The internal consistency of calculated water temperatures analysed using co-occurring phosphate and carbonate fossils and different phosphate and carbonate temperature equations (the latter include Kim and O'Neil's [153]; Anderson and Arthur's [8] and Kim et al.'s [159] equations) was tested by Lécuyer et al. [202]. These authors have also presented a new temperature equation (12) combining data from modern lingulids and shark teeth, which yields the most consistent phosphate-carbonate temperature estimates:

$$T(^{\circ}\text{C}) = 117.4 - 4.50 \times (\delta^{18}\text{O}_{\text{phosphate}} - \delta^{18}\text{O}_{\text{water}}) \quad (12)$$

where δ¹⁸O_{phosphate} is the oxygen isotope composition of carbonate and δ¹⁸O_{water} is the oxygen isotope composition of water, both reported versus the VSMOW scale.

Application of all corrections to the oxygen isotope phosphate temperature scales reduces a scatter in the temperatures calculated to less than 5 °C, which is much lower than the difference reported previously (cf. [200]). Temperatures calculated using various oxygen isotope equations for calcium phosphate can be easily compared using the calculator available in Supplementary Materials to this article (Table S2, List S2).

4. Vital and Habitat Effects

4.1. Calcareous Skeletons

Many organisms secrete calcium carbonate out of isotope equilibrium with water and, hence, their δ¹⁸O values are inconsistent with fractionation predicted by commonly applied oxygen temperature scales. These phenomena may be related to carbonate precipitation from body fluids, which are not fully equilibrated with ambient water, or the transformation of precursor, amorphous mineral phases [21]. Disequilibrium precipitation due to vital fractionation effects is common among some groups of marine animals including calcareous algae, foraminifers, corals and echinoderms ([206]; Figure 7). In fact, disequilibrium precipitation of oxygen isotopes is less common than carbon isotope disequilibria, and δ¹⁸O values of skeletons of many animal groups such as sclerosponges, molluscs or some portion of brachiopod shells generally approach expected isotope equilibria (cf. [16,21]).

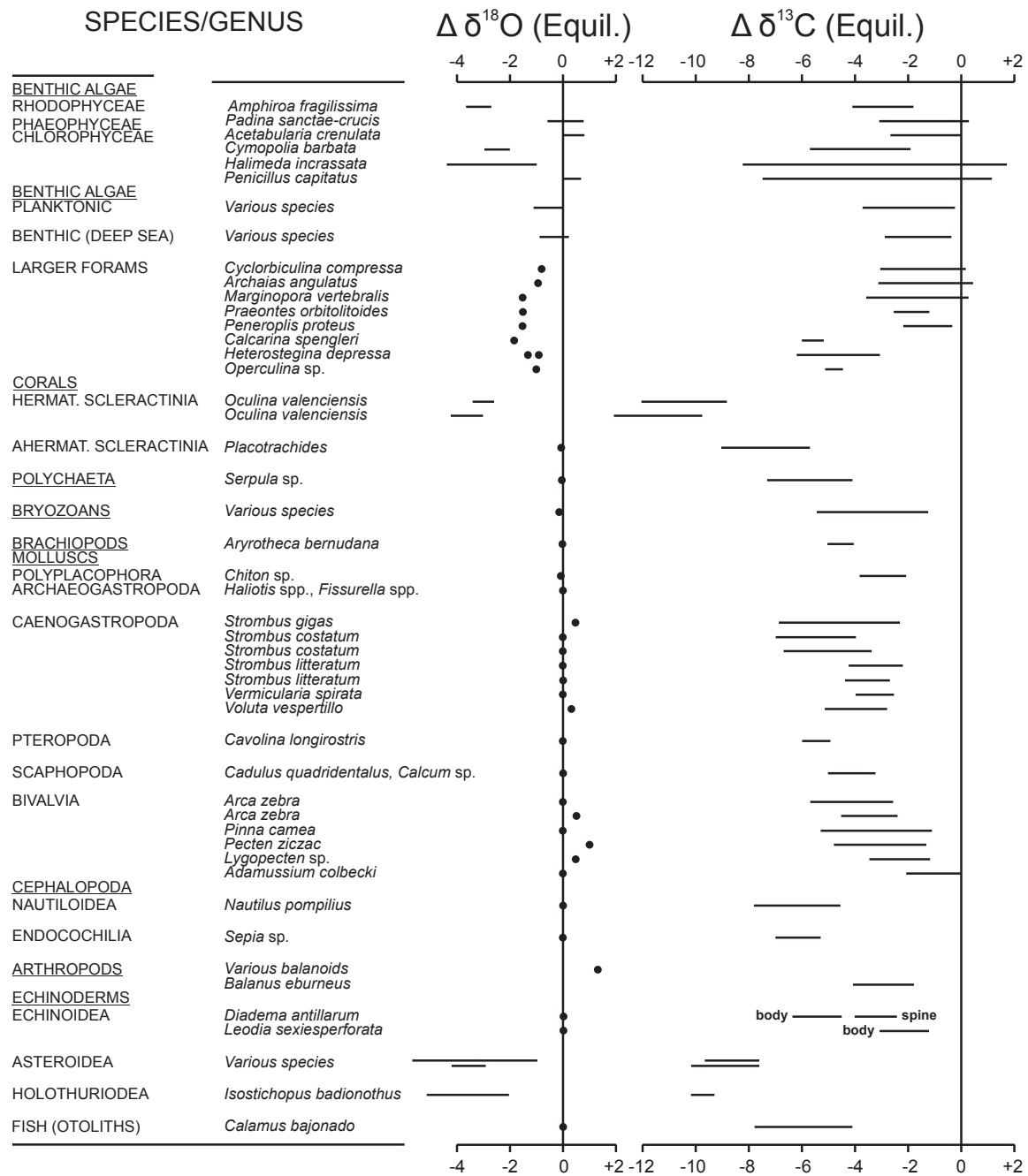


Figure 7. Oxygen (and carbon) isotope departures from isotope equilibrium in recent calcareous skeletons of various animal groups (reproduced with permission from Wefer and Berger [206]. “Isotope paleontology: growth and composition of extant calcareous species”. Marine Geology, 1991, v. 100, p. 207–248. Copyright Elsevier 2021).

Commonly known vital effects can be divided into kinetic and metabolic ones. The kinetic effects are attributed by McConnaughey [207,208] to discrimination of heavy ^{18}O and ^{13}C isotopes during CO_2 hydration and hydroxylation, which is favoured by a rapid shell growth. In the model of Adkins et al. [209] these effects are, however, linked to changing proportions of HCO_3^- and CO_3^{2-} ions at the calcification site regulated by calcification rate-dependent pH gradient between the cell wall and the extracellular calcifying fluid (ECF). In other, mixed models of Rollion-Bard et al. [210] and Chen et al. [211], the kinetic isotope shifts are related to pH variations and the time of O isotope equilibration between dissolved inorganic carbon (DIC) and water during the hydration and hydroxylation processes or, respectively, to the effect of variable activity of the enzyme carbonic anhydrase,

which buffers the pH, increases DIC concentration in ECF and affects the reaction kinetics. Simultaneous depletion in heavy isotopes, typical of organisms exerting kinetic fractionation, such as corals, is visualized by the strong, positive correlation between carbonate $\delta^{18}\text{O}$ and $\delta^{13}\text{C}$ values [207,208]. In rare cases, at the high calcification rate, high pH gradient and maximum CO_2 flux throughout the cell wall, constant $\delta^{13}\text{C}$ values may be maintained at decreasing $\delta^{18}\text{O}$ values, linked to kinetic fractionation [209]. Metabolic effects, which involve single $\delta^{13}\text{C}$ shifts related to the respiration or photosynthesis, may disrupt linear isotope trends of kinetic fractionation [207,212–214]. The presence of kinetic effects does not preclude palaeotemperature determinations, in some cases. The analysis of $\delta^{13}\text{C}$ vs. $\delta^{18}\text{O}$ regression lines of modern cold-water corals may be, for example, used for the retrieval of ambient water temperatures with an accuracy better than ± 2 °C, assuming that the $\delta^{13}\text{C}$ value of DIC is known or estimated [215–218].

The carbonate ion concentration in ambient water, dependent on water pH value, is another factor that frequently affects oxygen (and carbon) isotope values of unicellular, calcifying organisms including foraminifera tests, coccolithophores and calcareous dinoflagellates (cf. [219–223]). The greatest change in carbonate $\delta^{18}\text{O}$ values occurs in the 6–8 pH range [223]. The measured range of foraminiferal $\delta^{18}\text{O}$ values may additionally be dependent on pH variations within the water column and influenced by $\delta^{18}\text{O}$ shifts related to symbiotic activity in planktonic foraminifera species (cf. [186]). The carbonate ion effect may also be partially responsible for the scatter of $\delta^{18}\text{O}$ values of different epifaunal and infaunal foraminifera species due to pH variations in the sediment column [18]. High-amplitude variations in seawater pH values (e.g., throughout the Palaeocene–Eocene Thermal Maximum or glacial and interglacial transitions) and prolonged fluctuations in global seawater chemistry may produce significant temporal shifts in the foraminiferal oxygen isotope record [18,221,223–225].

Slightly lower pH values of body fluids of modern molluscs and brachiopods (7.2 to 7.5) compared to that of seawater (8.0) may theoretically be a source of constant oxygen isotope offsets to abiotic marine cements (cf. [21]). Although there is no information that variations in CO_3^{2-} ion concentration in surrounding water may affect the oxygen isotope composition of skeletons of most multicellular marine organisms, recently reported data suggest its impact on $\delta^{18}\text{O}$ values of artificially grown brachiopods [226].

Different intensities of the carbonate ion effect, related to the presence or the lack of symbionts, along with kinetic effects, may explain differences in oxygen isotope signatures of different size fractions of planktic and benthic foraminifera (cf. [183,186,227,228]). It is worth noting that environmental (micro)habitat effects of particular foraminiferal taxa related to the occupation of a specific depth in the water column or position in the sediment may be superimposed on isotopic shifts caused by kinetic or carbonate ion effects (cf. [77,85,179,182,229]). This can increase the entire bias and scatter of foraminiferal $\delta^{18}\text{O}$ values (cf. Figure 8).

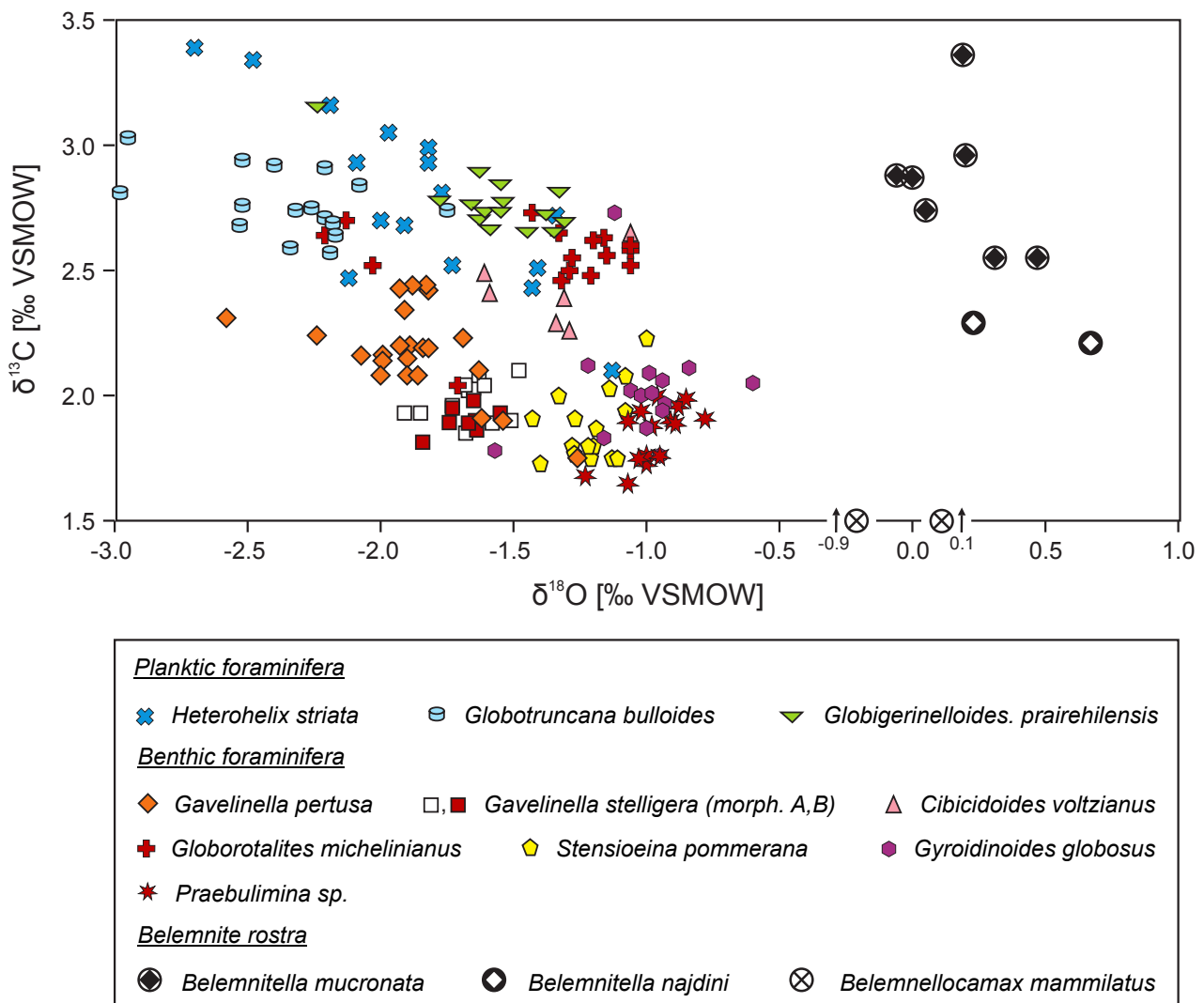


Figure 8. $\delta^{18}\text{O}$ and $\delta^{13}\text{C}$ values of individual benthic and planktic foraminifera tests and belemnitellid belemnite rostra from the Lower–Upper Campanian boundary (Upper Cretaceous, Mielnik, Eastern Poland; data of Bojanowski et al. [230] and Dubicka et al. [77]). Note a significant spread of foraminiferal $\delta^{18}\text{O}$ values related to vital and habitat effects. Although high *Gyroidinoides globosus* and *Praebulimina* sp. $\delta^{18}\text{O}$ values are expected to be close to isotope equilibrium (cf. [77]), ca. 1.0‰ higher belemnite $\delta^{18}\text{O}$ values may show different point of oxygen isotope equilibrium or specific oxygen isotope fractionation in the rostra from the Belemnitellidae belemnite family.

Although inner parts of secondary and tertiary layers, which form a major portion of brachiopod shells, are usually regarded as precipitated close to oxygen (and carbon) isotope equilibrium, the outer part of secondary layer and areas of specialised shell structures (hinge, brachidium, foramen, interarea and muscle scars) as well as thin primary layer of brachiopods show significant ^{18}O depletion related to kinetic effects [162,164,231–234]. In addition, more or less significant kinetic effects have recently been reported from bulk secondary layer of some terebratulid brachiopod taxa [234–236]. Oxygen isotope disequilibria are also observed in certain parts of bivalve shells e.g., fast growing areas of modern scallops [237], the earliest, juvenile portion of oyster carbonate [238] or shell increments affected by metabolic stress [239]. This emphasises a role of the selection of the least affected, by vital effects, shell zones for analysis of ancient water oxygen isotope signal.

Distinction between vital and (micro) habitat effects in the sedimentary record of ancient marine environments may be difficult because of the presence of the sole remnants of extinct organisms of unknown physiology or wide-spread organisms that settle various

depth niches. A comparison of oxygen isotope values of coeval fossils is a valuable proxy for determination of equilibrium isotope signal, but it has been only occasionally made. For example, a scatter of $\delta^{18}\text{O}$ values of different Upper Cretaceous foraminiferal taxa and their offset to the values of co-occurring belemnite rostra, as related to vital and habitat effects, is observed (cf. [77,230]; Figure 8).

Remarkable also is a comparison between $\delta^{18}\text{O}$ values of co-occurring benthic calcitic bivalves, brachiopods and belemnite rostra, which are often regarded as necto-benthic. Conducted isotope studies have shown various results, i.e., (1) similar $\delta^{18}\text{O}$ values of coeval Jurassic belemnite rostra and oyster shells [60,78,240], (2) similar $\delta^{18}\text{O}$ values of Jurassic–Cretaceous belemnite rostra and brachiopod shells [58,108,241], (3) similar $\delta^{18}\text{O}$ values of Jurassic belemnite rostra, oyster and brachiopod shells [242], (4) ca. 0.5‰ higher $\delta^{18}\text{O}$ values of Jurassic belemnite rostra compared to the oxygen isotope values of oyster shells [46,243], (5) ca. 1‰ higher $\delta^{18}\text{O}$ values of Cretaceous belemnite rostra compared to the oxygen isotope values of brachiopod shells [52], (6) ca. 1‰ higher $\delta^{18}\text{O}$ values of Cretaceous belemnite rostra compared to the oxygen isotope values of inoceramid and brachiopod shells [244], (7) 0.5 to 2‰ higher $\delta^{18}\text{O}$ values of Jurassic belemnite rostra compared to the values of co-occurring oyster and brachiopod shells [56,245]. Apart from the results of Alberti et al. [56,245], which might reflect migratory behaviour of investigated Tethyan Belemnopseidae (=Mesohibolitidae) and Duvalidae belemnites, possibly related to their post-spawning mortality, in the shallow Kachchh basin of India (cf. [246]) and the Morondava basin of Madagascar (cf. [247]), most elevated belemnite $\delta^{18}\text{O}$ values are derived from the Boreal belemnite groups, i.e., Jurassic *Cylindroteuthidae* belemnite family (data of Anderson et al. [46] and Mettam et al. [243]) and Cretaceous *Belemnitellidae* belemnite family (data of Voigt et al. [52] and Wilmsen and Niebuhr [244]). Interestingly, distinctly higher (by 0.8‰) $\delta^{18}\text{O}$ values of uppermost Middle–Upper Jurassic Boreal *cylindroteuthid* belemnites compared to the oxygen isotope values of co-occurring Tethyan belemnopseid belemnites have been reported by Wierzbowski et al. [55] from the Russian Platform. This observation is in line with data of Ditchfield [248] showing ca. 0.5‰ difference between $\delta^{18}\text{O}$ values of coeval Upper Jurassic *cylindroteuthid* and belemnopseid belemnite rostra from the Tordenskjoldberget Member of the Kongsøya Formation of Svalbard as well as the data of Price et al. [249] showing ca. 5 °C lower temperatures calculated from $\delta^{18}\text{O}$ values of *cylindroteuthid* belemnite rostra compared to those calculated from co-occurring aragonitic shells of *Belemnoteuthis* belemnites, *Kosmoceras* ammonites, *Mesosacella* bivalves, and aragonitic phragmocones of the same *cylindroteuthid* belemnites, whose rostra were sampled previously.

Noteworthy, Price et al. [250] have also observed a remarkable difference between belemnite and brachiopod $\delta^{18}\text{O}$ values in the long-term Jurassic–Lower Cretaceous dataset with belemnite data points being biased towards lower temperature estimates (Figure 9). The high belemnite $\delta^{18}\text{O}$ values are, hence, considered to be responsible for the occurrence of a so-called Jurassic–Early Cretaceous negative temperature anomaly, as the temperature trend based on sole brachiopod data shows a prolonged Mesozoic warm period ([250]; Figure 9).

High belemnite $\delta^{18}\text{O}$ values, especially apparent among boreal belemnite families, can be interpreted as a result of (1) the migratory life style of these animals, which lived in deeper and cooler waters; (2) their selective origin from mid- and high palaeolatitudes in the common datasets [250]; (3) non-equilibrium oxygen isotope fractionation in belemnite rostra or other skeleton parts of studied fossils [249,250]; or (4) cementation of originally porous belemnite rostra during early marine diagenesis (cf. [251,252]). Based on the comparison between $\delta^{18}\text{O}$ values of belemnites and co-occurring fossils as well as careful screening of belemnite rostra for the preservation state, theories of discriminatory selection of belemnite data points or their alteration should be disregarded (see discussion in Wierzbowski et al. [253] and Vickers et al. [254]). This may point to the specific oxygen isotope fractionation of belemnite rostra as a source of the observed offset in $\delta^{18}\text{O}$ values. A somewhat different oxygen isotope fractionation of the rostra of Boreal belemnite

groups, which might have been closer to the real equilibrium predicted for slow-growing inorganic calcite by Coplen [154], can also be suggested on the basis of clumped isotope data [253–255]. Interestingly, positive $\delta^{18}\text{O}$ shifts from isotope equilibrium calculated on the basis of traditional oxygen isotope equations are also observed in deep-water modern oyster shells characterized by extremely slow growth rates [256], cold water limpets [257], and calcitic barnacles being a group of arthropods [258]. This shows the possibility of the maintenance of different points of oxygen isotope equilibrium in some calcitic fossils e.g., those characterized by a very slow growth rate. On the other hand, lower $\delta^{18}\text{O}$ values of terebratulid brachiopods, which, contrary to rhynchonellids, possess perforated shells (see Figure 3) and frequently exert kinetic fractionation (cf. [234]), may bias the brachiopod oxygen isotope trend to higher temperature values. Therefore, both boreal belemnite and terebratulid brachiopod $\delta^{18}\text{O}$ data should be treated with caution while constructing long-term isotope temporal trends.

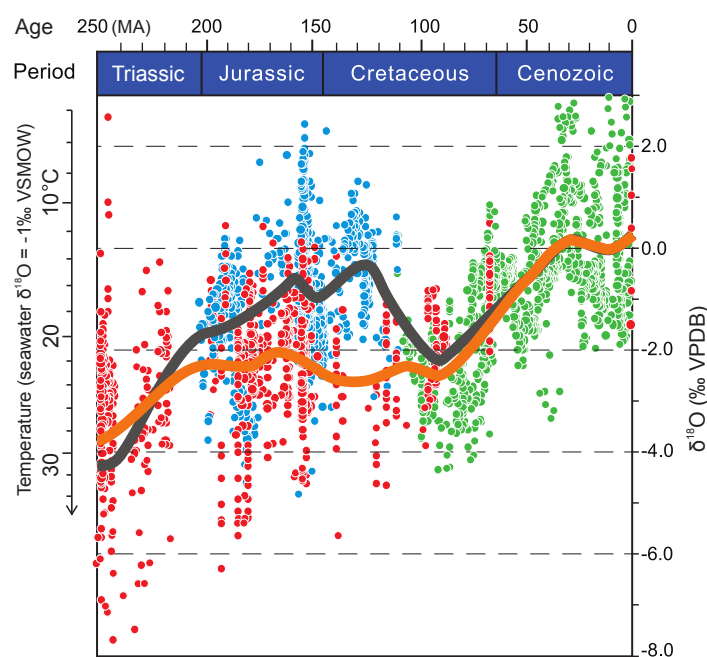


Figure 9. Evolution of published Mesozoic–Cenozoic $\delta^{18}\text{O}$ values. Brachiopod data (red circles), belemnite data (blue circles), planktic foraminifera (green circles). Smoothed curves for all data (dark grey curve) and brachiopod-foraminifera only data (orange curve). The orange curve devoid of belemnite data shows a prolonged warm period during the Jurassic and the Cretaceous (after Price et al. [250], modified). The temperature scale depicted for comparative purposes is based on Anderson and Arthur’s [8] equation and the assumed average oxygen isotope composition for the non-glacial Earth.

All of these facts emphasise the importance of careful selection of studied material and its screening for potential taxonomical bias as based on the comparison of oxygen isotope values between various coeval fossils. Such comparison is a valuable tool for retrieving reliable long-term oxygen isotope trends, which should reflect original temperature and chemistry changes of ancient water devoid of influence by vital and habitat animal effects.

4.2. Apatite Skeletons

It is generally assumed that $\delta^{18}\text{O}$ values of biophosphate track perfectly $\delta^{18}\text{O}$ values of body fluids owing to rapid isotopic exchange involving adenosine triphosphate (ATP) mechanisms common to all organisms [13]. Oxygen isotope composition of body water of aquatic animals, especially those using gills, is also expected to be in perfect isotope equilibrium with ambient water owing to rapid transcutaneous and trans-gill water exchange [259]. This shows the usefulness of oxygen isotope composition of phosphatic skeletons of marine animals for direct reconstruction of ancient water temperatures and chemistry.

Despite the facts mentioned above, the carbonate tooth phase of marine cetaceans, being air-breathers, and the phosphatic tooth phase of semiaquatic crocodylians show up to 2‰ $\delta^{18}\text{O}$ value enrichments, which might be related to metabolic factors [260,261]. Similar isotope enrichment is suggested for tooth phosphate of Mesozoic ichthyosaurs as their oxygen isotope ratios are shifted from the predicted range of values for endothermic animals [118]. Interestingly, the study of intra-tooth record in enamel $\delta^{18}\text{O}$ values of an Upper Jurassic ichthyosaur has shown an ontogenic increase (by ~2‰), which may be related to long-distance migrations of these animals [79]. The migration effects may, thus, be responsible for the observed offsets of bulk tooth $\delta^{18}\text{O}$ values of actively swimming marine animals from the equilibrium values expected for a local basin, where they were caught or their remains were found. In addition, unusually high $\delta^{18}\text{O}$ values of tooth enamel of specialised Jurassic and Cretaceous lungfishes, which lived in both marine and freshwater environments and were able to use gas bladder in hypoxic environment, e.g., in isolated lagoons, may ambiguously be linked either to specific water chemistry or metabolic factors related to episodes of strongly limited water exchange through gills and skin (cf. [79,262]). It is of importance as the remains of diadromous fishes may be found in marginal sea environments.

5. Oxygen Isotope Composition of Seawater and Habitat Depth

Palaeotemperatures based on the oxygen isotope composition of marine carbonates can be calculated only if a certain value of the ancient water oxygen isotope ratio is assumed. A global, average $\delta^{18}\text{O}_{\text{seawater}}$ value of -1‰ SMOW, as characteristic of the non-glacial Earth, is traditionally used in calculations of oxygen isotope temperatures for greenhouse periods of Earth history [160]. The $\delta^{18}\text{O}_{\text{seawater}}$ value increased during glaciation periods and its estimated relationship with the glacially induced sea-level changes is implied to be $0.010 \pm 0.001\text{‰ m}^{-1}$ [263]. Therefore, changes in both temperatures and ice volume are recorded in many isotope datasets, e.g., the Cenozoic foraminiferal $\delta^{18}\text{O}$ trends [264,265], which also co-vary with glaciostatic sea-level changes [266].

The assumption of a uniform, global $\delta^{18}\text{O}_{\text{seawater}}$ value is a vast simplification. This is because of significant spatial and temporal variability of oxygen isotope composition and salinity of surface ocean layer and water of marginal seas, both of which are dependent on evaporation rate and freshwater flux. In addition, the use of estimated average greenhouse $\delta^{18}\text{O}_{\text{seawater}}$ value, based on modern isotope models, is controversial for the early Palaeozoic because of the postulated long-term drift of seawater oxygen isotope composition (cf. [26–28]). An assumption of the water $\delta^{18}\text{O}$ value for a particular ancient basin, water depth and location possesses, therefore, a major difficulty that often cannot be solved in a reliable way. This translates into significant uncertainty of palaeotemperature estimates.

Deep water masses of modern oceans have relatively uniform $\delta^{18}\text{O}$ values, oscillating between -0.6‰ VSMOW in a case of Antarctic Bottom Water (AABW) and 0.1‰ VSMOW in a case of North Atlantic Deep Water (NADW; [267,268]). $\delta^{18}\text{O}$ values of surface waters of modern oceans vary considerably (Figure 10; [269,270]). Evaporation of seawater in subtropical regions, including restricted Red and Mediterranean Seas, induces up to ca. 2‰ increase in water $\delta^{18}\text{O}$ value. Significant negative shifts in $\delta^{18}\text{O}$ values (up to -4‰ VSMOW), well-visible in high latitudes of the northern hemisphere, arise because of freshwater input (Figure 10). Even larger ^{18}O depletions are noted in the proximity of the mouths of big rivers and in the restricted high latitude basins, such as the Baltic Sea (cf. [271]). This is because of low air temperatures and long-distance transport of moisture, which render low $\delta^{18}\text{O}$ values of high-latitude precipitation according to a Rayleigh distillation process, e.g., mean $\delta^{18}\text{O}_{\text{precipitation}}$ value, which is fairly constant (ca. -5‰ VSMOW) at the sea surface in the low ($0\text{--}40^\circ$) latitudes, gradually decreases down to ca. -25‰ VSMOW at 80° latitude (cf. [272–275]). For this reason, a distinct decline in seawater $\delta^{18}\text{O}$ values towards the poles is observed above 40°N and 40°S (Figure 10). Distinct negative shifts in $\delta^{18}\text{O}$ values of surface waters in high-latitude regions are also predicted in the mid-Cretaceous and Early Paleogene ocean water circulation models

([276,277]). The same applies to modelled decreases in salinity of Middle Jurassic high latitude basins [278].

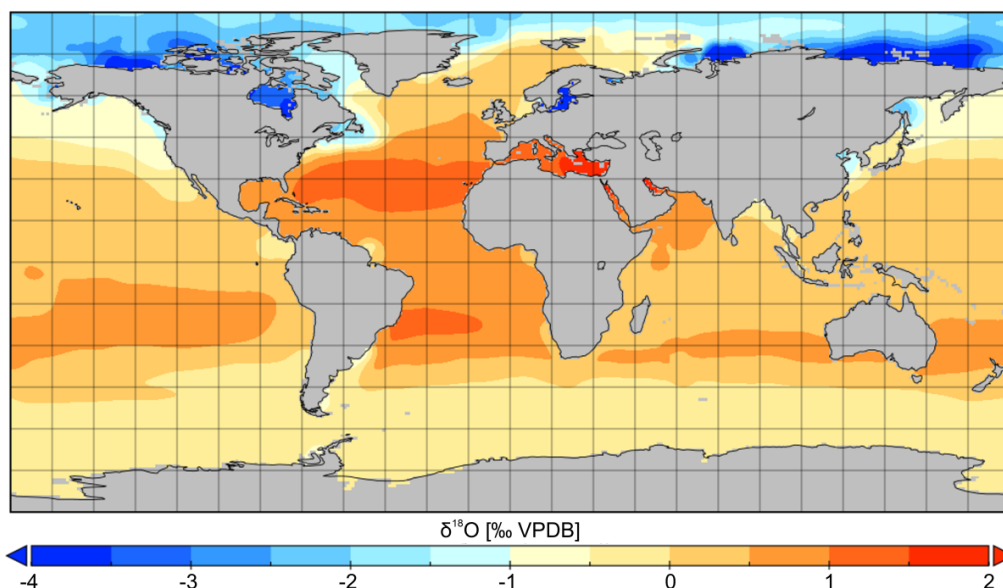


Figure 10. Gridded dataset of surface water $\delta^{18}\text{O}$ values of modern oceans (after Schmidt et al. [269] and LeGrande and Schmidt [270]).

A universal model of the relationship between salinity (S) and water $\delta^{18}\text{O}$ values, which may be helpful in oxygen isotope studies, has been presented by Railsback et al. [279]. It is based on modern observations of the existence of the two general linear dependences consisting of the low salinity trend (13), whose slope is determined by the freshwater runoff, and the high salinity trend (14) determined by evaporation.

$$\delta^{18}\text{O} (\text{‰ VSMOW}) = \delta^{18}\text{O}_0 + \Delta f_w / S_0 \times (S - S_0) \quad (13)$$

where $\delta^{18}\text{O}_0$ is the mean oxygen isotope composition of seawater, Δf_w is the difference between mean seawater $\delta^{18}\text{O}$ value and the value of local freshwater flux, and S_0 is mean seawater salinity.

$$\delta^{18}\text{O} (\text{‰ VSMOW}) = \delta^{18}\text{O}_0 + m_e \times (S - S_0) \quad (14)$$

where m_e is the evaporative enrichment parameter and other symbols are the same as in Equation (13).

The inflection point that divides both trends lies nowadays at slightly higher salinity and $\delta^{18}\text{O}$ value than the global average (34.7 ppt and 0.5‰ VSMOW) due to the presence of deep-water masses of decreased salinity, which originate in Polar regions, but it may have been located at mean salinity and $\delta^{18}\text{O}$ value in the past (34.0 ppt and -1.0‰ VSMOW) due to the presence of dense, saline bottom waters during greenhouse periods [279]. A 0.35‰/ppt value of the evaporative enrichment parameter (m_e), used in the model, is applied by analogy to the modern Mediterranean Sea and Red Sea. On the other hand, the 10‰ difference between mean seawater $\delta^{18}\text{O}$ value and the value of local freshwater flux (Δf_w) may be assumed for some Ordovician and Cretaceous basins [279–281]. Similarly, 8‰ difference is assumed for Late Jurassic basins of central Poland and the Russian Platform [253,282]. The latter parameter should, however, be taken individually depending on latitude and climate mode, e.g., the mean $\delta^{18}\text{O}$ value of freshwater flux decreases down to ca. 21‰ VSMOW in modern high latitude regions [279].

Another approach, used by Zachos et al. [283], is a direct calibration of oxygen isotope ratios of Cenozoic foraminifera from open oceanic drilling sites to the present-day distribution of sea surface $\delta^{18}\text{O}$ values from the southern hemisphere, which shows harmonized

spatial, isotope trends. The relationship (15) presented by Zachos et al. [283] is based on available seawater $\delta^{18}\text{O}$ data for the latitudes between 0 and 70°S.

$$\delta^{18}\text{O} (\text{‰ VSMOW}) = 0.576 + 0.041x - 0.0017x^2 + 1.35 \times 10^{-5}x \quad (15)$$

where x is the absolute latitudes in degrees.

Significant variations in salinity and water $\delta^{18}\text{O}$ values occurring in shallow coastal areas and restricted marginal seas are of special interest to geochemists who deal with Palaeozoic and Mesozoic data because of the lack of nearly all deep-sea sediments associated with oceanic crust older than 180 Ma (cf. [284]). Several studies of carbonate and phosphate fossils from ancient, epicontinental basins have shown low and variable $\delta^{18}\text{O}$ values linked to local freshwater input and, in a few cases, enhanced evaporation occurring in subtropical basins (cf. [80,145,146,253,285–289]).

Major decreases in salinity and water $\delta^{18}\text{O}$ values can be manifested by a retreat of stenohaline organisms (e.g., echinoderms and brachiopods), sedimentological and geochemical proxies (including correlation between $\delta^{18}\text{O}$ variations and sea-level changes or shell $^{87}\text{Sr}/^{86}\text{Sr}$ ratios, a significant co-variance between shell $\delta^{18}\text{O}$ and $\delta^{13}\text{C}$ values or a loss of the relationship between $\delta^{18}\text{O}$ values and Mg/Ca ratios of some biogenic calcites, cf. [20,80,145,146,253,282,288–292]) but minor salinity fluctuations are difficult to trace. They can be found using independent palaeotemperature tracers such as the clumped isotope composition of carbonate fossils (see next section and reference therein) or organic geochemical indices (cf. [290,291,293–297]), both of which are, however, often not available. The reconstruction of circulation changes and mixing of water masses in epeiric basins is also complicated. Inferences in this matter can be made based on sets of palaeogeographical reconstructions, analysis of faunistic migrations or neodymium isotope ratios (cf. [253,282,298–301]).

Thermal gradient in the water column and the effect of temporal bathymetry changes on temperatures recorded in skeletons of benthic and necto-benthic organisms as well as specific thermal regimes of epeiric sea basins are another problem that should be carefully considered. Temperatures of the mixed layer of the water column (usually above 50 m) are relatively uniform but show seasonal changes. They drop suddenly in the thermocline layer, located below (Figure 11; [302]). Temperatures of surface waters of restricted, shallow epicontinental basins located in the middle and low latitudes tend to be consistently higher and seasonally more variable than those of open oceanic basins [303]. Temporal bathymetry variations or variations of thermal regime of particular basins, related to water circulation, can significantly affect carbonate and phosphate $\delta^{18}\text{O}$ records. Such variations may be confused with climatic oscillations in certain cases, causing heterogeneity of palaeoclimatic data. Preferential analyses of samples derived from restricted, epeiric seas can also be a source of a long-term increase in temperatures estimated for ancient geological periods [303]. The determination of local effects of palaeobathymetry and palaeocirculation changes on water temperatures is often possible based on careful sedimentological and palaeogeographical examinations.

An example of such analysis is discussion of the sources of $\delta^{18}\text{O}$ variations observed in the stratigraphically well-constrained uppermost Callovian–mid-Kimmeridgian (Middle–Upper Jurassic) oxygen isotope dataset of benthic (brachiopod and bivalve shells) and necto-benthic (belemnite rostra) calcitic fossils from central Poland ([58,79]; Figure 12). All of the studied fossils are assumed to have been precipitated in the oxygen isotope equilibrium.

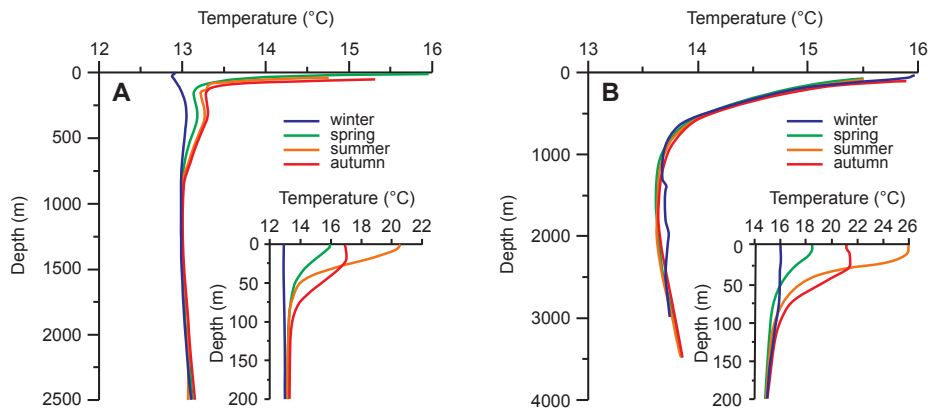


Figure 11. Seasonally averaged vertical profiles of water temperatures for (A) the Gulf of Lion in the western Mediterranean, and (B) the southern part of the Ionian Sea in the eastern Mediterranean (after Manca et al. [302], modified). The Mediterranean Sea is devoid of cold, bottom waters of Polar origin, and may be an analogy to ancient, epicontinental seas.

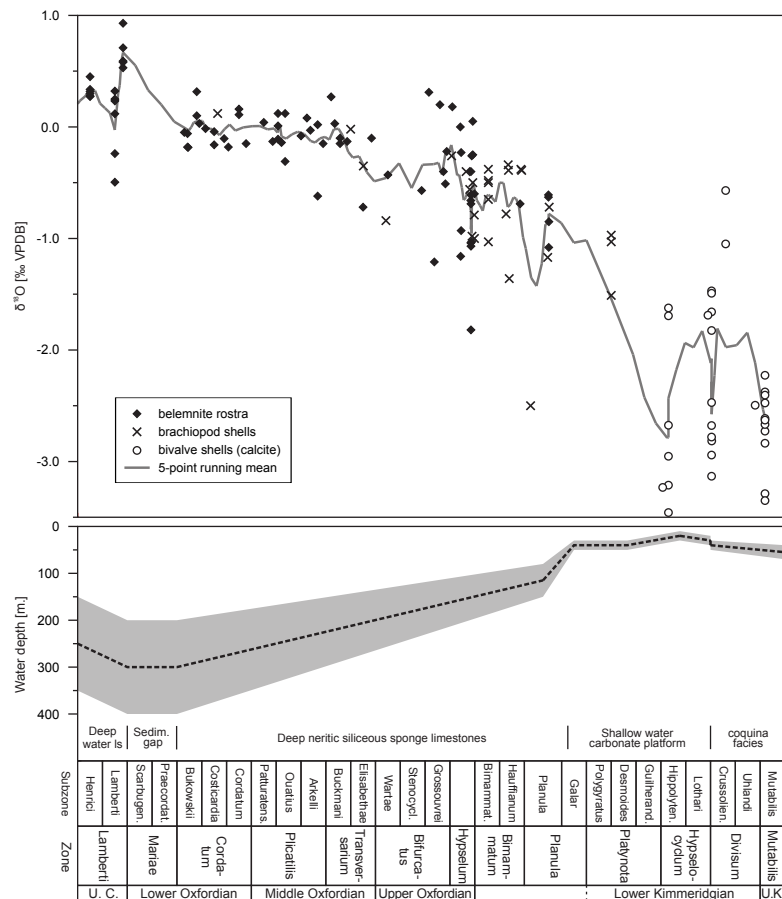


Figure 12. $\delta^{18}\text{O}$ record of uppermost Callovian–mid-Kimmeridgian (Middle–Upper Jurassic) belemnite rostra and brachiopod and bivalve (oyster, *Trichites*) shells (after Wierzbowski [58,79,108] and Wierzbowski et al. [304]) along with palaeobathymetry and sedimentary changes in the mid-Polish basin (the Polish Jura Chain and the SW margin of the Holy Cross Mountains; after Matyja nad Wierzbowski [305], Pisera [306], Wierzbowski et al. [307], Wierzbowski et al. [304], Matyja [308] and Wierzbowski [79,309,310]). The temporal oxygen isotope record is significantly affected by bathymetry variations, which induced a gradual increase in bottom temperatures and palaeocirculation and palaeogeography of the basin, which were responsible for salinity variations. A rapid salinity decrease likely occurred in the mid-Kimmeridgian.

A major, Oxfordian–Kimmeridgian drop in the $\delta^{18}\text{O}$ values (of ca. 2.5‰) of well-preserved fossils corresponds to gradual shallowing of the mid-Polish basin manifested by replacement of deep-water facies by shallow-water facies and final restriction of the sea area (cf. [58,79,308–311]). The palaeo-oceanographic factors probably induced bottom water warming and water circulation changes responsible for a pronounced decrease in water salinity. The main turning points in the depositional history of the basin include Middle–Late Callovian sea-level rise culminating into a maximal flooding surface visible as a sedimentary gap at the Callovian–Oxfordian boundary [304,311]. Deep-water, nertic sponge biofacies occurred in the mid-Polish basin during the Oxfordian. The sponge biofacies likely developed at the water depth of at least 100–300 m in the area of the Polish Jura Chain. This is deduced from a lack of hermatypic corals and a pronounced bottom relief of ca. 200 m between cyanobacteria-sponge bioherms and lowered interbiohermal areas [305,306]. At the end of the Planula Chron of the Early Kimmeridgian, the tops of cyanobacteria-sponge bioherms in the Polish Jura Chain were settled by hermatypic corals, which usually grow in the upper part of the photic zone (down to 40 m depth; [305,307]). The interbiohermal zones of the Polish Jura Chain and its margins were filled at the same time with micritic limestones of high thickness, which preceded the appearance of shallow water carbonate deposits [310]. A careful examination of sedimentological and faunistic data reveal, however, subtle signs of the shallowing already at the end of the interval of the dominance of deep-water facies, i.e., significant acceleration of the carbonate production in the study area and a gradual retreat of deep-water cephalopod fauna (cf. [58,108,305,312]). The Lower Kimmeridgian of central Poland is marked by the occurrence of shallow water oolitic and chalky limestones, deposited above fair-weather and storm wave bases, with maximal regression surface of the lowstand system tract dated to the middle part of the Hypselocyclus Zone [79,308–310]. The extremely shallow Lower Kimmeridgian facies are overlain by moderately shallow marly-limestone deposits of the Lower–Upper Kimmeridgian boundary with common condensations and bivalve coquinas, which bear a slightly transgressive character [79,308–310].

A pronounced increase in bottom water temperatures and a salinity drop are likely responsible for a marked decrease in $\delta^{18}\text{O}$ values (of ca. 2.5‰) noted in the Upper Oxfordian–Lower Kimmeridgian (Figure 12). The shallowing occurred after the global Late Callovian–Early Oxfordian sea level highstand (cf. [313,314]) typical of many areas. It may explain numerous, coeval negative $\delta^{18}\text{O}$ shifts recorded in various basins of Europe, including the Anglo-Paris basin, Russian Platform, Scotland and Western Carpathians [55,59,120,315–317]. The oxygen isotope data from epeiric European basins probably contributed to the major negative Upper Oxfordian–Lower Kimmeridgian $\delta^{18}\text{O}$ shift visible in the compilation of the Jurassic oxygen isotope data of Dera et al. [318]. Interestingly, no decrease in $\delta^{18}\text{O}$ values is observed in coeval datasets from the southern hemisphere [56,57,245,319]. In addition, the newly obtained TEX₈₆ biomarker and clumped isotope records of the Falkland Plateau, Russian Platform and Scotland point to constant seawater temperatures during the Late Jurassic and the stable Earth climate of that period [253–255,320].

6. Precise Sampling Methods

6.1. Microsampling Techniques

Precise mechanical microsampling by means of mini scalpels or microdrills, though time-consuming, has great potential for reconstruction of seasonal, annual or ontogenic oxygen isotope variations of macrofossils. It can be used for the determination of seasonality of ancient climates and palaeoenvironmental settings, assessment of the shell growth rate, and migration patterns as well as changeable intensity of vital effects, which are dependent on the metabolic activity of animals. The resolution of microsampling depends on the size and shape of studied fossils and the used technical methods. In the case of carbonate macrofossils, good resolution of sampling (50–100 μm distance for each sampling interval) can be obtained using computer micromill devices (cf. [217,218,256,321–323]).

High-resolution oxygen isotope profiles across modern shallow-water oyster shells, built of low-Mg calcite, have substantiated near equilibrium precipitation of oxygen isotopes in their skeletons and annual cyclicity of the $\delta^{18}\text{O}$ values related to seasonal changes in water temperature and salinity (cf. [165–170]). In addition, cessation lines of the growth of oyster shells can be linked, using precise microsampling, to periods of high summer temperatures and low winter temperatures. Minor negative deviations (up to -0.8‰) from equilibrium values were, nevertheless, observed in some cold month increments of modern shallow-water oysters [167]. Elevated and scattered $\delta^{18}\text{O}$ values of modern deep-water oysters, which are shown to be ca. 0.5‰ higher than the equilibrium oxygen isotope values, are, on the other hand, interpreted as a result of extremely slow precipitation rates in specific, bathyal conditions ([256]; see also discussion in Section 4.1. Calcareous skeletons).

Other examples of the reconstruction of life style and vital effects of organisms based on microsampling are studies of internal variability of $\delta^{18}\text{O}$ values of calcitic belemnite rostra. Previous studies based on coarse sampling methods and specimens not screened for diagenetic alteration showed significant variability of belemnite $\delta^{18}\text{O}$ values, which, despite the efforts made, could not have been explained by primary, palaeoenvironmental or metabolic factors (cf. [3,324]). High resolution microsampling of well-preserved belemnopseid belemnite rostra has, however, shown little variability of $\delta^{18}\text{O}$ values interpreted as a result of deeper, demersal habit of these organism, which lived below the surface mixing zone at relatively constant water temperatures (cf. [78,321,325]; see also Figure 13). Little internal variability of belemnite $\delta^{18}\text{O}$ values may also arise because of their short life span, which is deduced to be, generally, less than 1 year, as based on counting of daily growth rings of the rostra (cf. [326]). Simultaneous, high-amplitude intra-rostral $\delta^{13}\text{C}$ variations (Figure 13) likely arise because of varying intensity of internal metabolic processes [322]. They are similar to large (up to 3‰) internal carbon isotope variations reported from cuttlebones of wild and cultured *Sepia officinalis*, being a close relative of extinct belemnites [327]. Particularly, the modern *Sepia officinalis*' cuttlebone is found to be precipitated in approximate oxygen isotope equilibrium with ambient water [327,328], as suggested for rostra of extinct belemnopseid belemnites.

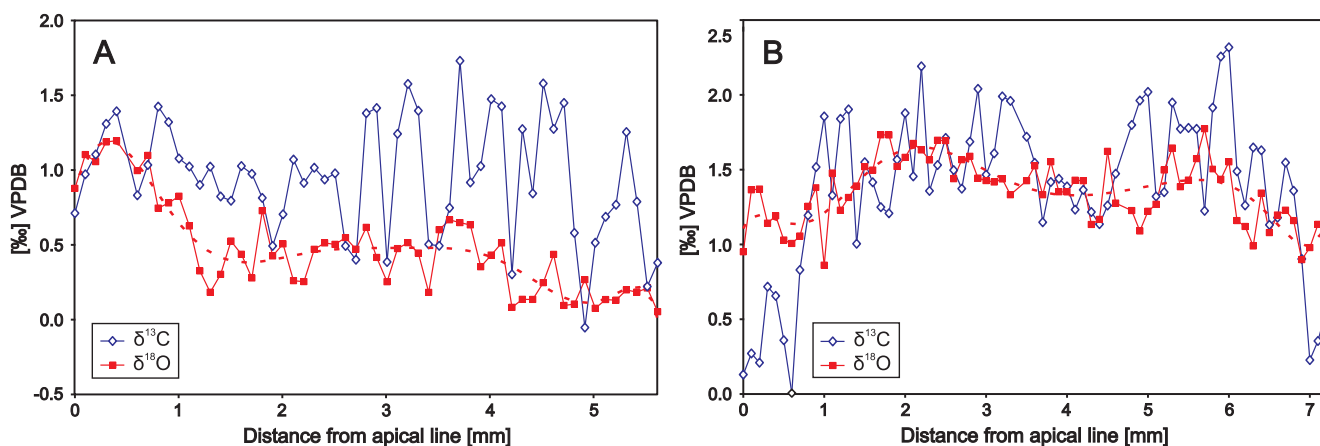


Figure 13. Ontogenetic $\delta^{18}\text{O}$ trends throughout the Lower Bathonian (Middle Jurassic) belemnite rostra: (A) *Hibolithes beyrichi* and (B) *Hibolithes hastatus* from central Poland. Average $\delta^{18}\text{O}$ trends are shown (reproduced with permission from Wierzbowski and Joachimski [322] “Stable isotopes, elemental distribution, and growth rings of belemnopseid belemnite rostra: proxies for belemnite life habitat”. Palaios, 2009, v. 24, p. 377–386. Copyright SEPM 2021).

6.2. Ion Microprobe

The highest resolution of oxygen isotope sampling of skeletal carbonates and phosphates can be obtained using the secondary ion mass spectrometry (SIMPS) method. Basic ion microprobe studies based on $10\text{--}20\ \mu\text{m}$ spot analyses have allowed determination of internal variability of oxygen isotope ratios of small macrofossils and selected microfossils such as small vertebrate teeth, fish otoliths, conodont elements or large foraminifera tests (cf. [41,88,130,329–332]). More accurate sampling, characterized by a few micrometre

spots at reasonable precision of isotope measurements, may be obtained using modern, multi-collector ion microprobes of high mass resolution (cf. [333–336]). The new nanoSIMS devices additionally enable nanometre scale imaging of the distribution of the oxygen isotope ratio in selected areas of microsamples (cf. [94,337]).

The results of ion microprobe analyses of the oxygen isotope ratio are affected by the instrumental mass fractionation occurring during the sputtering, transmission, and detection of secondary ions [330,338]. Therefore, homogenous standards of the same chemical composition and crystal structure as the studied samples should be used to calibrate the results and obtain highly accurate oxygen isotope analyses. Unfortunately, a source of observable bias can be the referencing of oxygen isotope ratios of biogenic carbonates or phosphates to those of inorganic calcites or apatites used as microprobe standards. This is due to the potential admixture of foreign ions derived from organic or inorganic impurities in biogenic samples, differences in their crystallinity and the presence of crystal-lattice distortions.

A negative offset of ca. 0.5‰ and 1.0‰, between biogenic aragonite and calcite samples, respectively, measured using the SIMS method and traditional gas isotope ratio mass spectrometry (GIRS) of bulk CO₂ derived from acid digestion of carbonates has been observed [335,336,339,340]. It is related to the admixture of water or organic matter molecules evidenced by negative correlation between measured $\delta^{18}\text{O}$ values and OH/O ratio of biogenic carbonates [336,339]. A significant effect of minor element concentrations in carbonates on SIMS analyses also has been demonstrated [341]. On the other hand, there is no agreement on instrumental bias of measured oxygen isotope ratios of marine apatite fossils (crown tissue of conodont elements and enameloid of shark teeth) by means of the SIMS and GIRS methods. Some of the data show no systematic instrumental bias [130,342], the other positive 0.6‰ offset in SIMS $\delta^{18}\text{O}$ values [129]. The observed instrumental bias may, however, be related to remnants of body tissue in bulk conodont elements analysed using the GIRS method (cf. [129]) or position-specific isotope fractionation in biogenic apatites revealed at certain instrument settings of an ion microprobe [343]. The lack of significant instrumental bias in some conodont or fish teeth $\delta^{18}\text{O}$ values, measured using SIMPS, may be related to relatively low content of carbonate and hydroxy groups in fluorapatites (cf. [344]). For instance, the carbonate content of ca. 1.8 wt.%, and <2.5 wt.% has been reported for crown tissue of conodont elements and enameloid layer of modern shark teeth, respectively [345,346]. In addition, significant reduction of the content of hydroxyl groups in fossil teeth of higher vertebrates is a consequence of ubiquitous transformation of metastable hydroxyapatite into fluorapatite in diagenetic environments (cf. [140–142]). A larger discrepancy between oxygen isotope measurements (up to 1–2‰) of teeth of modern terrestrial mammals, composed of hydroxyapatites, has been observed between the SIMS and GIRS methods [347]. However, oxygen isotope studies of modern or archaeological materials are outside the scope of the present paper.

Ion microprobe studies have revealed a 1–2‰ difference between $\delta^{18}\text{O}$ values of normal portions of planktic foraminiferal tests and those of gametogenic crusts precipitated during the final life stage of ontogenetic development [333,335]. The degree of test encrustation should, therefore, be taken into account while interpreting foraminiferal oxygen isotope values. The same method has been used to show submicrometer or micron-scale diagenetic alteration of calcitic tests of planktic foraminifera and to demonstrate that reliable oxygen isotope signals may still be preserved in their internal parts [88,94]. The ion microprobe analysis has been also used to show detailed thermal evolution of Palaeozoic and Triassic seas, based on $\delta^{18}\text{O}$ values of single, well-preserved conodont elements [342,344]. It has also demonstrated a significant internal and taxonomical variability of conodont $\delta^{18}\text{O}$ values, which can be assigned to differences in the life-styles of various conodont taxa [130,332,348].

The ca. 2‰ ontogenetic increase in $\delta^{18}\text{O}$ values of the enamel layer of Upper Jurassic ichthyosaur teeth from central Poland, determined using the ion microprobe method, is predominantly linked to long-distance migrations of these reptiles, but the effect of

changing metabolic factors cannot be completely excluded ([41]; Figure 14). The studies of the ontogenetic record of enamel(oid) layer of fossil teeth opens a potential, new way for studies of animal migrations and determination of water $\delta^{18}\text{O}$ value as based on the assumption that oxygen isotope composition of the latest ontogenetic stage of endothermic marine creatures was precipitated in local settings of a sedimentary basin at isotope equilibrium arising from the constant body temperature.

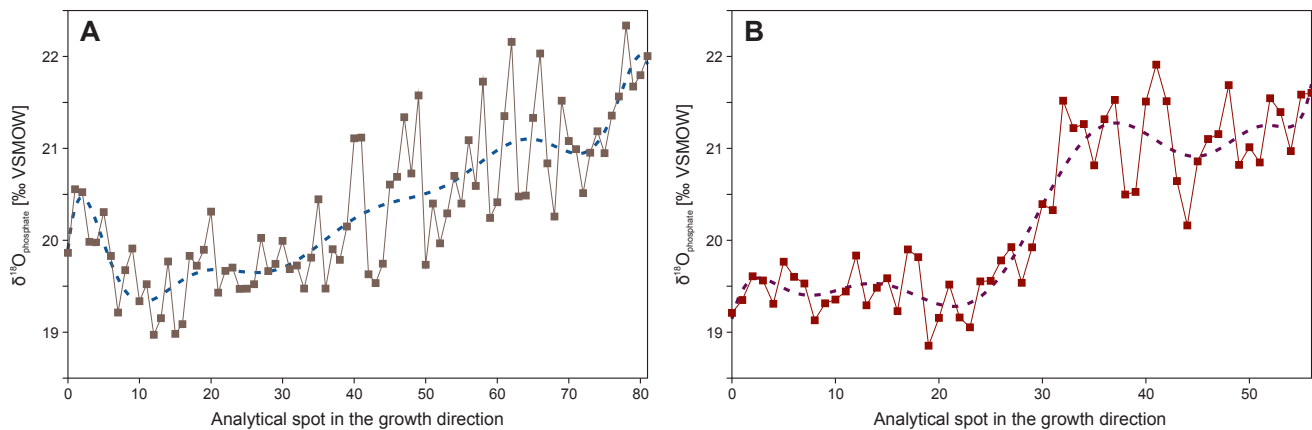


Figure 14. Ontogenetic $\delta^{18}\text{O}$ trends throughout the enamel layer of two teeth (samples (A) and (B)) of mid-Tithonian (Upper Jurassic) ichthyosaur (*Cryptopterygius kielanae*) from central Poland. Early portion of the enamel is characterized by low $\delta^{18}\text{O}$ values ($\sim 19.4\%$ VSMOW), and ontogenetic increases to $\sim 21.9\%$ and $\sim 21.4\%$ VSMOW in samples A and B, respectively, are observed. Average $\delta^{18}\text{O}$ trends are shown (reproduced with permission from Wierzbowski et al. [41]. “Oxygen isotope profiles of uppermost Jurassic vertebrate teeth and oyster shells: a record of paleoenvironmental changes and animal habitats”. *Palaios*, 2019, v. 34, p. 585–599. Copyright SEPM 2021).

7. Clumped Isotopes

The new, clumped isotope method is based on the analysis of relative abundances of mass 47 isotopologues (primarily $^{13}\text{C}^{18}\text{O}^{16}\text{O}$) in the carbonate (calcite or aragonite) mineral lattice (measured actually in acid-liberated CO_2) that are dependent on the precipitation temperature. Unlike the classical oxygen isotope method, clumped isotope palaeothermometry is independent of the composition of ambient water. It makes possible solving the basic problem of the uncertainty of temperature calculations related to unknown oxygen isotope composition of ancient water [349,350]. Although very promising, the clumped isotope palaeothermometry of carbonates is limited by the susceptibility of the clumped isotope composition to diagenetic alteration (cf. [351–353]), sophisticated and expensive analytical techniques (cf. [354]), gradually evolving temperature calibrations and normalization procedures as well as the still considerable uncertainty of a single Δ_{47} measurement (cf. [355–368]).

The solid-state re-ordering of C-O bonds can affect carbonate Δ_{47} values without visible microstructure or chemical changes. Passey and Henkes [351] and Henkes et al. [352] have demonstrated that partial re-ordering of C-O bonds in calcite occurs starting from the temperature range of 100–120 °C. Modelling by Stolper and Eiler [353] suggests, however, that prolonged exposure of calcites to burial temperatures of 80–100 °C may induce small shifts in their Δ_{47} values owing to a slow rate of diffusion and internal exchange reactions. The clumped isotope composition of aragonite is more susceptible to C-O bond re-ordering, and aragonite Δ_{47} values were significantly modified during heating at 100 °C [369,370]. However, clumped isotope composition of some fossils such as benthic foraminifera is shown to be relatively resistant to diagenetic alteration during shallow burial diagenesis at the sea floor [371].

The possibility of carbonate bond re-ordering related to thermal alteration of deposits imposes a more complex approach to screening of diagenetic processes before conducting clumped isotope analyses. Such investigations should be based not only on

the well-established, physical and chemical screening methods of carbonates (see Section 2. Diagenetic alteration) but also on the evaluation of thermal alteration and/or burial history of sediments. One should notice that the determination of thermal alteration using common organic matter indices cannot be applied in many cases, e.g., because of the scarcity of organic matter in some deposits. In addition, the maturation process of kerogen, which can be traced using vitrinite reflectance or Rock-Eval pyrolysis, starts below 100 °C only in a case of the most reactive kerogen IIS/II types (cf. [127,372]). The biomarker data substantiating low thermal degradation of organic matter can be helpful, if available, for studied deposits and localities (cf. [253,254]). A different, more or less reliable approach is used by some authors, e.g., Finnegan et al. [373] and Petersen et al. [374] studied primary and diagenetic mineral phases to show that the former are not equilibrated with diagenetic fluids, Dennis et al. [287] claim that a lack of the relationship between their Δ_{47} values and both the microstructure preservation and diagenetic Sr content of aragonite fossils is evidence against burial diagenesis of sediments, and Vickers et al. [254] use mapping of trace element content and crystallographic axis analyses to substantiate that studied belemnite rostra are well-preserved, independently from the evaluation of the burial history of sediments. On the other hand, Henkes et al. [32] use a C-O bond re-ordering model to distinguish between unaffected and re-ordered brachiopod Δ_{47} values for certain locations characterized by different burial temperatures.

Despite the common equilibrium precipitation of clumped isotopes in biogenic calcites and aragonites, kinetic effects, which induce Δ_{47} offsets, are observed or suggested in cold water benthic and planktic foraminifera [355,357], rapidly growing hermatypic corals [375,376], deep-water corals [359,377], and temperate- to cold-water brachiopods characterized by fast growth rates [234]. Bajnai et al. [367] have shown that dual analyses of carbonate Δ_{47} and Δ_{48} values allow identification of biomineral phases (e.g., corals) affected by kinetic fractionation of clumped isotopes and, in some cases, retrieval of the original palaeotemperature signal.

An increasing number of clumped isotope studies based on well-preserved carbonate fossils of the Palaeozoic to Paleogene age has been published. The clumped isotope method is employed for the calculation of water temperatures, their temporal evolution, the reconstruction of ancient water $\delta^{18}\text{O}$ value, its salinity, latitudinal temperature gradients and temporal temperature variations (cf. [32,253–255,287,371,373,374,378–381]). Although more Δ_{47} data are necessary to document long-term variations in the Earth climate and some of the older data need re-calculation due to changes in laboratory procedures or accepted temperature equations, some of the results are remarkable. For example, the study of clumped isotope composition of exceptionally well-preserved uppermost Middle–Upper Jurassic belemnite rostra and ammonite shells from the Russian Platform has shown relatively stable water temperatures and a decrease in salinity of the restricted Middle Russian Sea during the Late Oxfordian–Early Kimmeridgian as a result of a sea-level fall and progressive isolation of this basin ([253]; Figure 15). The clumped isotope data are in line with increasing provincialism of cephalopod faunas in the area of the Russian Platform during the Oxfordian–Kimmeridgian transition and gradual retreat of deep-water ostracod and planktic foraminifera (cf. [253,382–386]). The clumped isotope data contradict earlier theories of global cooling at the Middle–Late Jurassic transition and subsequent warming, which were largely documented based on Russian belemnite $\delta^{18}\text{O}$ data (cf. [315,316,387]). They also show relative stability of the latest Middle–Late climate and point to the dominant effect of palaeo-oceanographic changes in the carbonate $\delta^{18}\text{O}$ record of shallow, epicontinental sea basins of northern Europe.

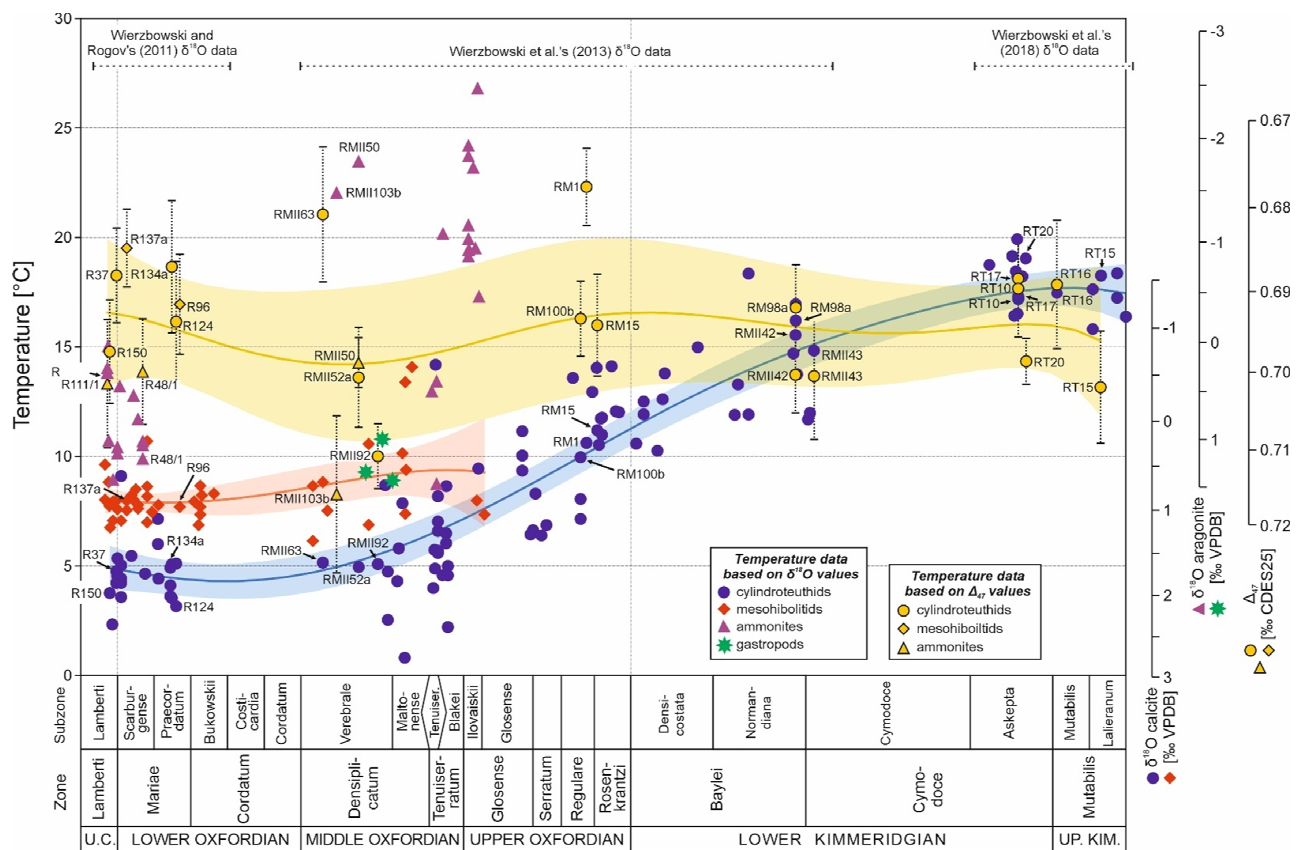


Figure 15. Isotope data and palaeotemperatures calculated from $\delta^{18}\text{O}$ and Δ_{47} (CDES 25) values of well-preserved calcareous fossils from the uppermost Callovian–lowermost Upper Kimmeridgian (Middle–Upper Jurassic) of the Russian Platform (after Wierzbowski et al. [253]). The oxygen isotope temperatures are calculated using the equations of Friedman and O’Neil [150] and Böhm et al. [158] for calcite and aragonite fossils, respectively, assuming $\delta^{18}\text{O}_{\text{water}}$ value of -1‰ VSMOW. The clumped isotope temperatures are calculated using the equation of Wacker et al. [361]. Temperature data points derived from $\delta^{18}\text{O}$ and Δ_{47} (CDES 25) values of the same samples are marked with sample numbers. Smoothed curves and corresponding 95% confidence intervals (blue, red, and yellow areas) are generated using a locally weighted second order polynomial regression with a bandwidth of 5 stratigraphical units, i.e., ca. 0.3 Myr. The $\delta^{18}\text{O}$ data were compiled from Wierzbowski and Rogov [388], Wierzbowski et al. [55] and Wierzbowski et al. [253]—see marked data ranges.

8. Conclusions

In this study are discussed proven procedures of palaeoenvironmental analysis based on oxygen isotope composition of skeletal calcium carbonate and calcium phosphate as well as major methodological difficulties associated with the selection of the well-preserved fossils and retrieval of the original oxygen isotope signal. The discussed, most reliable, reasoning methods could be used for reconstruction of ancient water salinity and calculation of the palaeotemperature of ancient marine basins.

Different techniques for screening the preservation state of skeletal carbonate and phosphates were reviewed with an emphasis on standardised chemical procedures based on minor and trace elemental proxies, which could be used in the case of carbonate and phosphate macrofossils, or determination of the microstructure preservation of microfossils. The published oxygen isotope temperature equations were compiled to show their differences and applicability to various fossils. The same applied to mathematical corrections, which were necessary for some equations due to later modifications in instrumental or experimental settings compared to those used during their formulation. Special attention was given to various vital and habitat effects, which may affect the oxygen isotope values of particular fossils, generating $\delta^{18}\text{O}$ offsets from expected isotope equilibrium. In particular, high $\delta^{18}\text{O}$ values of belemnite rostra were interpreted as reflecting different states

of oxygen isotope equilibrium closer to that of slowly precipitated inorganic calcite. The effect of palaeoceanographic factors, such as variations in water salinity and bathymetry, on the oxygen isotope record of shallow marine basins was additionally demonstrated. They could be analysed using sedimentological and faunistic data. The study was also devoted to the applicability of novel analytical methods such as microsampling (including ion microprobe analysis) and clumped isotope thermometry. They can be used for analysis of primary high-resolution seasonal and ontogenic variations of oxygen isotope ratios or water salinity changes and measurements of absolute temperatures of precipitation of biogenic carbonates.

Supplementary Materials: The following are available online at <https://www.mdpi.com/article/10.3390/geosciences11100419/s1>, Table S1: Carbonate temperature calculator; Table S2: Phosphate temperature calculator; List S1: Carbonate temperature calculator_notes; List S2: Phosphate temperature calculator_notes.

Funding: The study was supported by the PGI-NRI statutory funds (Project No. 62.9012.2032.00.0).

Institutional Review Board Statement: Not applicable.

Informed Consent Statement: Not applicable.

Data Availability Statement: Not applicable.

Acknowledgments: Zofia Dubicka is thanked for providing photos of foraminiferal microstructure shown in Figure 1, and Gregory Price for providing the original version of the diagram with Mesozoic-Cenozoic $\delta^{18}\text{O}$ trends depicted in Figure 9. Two anonymous reviewers are acknowledged for comments and suggested improvements.

Conflicts of Interest: The author declares no conflict of interest. The funder had no role in the design of the study, interpretation of data, writing of the manuscript, or in the decision to publish the results.

References

1. Urey, H.C. The thermodynamic properties of isotopic substances. *J. Chem. Soc.* **1947**, 562–581. [[CrossRef](#)]
2. McCrea, J.M. On the isotopic chemistry of carbonates and a paleotemperature scale. *J. Chem. Phys.* **1950**, *18*, 849–857. [[CrossRef](#)]
3. Urey, H.C.; Lowenstam, H.A.; Epstein, S.; McKinney, C.R. Measurement of paleotemperatures and temperatures of the upper cretaceous of England, Denmark, and the southeastern United States. *GSA Bull.* **1951**, *62*, 399–416. [[CrossRef](#)]
4. Epstein, S.; Buchsbaum, R.; Lowenstam, H.; Urey, H.C. Carbonate-water isotopic temperature scale. *GSA Bull.* **1951**, *62*, 417–425. [[CrossRef](#)]
5. Epstein, S.; Buchsbaum, R.; Lowenstam, H.A.; Urey, H.C. Revised carbonate-water isotopic temperature scale. *GSA Bull.* **1953**, *64*, 1315–1326. [[CrossRef](#)]
6. Longinelli, A.; Nuti, S. Revised phosphate-water isotopic temperature scale. *Earth Planet. Sci. Lett.* **1973**, *19*, 373–376. [[CrossRef](#)]
7. Kolodny, Y.; Luz, B.; Navon, O. Oxygen isotope variations in phosphate of biogenic apatites, I. Fish bone apatite—rechecking the rules of the game. *Earth Planet. Sci. Lett.* **1983**, *64*, 398–404. [[CrossRef](#)]
8. Anderson, T.F.; Arthur, M.A. Stable isotopes of oxygen and carbon and their application to sedimentologic and paleoenvironmental problems. In *Stable Isotopes in Sedimentary Geology: SEPM Short Course No. 10*; Arthur, M.A., Anderson, T.F., Kaplan, I.R., Veizer, J., Land, L.S., Eds.; Society of Economic Paleontologists and Mineralogists: Tulsa, OK, USA, 1983; pp. 1-1–1-151.
9. Veizer, J. Chemical diagenesis of carbonates: Theory and trace element technique. In *Stable Isotopes in Sedimentary Geology, SEPM Short Course No. 10*; Arthur, M.A., Anderson, T.F., Kaplan, I.R., Veizer, J., Land, L.S., Eds.; Society of Economic Paleontologists and Mineralogists: Tulsa, OK, USA, 1983; pp. 3-1–3-100.
10. Marshall, J.D. Climatic and oceanographic isotopic signals from the carbonate rock record and their preservation. *Geol. Mag.* **1992**, *129*, 143–160. [[CrossRef](#)]
11. Kolodny, Y.; Luz, B. Isotope signatures in phosphate deposits: Formation and diagenetic history. In *Isotopic Signatures and Sedimentary Records, Lectures Notes in Earth Sciences 43*; Clauer, N., Chaudhuri, S., Eds.; Springer: Berlin/Heidelberg, Germany, 1992; pp. 69–121.
12. Veizer, J. Depositional and diagenetic history of limestones: Stable and radiogenic isotopes. In *Isotopic Signatures and Sedimentary Records, Lectures Notes in Earth Sciences 43*; Clauer, N., Chaudhuri, S., Eds.; Springer: Berlin/Heidelberg, Germany, 1992; pp. 13–48. [[CrossRef](#)]
13. Kohn, M.J.; Cerling, T.E. Stable isotope composition of biological apatite. In *Phosphates. Reviews in Mineralogy & Geochemistry*; Kohn, M.J., Rakovan, J., Hughes, J.M., Eds.; Mineralogical Society of America, Geochemical Society: Chantilly, VA, USA, 2002; Volume 48, pp. 455–488.

14. Maslin, M.A.; Swann, G.E.A. Isotopes in marine sediments. In *Isotopes in Palaeoenvironmental Research, Developments in Palaeoenvironmental Research*; Leng, M.J., Ed.; Springer: Berlin/Heidelberg, Germany, 2006; Volume 10, pp. 227–290. [[CrossRef](#)]
15. Sharp, Z. *Principles of Stable Isotope Geochemistry*; Pearson Prentice Hall: Hoboken, NJ, USA, 2007; pp. 1–344.
16. Grossman, E.L. Applying oxygen isotope paleothermometry in deep time. In *Reconstructing Earth's Deep-Time Climate—The State of the Art in 2012, Paleontological Society Short Course, November 3, 2012*; Ivany, L.T., Huber, B.T., Eds.; The Paleontological Society: McLean, VA, USA, 2012; Volume 18, pp. 39–68.
17. Grossman, E.L. Oxygen isotope stratigraphy. In *The Geologic Time Scale*; Gradstein, F.M., Ogg, J.G., Schmitz, M., Ogg, G., Eds.; Elsevier: Amsterdam, The Netherlands, 2012; pp. 181–206.
18. Pearson, P.N. Oxygen isotopes in foraminifera: Overview and historical review. In *Reconstructing Earth's Deep-Time Climate—The State of the Art in 2012. Paleontological Society Short Course November 3, 2012. The Paleontological Society Papers*; Ivany, L.C., Huber, B.T., Eds.; The Paleontological Society: McLean, VA, USA, 2012; Volume 18, pp. 1–38.
19. Lea, D.W. Elemental and isotopic proxies of past ocean temperatures. In *Treatise on Geochemistry*, 1st ed.; Holland, H.D., Turekian, K.K., Eds.; Elsevier: Oxford, UK, 2003; Volume 6, pp. 391–432.
20. Lea, D.W. Elemental and isotopic proxies of past ocean temperatures. In *Treatise on Geochemistry*, 2nd ed.; Holland, H.D., Turekian, K.K., Eds.; Elsevier: Oxford, UK, 2014; Volume 8, pp. 373–397.
21. Immenhauser, A.; Schöne, B.R.; Hoffmann, R.; Niedermayr, A. Mollusc and brachiopod skeletal hard parts: Intricate archives of their marine environment. *Sedimentology* **2015**, *63*, 1–59. [[CrossRef](#)]
22. Banner, J.L.; Hanson, G.N. Calculation of simultaneous isotopic and trace element variations during water-rock interaction with applications to carbonate diagenesis. *Geochim. Cosmochim. Acta* **1990**, *54*, 3123–3137. [[CrossRef](#)]
23. Blake, R.; O'Neil, J.; Garcia, G. Oxygen isotope systematics of biologically mediated reactions of phosphate: I. Microbial degradation of organophosphorus compounds. *Geochim. Cosmochim. Acta* **1997**, *61*, 4411–4422. [[CrossRef](#)]
24. Sharp, Z.D. The effect of diagenesis on oxygen isotope ratios of biogenic phosphates. *Am. J. Sci.* **2000**, *300*, 222–237. [[CrossRef](#)]
25. Zazzo, A.; Lecuyer, C.; Mariotti, A. Experimentally-controlled carbon and oxygen isotope exchange between bioapatites and water under inorganic and microbially-mediated conditions. *Geochim. Cosmochim. Acta* **2004**, *68*, 1–12. [[CrossRef](#)]
26. Veizer, J.; Ala, D.; Azmy, K.; Bruckschen, P.; Buhl, D.; Bruhn, F.; Carden, G.A.; Diener, A.; Ebner, S.; Godderis, Y.; et al. $^{87}\text{Sr}/^{86}\text{Sr}$, $\delta^{13}\text{C}$ and $\delta^{18}\text{O}$ evolution of Phanerozoic seawater. *Chem. Geol.* **1999**, *161*, 59–88. [[CrossRef](#)]
27. Jaffrés, J.B.; Shields, G.; Wallmann, K. The oxygen isotope evolution of seawater: A critical review of a long-standing controversy and an improved geological water cycle model for the past 3.4 billion years. *Earth Sci. Rev.* **2007**, *83*, 83–122. [[CrossRef](#)]
28. Prokoph, A.; Shields, G.; Veizer, J. Compilation and time-series analysis of a marine carbonate $\delta^{18}\text{O}$, $\delta^{13}\text{C}$, $^{87}\text{Sr}/^{86}\text{Sr}$ and $\delta^{34}\text{S}$ database through Earth history. *Earth-Sci. Rev.* **2008**, *87*, 113–133. [[CrossRef](#)]
29. Goldberg, S.L.; Present, T.M.; Finnegan, S.; Bergmann, K.D. A high-resolution record of early Paleozoic climate. *Proc. Natl. Acad. Sci. USA* **2021**, *118*, 2013083118. [[CrossRef](#)]
30. Veizer, J.; Prokoph, A. Temperatures and oxygen isotopic composition of Phanerozoic oceans. *Earth-Sci. Rev.* **2015**, *146*, 92–104. [[CrossRef](#)]
31. Galili, N.; Shemesh, A.; Yam, R.; Brailovsky, I.; Sela-Adler, M.; Schuster, E.M.; Collom, C.; Bekker, A.; Planavsky, N.; Macdonald, F.A.; et al. The geologic history of seawater oxygen isotopes from marine iron oxides. *Science* **2019**, *365*, 469–473. [[CrossRef](#)]
32. Henkes, G.A.; Passey, B.H.; Grossman, E.; Shenton, B.J.; Yancey, T.E.; Pérez-Huerta, A. Temperature evolution and the oxygen isotope composition of Phanerozoic oceans from carbonate clumped isotope thermometry. *Earth Planet. Sci. Lett.* **2018**, *490*, 40–50. [[CrossRef](#)]
33. Hodel, F.; Macouin, M.; Trindade, R.; Triantafyllou, A.; Ganne, J.; Chavagnac, V.; Berger, J.; Rospabé, M.; Destrienneville, C.; Carlut, J.; et al. Fossil black smoker yields oxygen isotopic composition of Neoproterozoic seawater. *Nat. Commun.* **2018**, *9*, 1–7. [[CrossRef](#)]
34. Veizer, J. Chemical diagenesis of belemnite shells and possible consequences for paleotemperature determinations. *Neues Jahrb. Geol. P-A.* **1974**, *147*, 91–111.
35. Brand, U.; Veizer, J. Chemical diagenesis of a multicomponent carbonate system—1: Trace Elements. *J. Sediment. Res.* **1980**, *50*, 1219–1236. [[CrossRef](#)]
36. Ullmann, C.V.; Korte, C. Diagenetic alteration in low-Mg calcite from macrofossils: A review. *Geol. Q.* **2015**, *58*, 3–20. [[CrossRef](#)]
37. Ullmann, C.V.; Hesselbo, S.P.; Korte, C. Tectonic forcing of Early to Middle Jurassic seawater Sr/Ca. *Geology* **2013**, *41*, 1211–1214. [[CrossRef](#)]
38. Savard, M.M.; Veizer, J.; Hinton, R. Cathodoluminescence at low Fe and Mn concentrations; a SIMS study of zones in natural calcites. *J. Sediment. Res.* **1995**, *65*, 208–213. [[CrossRef](#)]
39. Dickson, J.A.D. Carbonate identification and genesis as revealed by staining. *J. Sediment. Res.* **1966**, *36*, 491–505. [[CrossRef](#)]
40. Nunn, E.V.; Price, G.D. Late Jurassic (Kimmeridgian–Tithonian) stable isotopes ($\delta^{18}\text{O}$, $\delta^{13}\text{C}$) and Mg/Ca ratios: New palaeoclimate data from Helmsdale, northeast Scotland. *Palaeogeogr. Palaeoclim. Palaeoecol.* **2010**, *292*, 325–335. [[CrossRef](#)]
41. Wierzbowski, H.; Błażejowski, B.; Tyborowski, D. Oxygen isotope profiles of uppermost jurassic vertebrate teeth and oyster shells: A record of paleoenvironmental changes and animal habitats. *Palaios* **2019**, *34*, 585–599. [[CrossRef](#)]
42. Barbin, V. Cathodoluminescence of carbonate shells: Biochemical vs diagenetic process. In *Cathodoluminescence in Geosciences*; Pagel, M., Barbin, V., Blanc, P., Ohnenstetter, D., Eds.; Springer: Berlin/Heidelberg, Germany, 2000; pp. 303–329. [[CrossRef](#)]

43. Barbin, V. Application of cathodoluminescence microscopy to recent and past biological materials: A decade of progress. *Miner. Pet.* **2013**, *107*, 353–362. [[CrossRef](#)]
44. Wendler, J.E.; Wendler, I.; Rose, T.; Huber, B.T. Using cathodoluminescence spectroscopy of Cretaceous calcareous microfossils to distinguish biogenic from early-diagenetic calcite. *Microsc. Microanal.* **2012**, *18*, 1313–1321. [[CrossRef](#)] [[PubMed](#)]
45. Barbin, V. Application of cathodoluminescence to carbonate diagenesis. In *Cathodoluminescence in Geosciences*; Pagel, M., Barbin, V., Blanc, P., Ohnenstetter, D., Eds.; Springer: Berlin/Heidelberg, Germany, 2000; pp. 271–301. [[CrossRef](#)]
46. Anderson, T.F.; Popp, B.; Williams, A.C.; Ho, L.-Z.; Hudson, J.D. The stable isotopic records of fossils from the Peterborough Member, Oxford Clay Formation (Jurassic), UK: Palaeoenvironmental implications. *J. Geol. Soc.* **1994**, *151*, 125–138. [[CrossRef](#)]
47. Jones, C.E.; Jenkyns, H.; Coe, A.; Stephen, H.P. Strontium isotopic variations in Jurassic and Cretaceous seawater. *Geochim. Cosmochim. Acta* **1994**, *58*, 3061–3074. [[CrossRef](#)]
48. Price, G.; Ruffell, A.H.; Jones, C.E.; Kalin, R.M.; Mutterlose, J. Isotopic evidence for temperature variation during the early Cretaceous (late Ryazanian–mid-Hauterivian). *J. Geol. Soc.* **2000**, *157*, 335–343. [[CrossRef](#)]
49. Rosales, I.; Quesada, S.; Robles, S. Primary and diagenetic isotopic signals in fossils and hemipelagic carbonates: The Lower Jurassic of northern Spain. *Sedimentology* **2001**, *48*, 1149–1169. [[CrossRef](#)]
50. Gröcke, D.R.; Price, G.D.; Ruffell, A.H.; Mutterlose, J.; Baraboshkin, E. Isotopic evidence for Late Jurassic–Early Cretaceous climate change. *Palaeogeogr. Palaeoclim. Palaeoecol.* **2003**, *202*, 97–118. [[CrossRef](#)]
51. Rosales, I.; Quesada, S.; Robles, S. Paleotemperature variations of Early Jurassic seawater recorded in geochemical trends of belemnites from the Basque–Cantabrian basin, northern Spain. *Palaeogeogr. Palaeoclim. Palaeoecol.* **2004**, *203*, 253–275. [[CrossRef](#)]
52. Voigt, S.; Wilmsen, M.; Mortimore, R.N.; Voigt, T. Cenomanian palaeotemperatures derived from the oxygen isotopic composition of brachiopods and belemnites: Evaluation of Cretaceous palaeotemperature proxies. *Acta Diabetol.* **2003**, *92*, 285–299. [[CrossRef](#)]
53. Price, G.; Mutterlose, J. Isotopic signals from late Jurassic–early Cretaceous (Volgian–Valanginian) sub-Arctic belemnites, Yatria River, Western Siberia. *J. Geol. Soc.* **2004**, *161*, 959–968. [[CrossRef](#)]
54. Price, G.D.; Rogov, M.A. An isotopic appraisal of the Late Jurassic greenhouse phase in the Russian Platform. *Palaeogeogr. Palaeoclim. Palaeoecol.* **2009**, *273*, 41–49. [[CrossRef](#)]
55. Wierzbowski, H.; Rogov, M.A.; Matyja, B.A.; Kiselev, D.; Ippolitov, A. Middle–Upper Jurassic (Upper Callovian–Lower Kimmeridgian) stable isotope and elemental records of the Russian Platform: Indices of oceanographic and climatic changes. *Glob. Planet. Chang.* **2013**, *107*, 196–212. [[CrossRef](#)]
56. Alberti, M.; Fürsich, F.T.; Pandey, D.K. The Oxfordian stable isotope record ($\delta^{18}\text{O}$, $\delta^{13}\text{C}$) of belemnites, brachiopods, and oysters from the Kachchh Basin (western India) and its potential for palaeoecologic, palaeoclimatic, and palaeogeographic reconstructions. *Palaeogeogr. Palaeoclim. Palaeoecol.* **2012**, *344–345*, 49–68. [[CrossRef](#)]
57. Alberti, M.; Fürsich, F.T.; Pandey, D.K.; Ramkumar, M. Stable isotope analyses of belemnites from the Kachchh Basin, western India: Paleoclimatic implications for the Middle to Late Jurassic transition. *Facies* **2011**, *58*, 261–278. [[CrossRef](#)]
58. Wierzbowski, H. Seawater temperatures and carbon isotope variations in central European basins at the Middle–Late Jurassic transition (Late Callovian–Early Kimmeridgian). *Palaeogeogr. Palaeoclim. Palaeoecol.* **2015**, *440*, 506–523. [[CrossRef](#)]
59. Arabas, A. Middle–Upper Jurassic stable isotope records and seawater temperature variations: New palaeoclimate data from marine carbonate and belemnite rostra (Pieniny Klippen Belt, Carpathians). *Palaeogeogr. Palaeoclim. Palaeoecol.* **2016**, *446*, 284–294. [[CrossRef](#)]
60. Korte, C.; Hesselbo, S.P. Shallow marine carbon and oxygen isotope and elemental records indicate icehouse-greenhouse cycles during the Early Jurassic. *Paleoceanography* **2011**, *26*, 4219. [[CrossRef](#)]
61. Žák, K.; Košťák, M.; Man, O.; Zakharov, V.; Rogov, M.; Pruner, P.; Rohovec, J.; Dzyuba, O.; Mazuch, M. Comparison of carbonate C and O stable isotope records across the Jurassic/Cretaceous boundary in the Tethyan and Boreal Realms. *Palaeogeogr. Palaeoclim. Palaeoecol.* **2011**, *299*, 83–96. [[CrossRef](#)]
62. Joachimski, M.M.; van Geldern, R.; Breisig, S.; Buggisch, W.; Day, J. Oxygen isotope evolution of biogenic calcite and apatite during the Middle and Late Devonian. *Acta Diabetol.* **2004**, *93*, 542–553. [[CrossRef](#)]
63. Van Geldern, R.; Joachimski, M.; Day, J.; Jansen, U.; Alvarez, F.; Yolkin, E.; Ma, X.-P. Carbon, oxygen and strontium isotope records of Devonian brachiopod shell calcite. *Palaeogeogr. Palaeoclim. Palaeoecol.* **2006**, *240*, 47–67. [[CrossRef](#)]
64. Korte, C.; Jasper, T.; Kozur, H.W.; Veizer, J. $\delta^{18}\text{O}$ and $\delta^{13}\text{C}$ of Permian brachiopods: A record of seawater evolution and continental glaciation. *Palaeogeogr. Palaeoclim. Palaeoecol.* **2005**, *224*, 333–351. [[CrossRef](#)]
65. Korte, C.; Jones, P.J.; Brand, U.; Mertmann, D.; Veizer, J. Oxygen isotope values from high-latitudes: Clues for Permian sea-surface temperature gradients and Late Palaeozoic deglaciation. *Palaeogeogr. Palaeoclim. Palaeoecol.* **2008**, *269*, 1–16. [[CrossRef](#)]
66. Armendáriz, M.; Rosales, I.; Quesada, C. Oxygen isotope and Mg/Ca composition of Late Viséan (Mississippian) brachiopod shells from SW Iberia: Palaeoclimatic and palaeogeographic implications in northern Gondwana. *Palaeogeogr. Palaeoclim. Palaeoecol.* **2008**, *268*, 65–79. [[CrossRef](#)]
67. Bruckschen, P.; Veizer, J. Oxygen and carbon isotopic composition of Dinantian brachiopods: Paleoenvironmental implications for the Lower Carboniferous of western Europe. *Palaeogeogr. Palaeoclim. Palaeoecol.* **1997**, *132*, 243–264. [[CrossRef](#)]
68. Bruckschen, P.; Oesmann, S.; Veizer, J. Isotope stratigraphy of the European Carboniferous: Proxy signals for ocean chemistry, climate and tectonics. *Chem. Geol.* **1999**, *161*, 127–163. [[CrossRef](#)]

69. Zuo, F.; Heimhofer, U.; Huck, S.; Adatte, T.; Erbacher, J.; Bodin, S. Climatic fluctuations and seasonality during the Kimmeridgian (Late Jurassic): Stable isotope and clay mineralogical data from the Lower Saxony Basin, Northern Germany. *Palaeogeogr. Palaeoclim. Palaeoecol.* **2018**, *517*, 1–15. [[CrossRef](#)]
70. Angiolini, L.; Jadoul, F.; Leng, M.J.; Stephenson, M.H.; Rushton, J.; Chenery, S.; Crippa, G. How cold were the Early Permian glacial tropics? Testing sea-surface temperature using the oxygen isotope composition of rigorously screened brachiopod shells. *J. Geol. Soc.* **2009**, *166*, 933–945. [[CrossRef](#)]
71. Morrison, J.O.; Brand, U. Geochemistry of recent marine invertebrates. *Geosci. Can.* **1986**, *13*, 237–254.
72. Brand, U.; Logan, A.; Hiller, N.; Richardson, J. Geochemistry of modern brachiopods: Applications and implications for oceanography and paleoceanography. *Chem. Geol.* **2003**, *198*, 305–334. [[CrossRef](#)]
73. Morse, J.W.; Mackenzie, F.T. *Geochemistry of Sedimentary Carbonates. Developments in Sedimentology*; Elsevier: Amsterdam, The Netherlands, 1990; Volume 48, 418p.
74. Grossman, E. Chemical variation in Pennsylvanian brachiopod shells—diagenetic, taxonomic, microstructural, and seasonal effects. *J. Sediment. Res.* **1996**, *66*, 1011–1022. [[CrossRef](#)]
75. Mii, H.S.; Grossman, E.L.; Yancey, T.E. Carboniferous isotope stratigraphies of North America: Implications for Carboniferous paleoceanography and Mississippian glaciation. *Geol. Soc. Am. Bull.* **1999**, *111*, 960–973. [[CrossRef](#)]
76. Bomou, B.; Deconinck, J.-F.; Pucéat, E.; Amédéo, F.; Joachimski, M.M.; Quillévéré, F. Isotopic seawater temperatures in the Albian Gault Clay of the Boulonnais (Paris Basin): Palaeoenvironmental implications. *Proc. Geol. Assoc.* **2016**, *127*, 699–711. [[CrossRef](#)]
77. Dubicka, Z.; Wierzbowski, H.; Wierny, W. Oxygen and carbon isotope records of Upper Cretaceous foraminifera from Poland: Vital and microhabitat effects. *Palaeogeogr. Palaeoclim. Palaeoecol.* **2018**, *500*, 33–51. [[CrossRef](#)]
78. Wierzbowski, H.; Joachimski, M. Reconstruction of late Bajocian–Bathonian marine palaeoenvironments using carbon and oxygen isotope ratios of calcareous fossils from the Polish Jura Chain (central Poland). *Palaeogeogr. Palaeoclim. Palaeoecol.* **2007**, *254*, 523–540. [[CrossRef](#)]
79. Wierzbowski, H. Palaeoenvironmental changes recorded in the oxygen and carbon isotope composition of Kimmeridgian (Upper Jurassic) carbonates from central Poland. *Geol. Q.* **2019**, *63*, 359. [[CrossRef](#)]
80. Danise, S.; Price, G.D.; Alberti, M.; Holland, S.M. Isotopic evidence for partial geochemical decoupling between a Jurassic epicontinental sea and the open ocean. *Gondwana Res.* **2020**, *82*, 97–107. [[CrossRef](#)]
81. Sexton, P.F.; Wilson, P.A.; Pearson, P. Microstructural and geochemical perspectives on planktic foraminiferal preservation: “Glassy” versus “Frosty”. *Geochem. Geophys. Geosyst.* **2006**, *7*, 12–19. [[CrossRef](#)]
82. Bice, K.L.; Huber, B.T.; Norris, R.D. Extreme polar warmth during the Cretaceous greenhouse? Paradox of the late Turonian $\delta^{18}\text{O}$ record at Deep Sea Drilling Project Site 511. *Paleoceanography* **2003**, *18*, 1031. [[CrossRef](#)]
83. Isaza-Londoño, C.; MacLeod, K.G.; Huber, B.T. Maastrichtian North Atlantic warming, increasing stratification, and foraminiferal paleobiology at three timescales. *Paleoceanography* **2006**, *21*, 1012. [[CrossRef](#)]
84. D’Haenens, S.; Bornemann, A.; Roose, K.; Claeys, P.; Speijer, R.P. Stable isotope paleoecology ($\delta^{13}\text{C}$ and $\delta^{18}\text{O}$) of Early Eocene *Zeauvigerina aegyptiaca* from the North Atlantic (DSDP site 401). *Austrian J. Earth Sci.* **2012**, *105*, 179–188.
85. Wendler, I.; Huber, B.T.; MacLeod, K.G.; Wendler, J.E. Stable oxygen and carbon isotope systematics of exquisitely preserved Turonian foraminifera from Tanzania—Understanding isotopic signatures in fossils. *Mar. Micropaleontol.* **2013**, *102*, 1–33. [[CrossRef](#)]
86. Reolid, M. Stable isotopes on foraminifera and ostracods for interpreting incidence of the Toarcian Oceanic Anoxic Event in Westernmost Tethys: Role of water stagnation and productivity. *Palaeogeogr. Palaeoclim. Palaeoecol.* **2014**, *395*, 77–91. [[CrossRef](#)]
87. Falzoni, F.; Petrizzo, M.R.; Clarke, L.J.; MacLeod, K.G.; Jenkyns, H.C. Long-term Late Cretaceous oxygen- and carbon-isotope trends and planktonic foraminiferal turnover: A new record from the southern midlatitudes. *GSA Bull.* **2016**, *128*, 1725–1735. [[CrossRef](#)]
88. Kozdon, R.; Kelly, C.; Kita, N.T.; Fournelle, J.; Valley, J. Planktonic foraminiferal oxygen isotope analysis by ion microprobe technique suggests warm tropical sea surface temperatures during the Early Paleogene. *Paleoceanography* **2011**, *26*, 3206. [[CrossRef](#)]
89. Schrag, D.P. Effects of diagenesis on the isotopic record of late paleogene tropical sea surface temperatures. *Chem. Geol.* **1999**, *161*, 215–224. [[CrossRef](#)]
90. Pearson, P.N.; Ditchfield, P.W.; Singano, J.; Harcourt-Brown, K.G.; Nicholas, C.J.; Olsson, R.K.; Shackleton, N.J.; Hall, M.A. Warm tropical sea surface temperatures in the Late Cretaceous and Eocene epochs. *Nature* **2001**, *413*, 481–487. [[CrossRef](#)] [[PubMed](#)]
91. Pearson, P.; van Dongen, B.; Nicholas, C.J.; Pancost, R.; Schouten, S.; Singano, J.M.; Wade, B. Stable warm tropical climate through the Eocene Epoch. *Geology* **2007**, *35*, 211. [[CrossRef](#)]
92. Ando, A.; Huber, B.T.; MacLeod, K.G.; Watkins, D.K. Early Cenomanian “hot greenhouse” revealed by oxygen isotope record of exceptionally well-preserved foraminifera from Tanzania. *Paleoceanography* **2015**, *30*, 1556–1572. [[CrossRef](#)]
93. MacLeod, K.G.; Huber, B.T.; Berrocoso, Á.J.; Wendler, I. A stable and hot Turonian without glacial $\delta^{18}\text{O}$ excursions is indicated by exquisitely preserved Tanzanian foraminifera. *Geology* **2013**, *41*, 1083–1086. [[CrossRef](#)]
94. Bernard, S.; Daval, D.; Ackerer, P.; Pont, S.; Meibom, A. Burial-induced oxygen-isotope re-equilibration of fossil foraminifera explains ocean paleotemperature paradoxes. *Nat. Commun.* **2017**, *8*, 1134. [[CrossRef](#)]
95. Bernard, S.; Daval, D.; Ackerer, P.; Pont, S.; Meibom, A. Reply to ‘No substantial long-term bias in the Cenozoic benthic foraminifera oxygen-isotope record’. *Nat. Commun.* **2018**, *9*, 2874. [[CrossRef](#)]

96. Evans, D.; Badger, M.P.S.; Foster, G.L.; Henehan, M.J.; Lear, C.H.; Zachos, J.C. No substantial long-term bias in the Cenozoic benthic foraminifera oxygen-isotope record. *Nat. Commun.* **2018**, *9*, 2875. [[CrossRef](#)] [[PubMed](#)]
97. Stahl, W.; Jordan, R. General considerations on isotopic paleotemperature determinations and analyses on Jurassic ammonites. *Earth Planet. Sci. Lett.* **1969**, *6*, 173–178. [[CrossRef](#)]
98. Forester, R.W.; Caldwell, W.G.E.; Oro, F.H. Oxygen and carbon isotopic study of ammonites from the Late Cretaceous Bearpaw Formation in southwestern Saskatchewan. *Can. J. Earth Sci.* **1977**, *14*, 2086–2100. [[CrossRef](#)]
99. Buchardt, B.; Weiner, S. Diagenesis of aragonite from Upper Cretaceous ammonites: A geochemical case-study. *Sedimentology* **1981**, *28*, 423–438. [[CrossRef](#)]
100. Dauphin, Y.; Denis, A. Analyse microstructurale des tests de mollusques du Callovien de Lukow (Pologne)—Com-paraison de l'état de conservation de quelques types structuraux majeurs. *Rev. Paléobiol.* **1990**, *9*, 27–36.
101. Dauphin, Y.; Denis, A. Diagenèse comparée des phases minérales et organiques solubles dans les tests aragonitiques de nautilus et d'ammonites. *Bull. Soc. Géol. Fr.* **1999**, *170*, 355–365.
102. Cochran, J.K.; Kallenberg, K.; Landman, N.H.; Harries, P.; Weinreb, D.; Turekian, K.K.; Beck, A.J.; Cobban, W.A. Effect of diagenesis on the Sr, O, and C isotope composition of late Cretaceous mollusks from the Western Interior Seaway of North America. *Am. J. Sci.* **2010**, *310*, 69–88. [[CrossRef](#)]
103. Knoll, K.; Landman, N.H.; Cochran, J.K.; MacLeod, K.; Sessa, J.A. Microstructural preservation and the effects of diagenesis on the carbon and oxygen isotope composition of Late Cretaceous aragonitic mollusks from the Gulf Coastal Plain and the Western Interior Seaway. *Am. J. Sci.* **2016**, *316*, 591–613. [[CrossRef](#)]
104. Gothmann, A.M.; Stolarski, J.; Adkins, J.F.; Schoene, B.; Dennis, K.J.; Schrag, D.P.; Mazur, M.; Bender, M.L. Fossil corals as an archive of secular variations in seawater chemistry since the Mesozoic. *Geochim. Cosmochim. Acta* **2015**, *160*, 188–208. [[CrossRef](#)]
105. Dubicka, Z.; Wierzbowski, H.; Pałczyńska, A. Can oxygen and carbon isotope ratios of Jurassic foraminifera be used in palaeoenvironmental reconstructions? *Palaeogeogr. Palaeoclim. Palaeoecol.* **2021**, *577*, 110554. [[CrossRef](#)]
106. Samtleben, C.; Munnecke, A.; Bickert, T.; Pätzold, J. Shell succession, assemblage and species dependent effects on the C/O-isotopic composition of brachiopods—Examples from the Silurian of Gotland. *Chem. Geol.* **2001**, *175*, 61–107. [[CrossRef](#)]
107. Fujioka, H.; Takayanagi, H.; Yamamoto, K.; Iryu, Y. The effects of meteoric diagenesis on the geochemical composition and microstructure of Pliocene fossil Terebratalia coreanica and Laqueus rubellus brachiopod shells from northeastern Japan. *Prog. Earth Planet. Sci.* **2019**, *6*, 45. [[CrossRef](#)]
108. Wierzbowski, H. Detailed oxygen and carbon isotope stratigraphy of the Oxfordian in Central Poland. *Acta Diabetol.* **2002**, *91*, 304–314. [[CrossRef](#)]
109. Krencker, F.-N.; Bodin, S.; Hoffmann, R.; Suan, G.; Mattioli, E.; Kabiri, L.; Föllmi, K.; Immenhauser, A. The middle Toarcian cold snap: Trigger of mass extinction and carbonate factory demise. *Glob. Planet. Chang.* **2014**, *117*, 64–78. [[CrossRef](#)]
110. Colombié, C.; Carcel, D.; Lécuyer, C.; Ruffel, A.; Schnyder, J. Temperature and cyclone frequency in Kimmeridgian Greenhouse period (late Jurassic). *Glob. Planet. Chang.* **2018**, *170*, 126–145. [[CrossRef](#)]
111. Dubicka, Z.; Peryt, D. Integrated biostratigraphy of Upper Maastrichtian chalk at Chełm (SE Poland). *Ann. Soc. Geol. Pol.* **2011**, *81*, 185–197.
112. Lécuyer, C.; Grandjean, P.; O'Neil, J.; Cappetta, H.; Martineau, F. Thermal excursions in the ocean at the Cretaceous—Tertiary boundary (northern Morocco): $\delta^{18}\text{O}$ record of phosphatic fish debris. *Palaeogeogr. Palaeoclim. Palaeoecol.* **1993**, *105*, 235–243. [[CrossRef](#)]
113. Picard, S.; Garcia, J.-P.; Lécuyer, C.; Sheppard, S.M.F.; Cappetta, H.; Emig, C.C. $\delta^{18}\text{O}$ values of coexisting brachiopods and fish: Temperature differences and estimates of paleo-water depths. *Geology* **1998**, *26*, 975–978. [[CrossRef](#)]
114. Billon-Bruyat, J.-P.; Lécuyer, C.; Martineau, F.; Mazin, J.-M. Oxygen isotope compositions of Late Jurassic vertebrate remains from lithographic limestones of western Europe: Implications for the ecology of fish, turtles, and crocodilians. *Palaeogeogr. Palaeoclim. Palaeoecol.* **2005**, *216*, 359–375. [[CrossRef](#)]
115. Kocsis, L.; Ósi, A.; Vennemann, T.; Trueman, C.N.; Palmer, M.R. Geochemical study of vertebrate fossils from the Upper Cretaceous (Santonian) Csehbánya Formation (Hungary): Evidence for a freshwater habitat of mosasaurs and pycnodont fish. *Palaeogeogr. Palaeoclim. Palaeoecol.* **2009**, *280*, 532–542. [[CrossRef](#)]
116. Bera, M.K.; Bhattacharya, K.; Sarkar, A.; Samanta, A.; Kumar, K.; Sahni, A. Oxygen isotope analysis of bone and tooth enamel phosphate from paleogene sediments: Experimental techniques and initial results. *J. Geol. Soc. India* **2010**, *76*, 275–282. [[CrossRef](#)]
117. Elrick, M.; Rieboldt, S.; Saltzman, M.; McKay, R.M. Oxygen-isotope trends and seawater temperature changes across the Late Cambrian Steptoean positive carbon-isotope excursion (SPICE event). *Geology* **2011**, *39*, 987–990. [[CrossRef](#)]
118. Bernard, A.; Lécuyer, C.; Vincent, P.; Amiot, R.; Bardet, N.; Buffetaut, E.; Cuny, G.; Fourel, F.; Martineau, F.; Mazin, J.-M.; et al. Regulation of Body Temperature by Some Mesozoic Marine Reptiles. *Science* **2010**, *328*, 1379–1382. [[CrossRef](#)]
119. Pouech, J.; Amiot, R.; Lécuyer, C.; Mazin, J.; Martineau, F.; Fourel, F. Oxygen isotope composition of vertebrate phosphates from Cherves-de-Cognac (Berriasian, France): Environmental and ecological significance. *Palaeogeogr. Palaeoclim. Palaeoecol.* **2014**, *410*, 290–299. [[CrossRef](#)]
120. Lécuyer, C.; Picard, S.; Garcia, J.-P.; Sheppard, S.M.F.; Grandjean, P.; Dromart, G. Thermal evolution of Tethyan surface waters during the Middle-Late Jurassic: Evidence from $\delta^{18}\text{O}$ values of marine fish teeth. *Paleoceanography* **2003**, *18*, 1076. [[CrossRef](#)]

121. Zazzo, A.; Lecuyer, C.; Sheppard, S.M.; Grandjean, P.; Mariotti, A. Diagenesis and the reconstruction of paleoenvironments: A method to restore original $\delta^{18}\text{O}$ values of carbonate and phosphate from fossil tooth enamel. *Geochim. Cosmochim. Acta* **2004**, *68*, 2245–2258. [[CrossRef](#)]
122. Shemesh, A. Crystallinity and diagenesis of sedimentary apatites. *Geochim. Cosmochim. Acta* **1990**, *54*, 2433–2438. [[CrossRef](#)]
123. Pucéat, E.; Reynard, B.; Lecuyer, C. Can crystallinity be used to determine the degree of chemical alteration of biogenic apatites? *Chem. Geol.* **2004**, *205*, 83–97. [[CrossRef](#)]
124. Thomas, D.B.; McGoverin, C.M.; Fordyce, R.E.; Frew, R.D.; Gordon, K.C. Raman spectroscopy of fossil bioapatite—A proxy for diagenetic alteration of the oxygen isotope composition. *Palaeogeogr. Palaeoclim. Palaeoecol.* **2011**, *310*, 62–70. [[CrossRef](#)]
125. Epstein, A.G.; Epstein, J.B.; Harris, L.D. Conodont color alteration—An index to organic metamorphism. In *Geological Survey Professional Paper 995*; United States Government Printing Office: Washington, DC, USA, 1977; pp. 1–27.
126. Rejebian, V.A.; Harris, A.G.; Huebner, J.S. Conodont color and textural alteration: An index to regional metamorphism, contact metamorphism, and hydrothermal alteration. *Geol. Soc. Am. Bull.* **1987**, *99*, 471–479. [[CrossRef](#)]
127. Dembicki, H. *Practical Petroleum Geochemistry for Exploration and Production*; Elsevier: Amsterdam, The Netherlands, 2017; p. 331. [[CrossRef](#)]
128. Joachimski, M.; Breisig, S.; Buggisch, W.; Talent, J.; Mawson, R.; Gereke, M.; Morrow, J.; Day, J.; Weddige, K. Devonian climate and reef evolution: Insights from oxygen isotopes in apatite. *Earth Planet. Sci. Lett.* **2009**, *284*, 599–609. [[CrossRef](#)]
129. Trotter, J.; Williams, I.S.; Barnes, C.R.; Männik, P.; Simpson, A. New conodont $\delta^{18}\text{O}$ records of Silurian climate change: Implications for environmental and biological events. *Palaeogeogr. Palaeoclim. Palaeoecol.* **2016**, *443*, 34–48. [[CrossRef](#)]
130. Wheeley, J.; Smith, M.P.; Boomer, I. Oxygen isotope variability in conodonts: Implications for reconstructing Palaeozoic palaeoclimates and palaeoceanography. *J. Geol. Soc.* **2012**, *169*, 239–250. [[CrossRef](#)]
131. Nöth, S. Conodont color (CAI) versus microcrystalline and textural changes in Upper Triassic conodonts from Northwest Germany. *Facies* **1998**, *38*, 165–173. [[CrossRef](#)]
132. Wierzbowski, H.; Szaniawski, H.; Błażejowski, B. Structural, chemical and isotope evidence for secondary phosphate mineralization of grasping spines of Early Palaeozoic chaetognaths. *Lethaia* **2021**, *54*, 245–259. [[CrossRef](#)]
133. Bocherens, H.; Brinkman, D.B.; Dauphin, Y.; Mariotti, A. Microstructural and geochemical investigations on Late Cretaceous archosaur teeth from Alberta, Canada. *Can. J. Earth Sci.* **1994**, *31*, 783–792. [[CrossRef](#)]
134. Kohn, M.; Schoeninger, M.J.; Barker, W.W. Altered states: Effects of diagenesis on fossil tooth chemistry. *Geochim. Cosmochim. Acta* **1999**, *63*, 2737–2747. [[CrossRef](#)]
135. Reynard, B.; Lecuyer, C.; Grandjean, P. Crystal-chemical controls on rare-earth element concentrations in fossil biogenic apatites and implications for paleoenvironmental reconstructions. *Chem. Geol.* **1999**, *155*, 233–241. [[CrossRef](#)]
136. Armstrong, H.; Pearson, D.; Griselin, M. Thermal effects on rare earth element and strontium isotope chemistry in single conodont elements. *Geochim. Cosmochim. Acta* **2001**, *65*, 435–441. [[CrossRef](#)]
137. Lecuyer, C.; Bogey, C.; Garcia, J.-P.; Grandjean, P.; Barrat, J.-A.; Floquet, M.; Bardet, N.; Pereda-Superbiola, X. Stable isotope composition and rare earth element content of vertebrate remains from the Late Cretaceous of northern Spain (Laño): Did the environmental record survive? *Palaeogeogr. Palaeoclim. Palaeoecol.* **2003**, *193*, 457–471. [[CrossRef](#)]
138. Trotter, J.A.; Eggins, S.M. Chemical systematics of conodont apatite determined by laser ablation ICPMS. *Chem. Geol.* **2006**, *233*, 196–216. [[CrossRef](#)]
139. Kamenov, G.D.; Lofaro, E.M.; Goad, G.; Krigbaum, J. Trace elements in modern and archaeological human teeth: Implications for human metal exposure and enamel diagenetic changes. *J. Archaeol. Sci.* **2018**, *99*, 27–34. [[CrossRef](#)]
140. Lübke, A.; Enax, J.; Loza, K.; Prymak, O.; Gaengler, P.; Fabritius, H.-O.; Raabe, D.; Epple, M. Dental lessons from past to present: Ultrastructure and composition of teeth from plesiosaurs, dinosaurs, extinct and recent sharks. *RSC Adv.* **2015**, *5*, 61612–61622. [[CrossRef](#)]
141. De Renzi, M.; Manzanares, E.; Marin-Monfort, M.D.; Botella, H. Comments on “Dental lessons from past to present: Ultrastructure and composition of teeth from plesiosaurs, dinosaurs, extinct and recent sharks” by A. Lübke, J. Enax, K. Loza, O. Prymak, P. Gaengler, H.-O. Fabritius, D. Raabe and M. Epple, *RSC Adv.*, 2015, 5, 61612. *RSC Adv.* **2016**, *6*, 74384–74388. [[CrossRef](#)]
142. Luebke, A.; Loza, K.; Patnaik, R.; Enax, J.; Raabe, D.; Prymak, O.; Fabritius, H.-O.; Gaengler, P.; Epple, M. Reply to the ‘Comments on “Dental lessons from past to present: Ultrastructure and composition of teeth from plesiosaurs, dinosaurs, extinct and recent sharks”’ by H. Botella et al., *RSC Adv.*, 2016, 6, 74384–74388. *RSC Adv.* **2017**, *7*, 6215–6222. [[CrossRef](#)]
143. Lecuyer, C.; Reynard, B.; Grandjean, P. Rare earth element evolution of Phanerozoic seawater recorded in biogenic apatites. *Chem. Geol.* **2004**, *204*, 63–102. [[CrossRef](#)]
144. Ségalen, L.; de Rafelis, M.; Lee-Thorp, J.A.; Maurer, A.-F.; Renard, M. Cathodoluminescence tools provide clues to depositional history in Miocene and Pliocene mammalian teeth. *Palaeogeogr. Palaeoclim. Palaeoecol.* **2008**, *266*, 246–253. [[CrossRef](#)]
145. Fischer, J.; Voigt, S.; Franz, M.; Schneider, J.W.; Joachimski, M.M.; Tichomirowa, M.; Götze, J.; Furrer, H. Palaeoenvironments of the late Triassic Rhaetian Sea: Implications from oxygen and strontium isotopes of hybodont shark teeth. *Palaeogeogr. Palaeoclim. Palaeoecol.* **2012**, *353–355*, 60–72. [[CrossRef](#)]
146. Fischer, J.; Schneider, J.W.; Voigt, S.; Joachimski, M.M.; Tichomirowa, M.; Tütken, T.; Götze, J.; Berner, U. Oxygen and strontium isotopes from fossil shark teeth: Environmental and ecological implications for Late Palaeozoic European basins. *Chem. Geol.* **2013**, *342*, 44–62. [[CrossRef](#)]

147. Wierzbowski, H. Effects of pre-treatments and organic matter on oxygen and carbon isotope analyses of skeletal and inorganic calcium carbonate. *Int. J. Mass Spectrom.* **2007**, *268*, 16–29. [[CrossRef](#)]
148. Craig, H. The measurement of oxygen isotope paleotemperatures. In *Proceedings of the Spoleto Conference on Stable Isotopes in Oceanographic Studies and Paleotemperatures*; Tongiorgi, E., Ed.; Consiglio Nazionale delle Ricerche: Pisa, Italy, 1965; pp. 161–182.
149. Coplen, T.B.; Kendall, C.; Hopple, J. Comparison of stable isotope reference samples. *Nat. Cell Biol.* **1983**, *302*, 236–238. [[CrossRef](#)]
150. Friedman, I.; O'Neil, J.R. *Compilation of Stable Isotope Fractionation Factors of Geochemical Interest, Data of Geochemistry*, 6th ed.; United States Department of the Interior: Washington, DC, USA, 1977; pp. KK1–KK12.
151. O'Neil, J.R.; Clayton, R.N.; Mayeda, T.K. Oxygen isotope fractionation in divalent metal carbonates. *J. Chem. Phys.* **1969**, *51*, 5547–5558. [[CrossRef](#)]
152. Hays, P.; Grossman, E. Oxygen isotopes in meteoric calcite cements as indicators of continental paleoclimate. *Geology* **1991**, *19*, 441–444. [[CrossRef](#)]
153. Kim, S.-T.; O'Neil, J.R. Equilibrium and nonequilibrium oxygen isotope effects in synthetic carbonates. *Geochim. Cosmochim. Acta* **1997**, *61*, 3461–3475. [[CrossRef](#)]
154. Coplen, T.B. Calibration of the calcite–water oxygen-isotope geothermometer at Devils Hole, Nevada, a natural laboratory. *Geochim. Cosmochim. Acta* **2007**, *71*, 3948–3957. [[CrossRef](#)]
155. Lynch-Stieglitz, J.; Curry, W.B.; Slowey, N.C. A geostrophic transport estimate for the Florida Current from the oxygen isotope composition of benthic foraminifera. *Paleoceanography* **1999**, *14*, 360–373. [[CrossRef](#)]
156. Marchitto, T.; Curry, W.; Lynch-Stieglitz, J.; Bryan, S.; Cobb, K.; Lund, D. Improved oxygen isotope temperature calibrations for cosmopolitan benthic foraminifera. *Geochim. Cosmochim. Acta* **2014**, *130*, 1–11. [[CrossRef](#)]
157. Grossman, E.; Ku, T.-L. Oxygen and carbon isotope fractionation in biogenic aragonite: Temperature effects. *Chem. Geol. Isot. Geosci. Sect.* **1986**, *59*, 59–74. [[CrossRef](#)]
158. Böhm, F.; Joachimski, M.; Dullo, W.-C.; Eisenhauer, A.; Lehnert, H.; Reitner, J.; Wörheide, G. Oxygen isotope fractionation in marine aragonite of coralline sponges. *Geochim. Cosmochim. Acta* **2000**, *64*, 1695–1703. [[CrossRef](#)]
159. Kim, S.-T.; O'Neil, J.R.; Hillaire-Marcel, C.; Mucci, A. Oxygen isotope fractionation between synthetic aragonite and water: Influence of temperature and Mg²⁺ concentration. *Geochim. Cosmochim. Acta* **2007**, *71*, 4704–4715. [[CrossRef](#)]
160. Shackleton, N.; Kennett, J.; Houtz, R. Paleotemperature history of the Cenozoic and the initiation of Antarctic glaciation: Oxygen and carbon isotope analyses in DSDP Sites 277, 279 and 281. *Initial Rep. Deep Sea Drill. Proj.* **1975**, *29*, 743–755. [[CrossRef](#)]
161. Zhou, G.-T.; Zheng, Y.-F. An experimental study of oxygen isotope fractionation between inorganically precipitated aragonite and water at low temperatures. *Geochim. Cosmochim. Acta* **2003**, *67*, 387–399. [[CrossRef](#)]
162. Carpenter, S.J.; Lohmann, K.C. $\delta^{18}\text{O}$ and $\delta^{13}\text{C}$ values of modern brachiopod shells. *Geochim. Cosmochim. Acta* **1995**, *59*, 3749–3764. [[CrossRef](#)]
163. James, N.P.; Bone, Y.; Kyser, T.K. Brachiopod $\delta^{18}\text{O}$ values do reflect ambient oceanography: Lecepode Shelf, southern Australia. *Geology* **1997**, *25*, 551–554. [[CrossRef](#)]
164. Parkinson, D.; Curry, G.B.; Cusack, M.; Fallick, A.E. Shell structure, patterns and trends of oxygen and carbon stable isotopes in modern brachiopod shells. *Chem. Geol.* **2005**, *219*, 193–235. [[CrossRef](#)]
165. Hong, W.; Keppens, E.; Nielsen, P.; Van Riet, A. Oxygen and carbon isotope study of the Holocene oyster reefs and paleoenvironmental reconstruction on the northwest coast of Bohai Bay, China. *Mar. Geol.* **1995**, *124*, 289–302. [[CrossRef](#)]
166. Kirby, M.X.; Soniat, T.M.; Spero, H. Stable isotope sclerochronology of Pleistocene and Recent oyster shells (*Crassostrea virginica*). *Palaios* **1998**, *13*, 560. [[CrossRef](#)]
167. Surge, D.; Lohmann, K.; Dettman, D.L. Controls on isotopic chemistry of the American oyster, *Crassostrea virginica*: Implications for growth patterns. *Palaeogeogr. Palaeoclim. Palaeoecol.* **2001**, *172*, 283–296. [[CrossRef](#)]
168. Surge, D.M.; Lohmann, K.C.; Goodfriend, G.A. Reconstructing estuarine conditions: Oyster shells as recorders of environmental change, Southwest Florida. *Estuar. Coast. Shelf Sci.* **2003**, *57*, 737–756. [[CrossRef](#)]
169. Titschack, J.; Zuschin, M.; Spötl, C.; Baal, C. The giant oyster *Hyotissa hyotis* from the northern Red Sea as a decadal-scale archive for seasonal environmental fluctuations in coral reef habitats. *Coral Reefs* **2010**, *29*, 1061–1075. [[CrossRef](#)]
170. Ullmann, C.V.; Wiechert, U.; Korte, C. Oxygen isotope fluctuations in a modern North Sea oyster (*Crassostrea gigas*) compared with annual variations in seawater temperature: Implications for palaeoclimate studies. *Chem. Geol.* **2010**, *277*, 160–166. [[CrossRef](#)]
171. Shackleton, N.J. Attainment of isotopic equilibrium between ocean water and benthonic foraminifera genus *Uvigerina*: Isotopic changes in the ocean during the last glacial. *Colloq. Int. C.N.R.S.* **1974**, *219*, 203–209.
172. Grossman, E. Stable isotopes in modern benthic foraminifera; a study of vital effect. *J. Foraminifer. Res.* **1987**, *17*, 48–61. [[CrossRef](#)]
173. Keigwin, L.D.; Corliss, B.H. Stable isotopes in late middle Eocene to Oligocene foraminifera. *GSA Bull.* **1986**, *97*, 335–345. [[CrossRef](#)]
174. McCorkle, D.C.; Corliss, B.H.; Emerson, S.R.; Keigwin, L.D. The influence of microhabitats on the carbon isotopic composition of deep-sea benthic foraminifera. *Paleoceanography* **1990**, *5*, 161–185. [[CrossRef](#)]
175. McCorkle, D.C.; Corliss, B.H.; Farnham, C.A. Vertical distributions and stable isotopic compositions of live (stained) benthic foraminifera from the North Carolina and California continental margins. *Deep. Sea Res. Part I Oceanogr. Res. Pap.* **1997**, *44*, 983–1024. [[CrossRef](#)]
176. Zachos, J.C.; Breza, J.R.; Wise, S.W. Early Oligocene ice-sheet expansion on Antarctica: Stable isotope and sedimentological evidence from Kerguelen Plateau, southern Indian Ocean. *Geology* **1992**, *20*, 569–573. [[CrossRef](#)]

177. Rathburn, A.; Corliss, B.; Tappa, K.; Lohmann, K. Comparisons of the ecology and stable isotopic compositions of living (stained) benthic foraminifera from the Sulu and South China Seas. *Deep. Sea Res. Part I Oceanogr. Res. Pap.* **1996**, *43*, 1617–1646. [[CrossRef](#)]
178. Duplessy, J.-C.; Labeyrie, L.; Waelbroeck, C. Constraints on the ocean oxygen isotopic enrichment between the Last Glacial Maximum and the Holocene: Paleooceanographic implications. *Quat. Sci. Rev.* **2002**, *21*, 315–330. [[CrossRef](#)]
179. Schmiedl, G.; Pfeilsticker, M.; Hemleben, C.; Mackensen, A. Environmental and biological effects on the stable isotope composition of recent deep-sea benthic foraminifera from the western Mediterranean Sea. *Mar. Micropaleontol.* **2004**, *51*, 129–152. [[CrossRef](#)]
180. Fontanier, C.; Mackensen, A.; Jorissen, F.; Anschutz, P.; Licari, L.; Griveaud, C. Stable oxygen and carbon isotopes of live benthic foraminifera from the Bay of Biscay: Microhabitat impact and seasonal variability. *Mar. Micropaleontol.* **2006**, *58*, 159–183. [[CrossRef](#)]
181. Basak, C.; Rathburn, A.E.; Pérez, M.E.; Martin, J.B.; Kluesner, J.W.; Levin, L.; De Deckker, P.; Gieskes, J.M.; Abriani, M. Carbon and oxygen isotope geochemistry of live (stained) benthic foraminifera from the Aleutian Margin and the Southern Australian Margin. *Mar. Micropaleontol.* **2009**, *70*, 89–101. [[CrossRef](#)]
182. Ishimura, T.; Tsunogai, U.; Hasegawa, S.; Nakagawa, F.; Oi, T.; Kitazato, H.; Suga, H.; Toyofuku, T. Variation in stable carbon and oxygen isotopes of individual benthic foraminifera: Tracers for quantifying the magnitude of isotopic disequilibrium. *Biogeosciences* **2012**, *9*, 4353–4367. [[CrossRef](#)]
183. Franco-Fraguas, P.; Costa, K.B.; Toledo, F.A.D.L. Stable isotope/test size relationship in *Cibicides wuellerstorfi*. *Braz. J. Oceanogr.* **2011**, *59*, 287–291. [[CrossRef](#)]
184. Erez, J.; Luz, B. Experimental paleotemperature equation for planktonic foraminifera. *Geochim. Cosmochim. Acta* **1983**, *47*, 1025–1031. [[CrossRef](#)]
185. Bouvier-Soumagnac, Y.; Duplessy, J.-C. Carbon and oxygen isotopic composition of planktonic foraminifera from laboratory culture, plankton tows and Recent sediment; implications for the reconstruction of paleoclimatic conditions and of the global carbon cycle. *J. Foraminif. Res.* **1985**, *15*, 302–320. [[CrossRef](#)]
186. Bemis, B.E.; Spero, H.; Bijma, J.; Lea, D.W. Reevaluation of the oxygen isotopic composition of planktonic foraminifera: Experimental results and revised paleotemperature equations. *Paleoceanography* **1998**, *13*, 150–160. [[CrossRef](#)]
187. Mulitza, S.; Boltovskoy, D.; Donner, B.; Meggers, H.; Paul, A.; Wefer, G. Temperature: $\delta^{18}\text{O}$ relationships of planktonic foraminifera collected from surface waters. *Palaeogeogr. Palaeoclim. Palaeoecol.* **2003**, *202*, 143–152. [[CrossRef](#)]
188. Jiménez-López, C.; Romanek, C.S.; Huertas, F.; Ohmoto, H.; Caballero, E. Oxygen isotope fractionation in synthetic magnesian calcite. *Geochim. Cosmochim. Acta* **2004**, *68*, 3367–3377. [[CrossRef](#)]
189. Tarutani, T.; Clayton, R.N.; Mayeda, T.K. The effect of polymorphism and magnesium substitution on oxygen isotope fractionation between calcium carbonate and water. *Geochim. Cosmochim. Acta* **1969**, *33*, 987–996. [[CrossRef](#)]
190. Brand, U.; Azmy, K.; Bitner, M.; Logan, A.; Zuschin, M.; Came, R.; Ruggiero, E. Oxygen isotopes and MgCO_3 in brachiopod calcite and a new paleotemperature equation. *Chem. Geol.* **2013**, *359*, 23–31. [[CrossRef](#)]
191. Day, C.; Henderson, G. Oxygen isotopes in calcite grown under cave-analogue conditions. *Geochim. Cosmochim. Acta* **2011**, *75*, 3956–3972. [[CrossRef](#)]
192. Dietzel, M.; Tang, J.; Leis, A.; Köhler, S.J. Oxygen isotopic fractionation during inorganic calcite precipitation — Effects of temperature, precipitation rate and pH. *Chem. Geol.* **2009**, *268*, 107–115. [[CrossRef](#)]
193. Gabitov, R.I.; Watson, E.B.; Sadekov, A.Y. Oxygen isotope fractionation between calcite and fluid as a function of growth rate and temperature: An in situ study. *Chem. Geol.* **2012**, *306–307*, 92–102. [[CrossRef](#)]
194. Watkins, J.M.; Nielsen, L.C.; Ryerson, F.J.; DePaolo, D.J. The influence of kinetics on the oxygen isotope composition of calcium carbonate. *Earth Planet. Sci. Lett.* **2013**, *375*, 349–360. [[CrossRef](#)]
195. Watkins, J.M.; Hunt, J.D.; Ryerson, F.J.; DePaolo, D.J. The influence of temperature, pH, and growth rate on the $\delta^{18}\text{O}$ composition of inorganically precipitated calcite. *Earth Planet. Sci. Lett.* **2014**, *404*, 332–343. [[CrossRef](#)]
196. Lécuyer, C.; Hutzler, A.; Amiot, R.; Daux, V.; Grosheny, D.; Otero, O.; Martineau, F.; Fourel, F.; Balter, V.; Reynard, B. Carbon and oxygen isotope fractionations between aragonite and calcite of shells from modern molluscs. *Chem. Geol.* **2012**, *332–333*, 92–101. [[CrossRef](#)]
197. Patterson, W.P.; Smith, G.R.; Lohmann, K.C. Continental paleothermometry and seasonality using the isotopic composition of aragonitic otoliths of freshwater fishes. *Sea Ice* **2013**, *78*, 191–202. [[CrossRef](#)]
198. Thorrold, S.; Campana, S.E.; Jones, C.M.; Swart, P. Factors determining $\delta^{13}\text{C}$ and $\delta^{18}\text{O}$ fractionation in aragonitic otoliths of marine fish. *Geochim. Cosmochim. Acta* **1997**, *61*, 2909–2919. [[CrossRef](#)]
199. Høie, H.; Otterlei, E.; Folkvord, A. Temperature-dependent fractionation of stable oxygen isotopes in otoliths of juvenile cod (*Gadus morhua* L.). *ICES J. Mar. Sci.* **2004**, *61*, 243–251. [[CrossRef](#)]
200. White, R.M.P.; Dennis, P.F.; Atkinson, T.C. Experimental calibration and field investigation of the oxygen isotopic fractionation between biogenic aragonite and water. *Rapid Commun. Mass. Spectrom.* **1999**, *13*, 1242–1247. [[CrossRef](#)]
201. Pucéat, E.; Joachimski, M.; Bouilloux, A.; Monna, F.; Bonin, A.; Motreuil, S.; Morinière, P.; Hénard, S.; Mourin, J.; Dera, G. Revised phosphate–water fractionation equation reassessing paleotemperatures derived from biogenic apatite. *Earth Planet. Sci. Lett.* **2010**, *298*, 135–142. [[CrossRef](#)]
202. Lécuyer, C.; Amiot, R.; Touzeau, A.; Trotter, J. Calibration of the phosphate $\delta^{18}\text{O}$ thermometer with carbonate–water oxygen isotope fractionation equations. *Chem. Geol.* **2013**, *347*, 217–226. [[CrossRef](#)]

203. Longinelli, A. Comment on work by Pucéat et al. (2010) on a revised phosphate–water fractionation equation. *Earth Planet. Sci. Lett.* **2013**, *377–378*, 378–379. [[CrossRef](#)]
204. Pucéat, E.; Joachimski, M.; Bouilloux, A.; Monna, F.; Bonin, A.; Motreuil, S.; Morinière, P.; Henard, S.; Mourin, J.; Dera, G.; et al. Reply on Comment by Longinelli (2013) on a revised phosphate–water fractionation equation. *Earth Planet. Sci. Lett.* **2013**, *377–378*, 380–382. [[CrossRef](#)]
205. Chenery, C.A.; Müldner, G.; Evans, J.; Eckardt, H.; Lewis, M. Strontium and stable isotope evidence for diet and mobility in Roman Gloucester, UK. *J. Archaeol. Sci.* **2010**, *37*, 150–163. [[CrossRef](#)]
206. Wefer, G.; Berger, W.H. Isotope paleontology: Growth and composition of extant calcareous species. *Mar. Geol.* **1991**, *100*, 207–248. [[CrossRef](#)]
207. McConnaughey, T. ^{13}C and ^{18}O isotopic disequilibrium in biological carbonates: I. Patterns. *Geochim. Cosmochim. Acta* **1989**, *53*, 151–162. [[CrossRef](#)]
208. McConnaughey, T. ^{13}C and ^{18}O isotopic disequilibrium in biological carbonates: II. In vitro simulation of kinetic isotope effects. *Geochim. Cosmochim. Acta* **1989**, *53*, 163–171. [[CrossRef](#)]
209. Adkins, J.F.; Boyle, E.A.; Curry, W.B.; Lutringer, A. Stable isotopes in deep-sea corals and a new mechanism for “vital effects”. *Geochim. Cosmochim. Acta* **2003**, *67*, 1129–1143. [[CrossRef](#)]
210. Rollion-Bard, C.; Chaussidon, M.; France-Lanord, C. pH control on oxygen isotopic composition of symbiotic corals. *Earth Planet. Sci. Lett.* **2003**, *215*, 275–288. [[CrossRef](#)]
211. Chen, S.; Gagnon, A.C.; Adkins, J.F. Carbonic anhydrase, coral calcification and a new model of stable isotope vital effects. *Geochim. Cosmochim. Acta* **2018**, *236*, 179–197. [[CrossRef](#)]
212. McConnaughey, T.A.; Burdett, J.; Whelan, J.F.; Paull, C.K. Carbon isotopes in biological carbonates: Respiration and photosynthesis. *Geochim. Cosmochim. Acta* **1997**, *61*, 611–622. [[CrossRef](#)]
213. Swart, P. Carbon and oxygen isotope fractionation in scleractinian corals: A review. *Earth Sci. Rev.* **1983**, *19*, 51–80. [[CrossRef](#)]
214. Prada, F.; Yam, R.; Levy, O.; Caroselli, E.; Falini, G.; Dubinsky, Z.; Goffredo, S.; Shemesh, A. Kinetic and metabolic isotope effects in zooxanthellate and non-zooxanthellate Mediterranean corals along a wide latitudinal gradient. *Front. Mar. Sci.* **2019**, *6*. [[CrossRef](#)]
215. Smith, J.E.; Schwarcz, H.P.; Risk, M.J.; McConnaughey, T.A.; Keller, N. Paleotemperatures from deep-sea corals: Overcoming ‘vital effects’. *Palaeos* **2000**, *15*, 25–32. [[CrossRef](#)]
216. Lutringer, A.; Blamart, D.; Frank, N.; Labeyrie, L. Paleotemperatures from deep-sea corals: Scale effects. In *Cold-Water Corals and Ecosystems*; Freiwald, A., Roberts, J.M., Eds.; Springer: Berlin, Germany, 2005; pp. 1081–1096. [[CrossRef](#)]
217. Marali, S.; Wisshak, M.; Correa, M.L.; Freiwald, A. Skeletal microstructure and stable isotope signature of three bathyal solitary cold-water corals from the Azores. *Palaogeogr. Palaeoclim. Palaeoecol.* **2013**, *373*, 25–38. [[CrossRef](#)]
218. Chaabane, S.; Correa, M.L.; Montagna, P.; Kallel, N.; Taviani, M.; Linares, C.; Ziveri, P. Exploring the oxygen and carbon isotopic composition of the Mediterranean red coral (*Corallium rubrum*) for seawater temperature reconstruction. *Mar. Chem.* **2016**, *186*, 11–23. [[CrossRef](#)]
219. Spero, H. Do planktic foraminifera accurately record shifts in the carbon isotopic composition of seawater ΣCO_2 ? *Mar. Micropaleontol.* **1992**, *19*, 275–285. [[CrossRef](#)]
220. Spero, H.; Lea, D.W. Intraspecific stable isotope variability in the planktic foraminifera *Globigerinoides sacculifer*: Results from laboratory experiments. *Mar. Micropaleontol.* **1993**, *22*, 221–234. [[CrossRef](#)]
221. Spero, H.J.; Bijma, J.; Lea, D.W.; Bemis, B.E. Effect of seawater carbonate concentration on foraminiferal carbon and oxygen isotopes. *Nat. Cell Biol.* **1997**, *390*, 497–500. [[CrossRef](#)]
222. Ziveri, P.; Thoms, S.; Probert, I.; Geisen, M.; Langer, G. A universal carbonate ion effect on stable oxygen isotope ratios in unicellular planktonic calcifying organisms. *Biogeosciences* **2012**, *9*, 1025–1032. [[CrossRef](#)]
223. Uchikawa, J.; Zeebe, R.E. Examining possible effects of seawater pH decline on foraminiferal stable isotopes during the Paleocene-Eocene Thermal Maximum. *Paleoceanography* **2010**, *25*, 2216. [[CrossRef](#)]
224. Lea, D.W.; Bijma, J.; Spero, H.J.; Archer, D. Implications of a carbonate ion effect on shell carbon and oxygen isotopes for glacial ocean conditions. In *Use of Proxies in Paleoceanography: Examples from the South Atlantic*; Fischer, G., Wefer, G., Eds.; Springer: Berlin/Heidelberg, Germany, 1999; pp. 513–522. [[CrossRef](#)]
225. Zeebe, R.E. Seawater pH and isotopic paleotemperatures of Cretaceous oceans. *Palaogeogr. Palaeoclim. Palaeoecol.* **2001**, *170*, 49–57. [[CrossRef](#)]
226. Ye, F.; Jurikova, H.; Angiolini, L.; Brand, U.; Crippa, G.; Henkel, D.; Laudien, J.; Hiebenthal, C.; Šmajgl, D. Variation in brachiopod microstructure and isotope geochemistry under low-pH–ocean acidification conditions. *Biogeosciences* **2019**, *16*, 617–642. [[CrossRef](#)]
227. Wilke, I.; Bickert, T.; Peeters, F.J. The influence of seawater carbonate ion concentration $[\text{CO}_3^{2-}]$ on the stable carbon isotope composition of the planktic foraminifera species *Globorotalia inflata*. *Mar. Micropaleontol.* **2006**, *58*, 243–258. [[CrossRef](#)]
228. Barras, C.; Duplessy, J.-C.; Geslin, E.; Michel, E.; Jorissen, F. Calibration of $\delta^{18}\text{O}$ of cultured benthic foraminiferal calcite as a function of temperature. *Biogeosciences* **2010**, *7*, 1349–1356. [[CrossRef](#)]
229. Friedrich, O.; Schmiedl, G.; Erlenkeuser, H. Stable isotope composition of Late Cretaceous benthic foraminifera from the southern South Atlantic: Biological and environmental effects. *Mar. Micropaleontol.* **2006**, *58*, 135–157. [[CrossRef](#)]

230. Bojanowski, M.J.; Dubicka, Z.; Minoletti, F.; Olszewska-Nejbert, D.; Surowski, M. Stable C and O isotopic study of the Campanian chalk from the Mielnik section (eastern Poland): Signals from bulk rock, belemnites, benthic foraminifera, nannofossils and microcrystalline cements. *Palaeogeogr. Palaeoclim. Palaeoecol.* **2017**, *465*, 193–211. [[CrossRef](#)]
231. Yamamoto, K.; Asami, R.; Iryu, Y. Carbon and oxygen isotopic compositions of modern brachiopod shells from a warm-temperate shelf environment, Sagami Bay, central Japan. *Palaeogeogr. Palaeoclim. Palaeoecol.* **2010**, *291*, 348–359. [[CrossRef](#)]
232. Yamamoto, K.; Asami, R.; Iryu, Y. Within-shell variations in carbon and oxygen isotope compositions of two modern brachiopods from a subtropical shelf environment off Amami-o-shima, southwestern Japan. *Geochem. Geophys. Geosyst.* **2010**, *11*, 10009. [[CrossRef](#)]
233. Penman, D.E.; Hönisch, B.; Rasbury, E.T.; Hemming, N.G.; Spero, H.J. Boron, carbon, and oxygen isotopic composition of brachiopod shells: Intra-shell variability, controls, and potential as a paleo-pH recorder. *Chem. Geology* **2013**, *340*, 32–39. [[CrossRef](#)]
234. Bajnai, D.; Fiebig, J.; Tomašových, A.; Garcia, S.M.; Rollion-Bard, C.; Raddatz, J.; Löffler, N.; Primo-Ramos, C.; Brand, U. Assessing kinetic fractionation in brachiopod calcite using clumped isotopes. *Sci. Rep.* **2018**, *8*, 533. [[CrossRef](#)] [[PubMed](#)]
235. Auclair, A.-C.; Joachimski, M.; Lecuyer, C. Deciphering kinetic, metabolic and environmental controls on stable isotope fractionations between seawater and the shell of *Terebratalia transversa* (Brachiopoda). *Chem. Geol.* **2003**, *202*, 59–78. [[CrossRef](#)]
236. Takayanagi, H.; Asami, R.; Otake, T.; Abe, O.; Miyajima, T.; Kitagawa, H.; Iryu, Y. Quantitative analysis of intraspecific variations in the carbon and oxygen isotope compositions of the modern cool-temperate brachiopod *Terebratulina crossei*. *Geochim. Cosmochim. Acta* **2015**, *170*, 301–320. [[CrossRef](#)]
237. Owen, R.; Kennedy, H.; Richardson, C. Isotopic partitioning between scallop shell calcite and seawater: Effect of shell growth rate. *Geochim. Cosmochim. Acta* **2002**, *66*, 1727–1737. [[CrossRef](#)]
238. Huyghe, D.; Emmanuel, L.; de Rafelis, M.; Renard, M.; Ropert, M.; Labourdette, N.; Lartaud, F. Oxygen isotope disequilibrium in the juvenile portion of oyster shells biases seawater temperature reconstructions. *Estuar. Coast. Shelf Sci.* **2020**, *240*, 106777. [[CrossRef](#)]
239. Hahn, S.; Rodolfo-Metalpa, R.; Griesshaber, E.; Schmahl, W.W.; Buhl, D.; Hall-Spencer, J.M.; Baggini, C.; Fehr, K.T.; Immenhauser, A. Marine bivalve shell geochemistry and ultrastructure from modern low pH environments: Environmental effect versus experimental bias. *Biogeosciences* **2012**, *9*, 1897–1914. [[CrossRef](#)]
240. Alberti, M.; Fürsich, F.T.; Abdelhady, A.A.; Andersen, N. Middle to Late Jurassic equatorial seawater temperatures and latitudinal temperature gradients based on stable isotopes of brachiopods and oysters from Gebel Maghara, Egypt. *Palaeogeogr. Palaeoclim. Palaeoecol.* **2017**, *468*, 301–313. [[CrossRef](#)]
241. Price, G.; Harwood, E. Isotopic analysis of belemnites and brachiopods from the Cretaceous (Albian) Hunstanton Red Chalk Formation (Hunstanton, Norfolk, UK). *Proc. Geol. Assoc.* **2012**, *123*, 479–485. [[CrossRef](#)]
242. Price, G.D.; Teece, C. Reconstruction of Jurassic (Bathonian) palaeosalinity using stable isotopes and faunal associations. *J. Geol. Soc.* **2010**, *167*, 1199–1208. [[CrossRef](#)]
243. Mettam, C.; Johnson, A.; Nunn, E.; Schöne, B.R. Stable isotope ($\delta^{18}\text{O}$ and $\delta^{13}\text{C}$) sclerochronology of Callovian (Middle Jurassic) bivalves (*Gryphaea (Bilobissa) dilobotes*) and belemnites (*Cylindroteuthis puzosiana*) from the Peterborough Member of the Oxford Clay Formation (Cambridgeshire, England): Evidence of palaeoclimate, water depth and belemnite behaviour. *Palaeogeogr. Palaeoclim. Palaeoecol.* **2014**, *399*, 187–201. [[CrossRef](#)]
244. Wilmsen, M.; Niebuhr, B. High-resolution Campanian–Maastrichtian carbon and oxygen stable isotopes of bulk-rock and skeletal components: Palaeoceanographic and palaeoenvironmental implications for the Boreal shelf sea. *Acta Geol. Pol.* **2017**, *67*, 47–74. [[CrossRef](#)]
245. Alberti, M.; Arabas, A.; Fürsich, F.T.; Andersen, N.; Ziólkowski, P. The Middle to Upper Jurassic stable isotope record of Madagascar: Linking temperature changes with plate tectonics during the break-up of Gondwana. *Gondwana Res.* **2019**, *73*, 1–15. [[CrossRef](#)]
246. Fürsich, F.; Singh, I.; Joachimski, M.; Krumm, S.; Schlirf, M. Palaeoclimate reconstructions of the Middle Jurassic of Kachchh (western India): An integrated approach based on palaeoecological, oxygen isotopic, and clay mineralogical data. *Palaeogeogr. Palaeoclim. Palaeoecol.* **2005**, *217*, 289–309. [[CrossRef](#)]
247. Geiger, M.; Schweigert, G. Toarcian–Kimmeridgian depositional cycles of the south-western Morondava Basin along the rifted continental margin of Madagascar. *Facies* **2006**, *52*, 85–112. [[CrossRef](#)]
248. Ditchfield, P.W. High northern palaeolatitude Jurassic–Cretaceous palaeotemperature variation: New data from Kong Karls Land, Svalbard. *Palaeogeogr. Palaeoclim. Palaeoecol.* **1997**, *130*, 163–175. [[CrossRef](#)]
249. Price, G.D.; Hart, M.B.; Wilby, P.R.; Page, K.N. Isotopic analysis of Jurassic (Callovian) mollusks from the Christian Malford Lagerstätte (UK): Implications for ocean water temperature estimates based on belemnites. *Palaios* **2015**, *30*, 645–654. [[CrossRef](#)]
250. Price, G.D.; Twitchett, R.J.; Wheeley, J.R.; Buono, G. Isotopic evidence for long term warmth in the Mesozoic. *Sci. Rep.* **2013**, *3*, 1438. [[CrossRef](#)] [[PubMed](#)]
251. Benito, M.I.; Reolid, M.; Viedma, C. On the microstructure, growth pattern and original porosity of belemnite rostra: Insights from calcite Jurassic belemnites. *J. Iber. Geol.* **2016**, *42*, 201–226. [[CrossRef](#)]
252. Hoffmann, R.; Richter, D.; Neuser, R.; Jöns, N.; Linzmeier, B.; Lemanis, R.; Füsseis, F.; Xiao, X.; Immenhauser, A. Evidence for a composite organic–inorganic fabric of belemnite rostra: Implications for palaeoceanography and palaeoecology. *Sediment. Geol.* **2016**, *341*, 203–215. [[CrossRef](#)]

253. Wierzbowski, H.; Bajnai, D.; Wacker, U.; Rogov, M.A.; Fiebig, J.; Tesakova, E.M. Clumped isotope record of salinity variations in the Subboreal Province at the Middle–Late Jurassic transition. *Glob. Planet. Chang.* **2018**, *167*, 172–189. [CrossRef]
254. Vickers, M.L.; Fernandez, A.; Hesselbo, S.P.; Price, G.D.; Bernasconi, S.M.; Lode, S.; Ullmann, C.V.; Thibault, N.; Hougaard, I.W.; Korte, C. Unravelling Middle to Late Jurassic palaeoceanographic and palaeoclimatic signals in the Hebrides Basin using belemnite clumped isotope thermometry. *Earth Planet. Sci. Lett.* **2020**, *546*, 116401. [CrossRef]
255. Vickers, M.; Bajnai, D.; Price, G.D.; Linckens, J.; Fiebig, J. Southern high-latitude warmth during the Jurassic–Cretaceous: New evidence from clumped isotope thermometry. *Geology* **2019**, *47*, 724–728. [CrossRef]
256. Wisshak, M.; Correa, M.L.; Gofas, S.S.; Salas, C.; Taviani, M.; Jakobsen, J.; Freiwald, A. Shell architecture, element composition, and stable isotope signature of the giant deep-sea oyster *Neopycnodonte zibrowii* sp. n. from the NE Atlantic. *Deep. Sea Res. Part I Oceanogr. Res. Pap.* **2009**, *56*, 374–407. [CrossRef]
257. Fenger, T.; Surge, D.; Schöne, B.; Milner, N. Sclerochronology and geochemical variation in limpet shells (*Patella vulgata*): A new archive to reconstruct coastal sea surface temperature. *Geochem. Geophys. Geosyst.* **2007**, *8*, 07001. [CrossRef]
258. Killingley, J.S.; Newman, W.A. ^{18}O fractionation in barnacle calcite: A barnacle paleotemperature equation. *J. Mar. Res.* **1982**, *40*, 893–902.
259. Kohn, M. Predicting animal $\delta^{18}\text{O}$: Accounting for diet and physiological adaptation. *Geochim. Cosmochim. Acta* **1996**, *60*, 4811–4829. [CrossRef]
260. Clementz, M.T.; Koch, P.L. Differentiating aquatic mammal habitat and foraging ecology with stable isotopes in tooth enamel. *Oecologia* **2001**, *129*, 461–472. [CrossRef]
261. Amiot, R.; Lecuyer, C.; Escarguel, G.; Billon-Bruyat, J.-P.; Buffet, E.; Langlois, C.; Martin, S.; Martineau, F.; Mazin, J.-M. Oxygen isotope fractionation between crocodylian phosphate and water. *Palaeogeogr. Palaeoclim. Palaeoecol.* **2007**, *243*, 412–420. [CrossRef]
262. Amiot, R.; Wang, X.; Lecuyer, C.; Buffet, E.; Boudad, L.; Cavin, L.; Ding, Z.; Fluteau, F.; Kellner, A.W.; Tong, H.; et al. Oxygen and carbon isotope compositions of middle Cretaceous vertebrates from North Africa and Brazil: Ecological and environmental significance. *Palaeogeogr. Palaeoclim. Palaeoecol.* **2010**, *297*, 439–451. [CrossRef]
263. Rohling, E.J. Oxygen Isotope Composition of Seawater. In *The Encyclopedia of Quaternary Science*; Elias, S.A., Ed.; Elsevier: Amsterdam, The Netherlands, 2013; Volume 2, pp. 915–922.
264. Zachos, J.; Pagani, M.; Sloan, L.; Thomas, E.; Billups, K. Trends, Rhythms, and Aberrations in Global Climate 65 Ma to Present. *Science* **2001**, *292*, 686–693. [CrossRef] [PubMed]
265. Cramer, B.S.; Miller, K.G.; Barrett, P.J.; Wright, J.D. Late Cretaceous–Neogene trends in deep ocean temperature and continental ice volume: Reconciling records of benthic foraminiferal geochemistry ($\delta^{18}\text{O}$ and Mg/Ca) with sea level history. *J. Geophys. Res. Space Phys.* **2011**, *116*, 12023. [CrossRef]
266. Abreu, V.S.; Anderson, J.B. Glacial Eustasy During the Cenozoic: Sequence Stratigraphic Implications. *AAPG Bull.* **1998**, *82*, 1385–1400. [CrossRef]
267. Craig, H.; Gordon, L.I. Deuterium and oxygen 18 variation in the ocean and the marine atmosphere. In *Proceedings of the Spoleto Conference on Stable Isotopes in Oceanographic Studies and Paleotemperatures*; Tongiorgi, E., Ed.; Consiglio Nazionale delle Ricerche: Pisa, Italy, 1965; pp. 1–22.
268. Bigg, G.R.; Rohling, E.J. An oxygen isotope data set for marine waters. *J. Geophys. Res. Space Phys.* **2000**, *105*, 8527–8535. [CrossRef]
269. Schmidt, G.A.; Bigg, G.R.; Rohling, E.J. Global Seawater Oxygen-18 Database, NASA Goddard Inst. of Space Sci., New York, NY, USA. 1999. Available online: <http://data.giss.nasa.gov/o18data/> (accessed on 6 April 2021).
270. LeGrande, A.N.; Schmidt, G. Global gridded data set of the oxygen isotopic composition in seawater. *Geophys. Res. Lett.* **2006**, *33*, 12604. [CrossRef]
271. Tornaiainen, J.; Lensu, A.; Vuorinen, P.J.; Sonninen, E.; Keinänen, M.; Jones, R.L.; Patterson, W.P.; Kiljunen, M. Oxygen and carbon isoscapes for the Baltic Sea: Testing their applicability in fish migration studies. *Ecol. Evol.* **2017**, *7*, 2255–2267. [CrossRef] [PubMed]
272. Craig, H. Isotopic Variations in Meteoric Waters. *Science* **1961**, *133*, 1702–1703. [CrossRef]
273. Dansgaard, W. Stable isotopes in precipitation. *Tellus* **1964**, *16*, 436–468. [CrossRef]
274. Rozanski, K.; Araguás-Araguás, L.; Gonfiantini, R. Isotopic Patterns in Modern Global Precipitation. *Magma Redox Geochem.* **2013**, *78*, 1–36. [CrossRef]
275. Bowen, G.J.; Wilkinson, B. Spatial distribution of $\delta^{18}\text{O}$ in meteoric precipitation. *Geology* **2002**, *30*. [CrossRef]
276. Zhou, J.; Poulsen, C.; Pollard, D.; White, T.S. Simulation of modern and middle Cretaceous marine $\delta^{18}\text{O}$ with an ocean-atmosphere general circulation model. *Paleoceanography* **2008**, *23*, 3223. [CrossRef]
277. Roberts, C.D.; LeGrande, A.N.; Tripathi, A. Sensitivity of seawater oxygen isotopes to climatic and tectonic boundary conditions in an early Paleogene simulation with GISS ModelE-R. *Paleoceanography* **2011**, *26*, 4203. [CrossRef]
278. Brunetti, M.; Vèrard, C.; Baumgartner, P.O. Modeling the Middle Jurassic ocean circulation. *J. Palaeogeogr.* **2015**, *4*, 371–383. [CrossRef]
279. Railsback, L.B.; Anderson, T.F.; Ackerly, S.C.; Cisne, J.L. Paleocceanographic modeling of temperature-salinity profiles from stable isotopic data. *Paleoceanography* **1989**, *4*, 585–591. [CrossRef]
280. Railsback, L. Influence of changing deep ocean circulation on the Phanerozoic oxygen isotopic record. *Geochim. Cosmochim. Acta* **1990**, *54*, 1501–1509. [CrossRef]

281. Woo, K.-S.; Anderson, T.F.; Railsback, L.B.; Sandberg, P.A. Oxygen isotope evidence for high-salinity surface seawater in the Mid-Cretaceous Gulf of Mexico: Implications for warm, saline deepwater formation. *Paleoceanography* **1992**, *7*, 673–685. [[CrossRef](#)]
282. Wierzbowski, H.; Dubicka, Z.; Rychliński, T.; Durska, E.; Olempska, E.; Błażejowski, B. Depositional environment of the Owadów-Brzezinki conservation Lagerstätte (uppermost Jurassic, central Poland): Evidence from microfacies analysis, microfossils and geochemical proxies. *Neues Jahrb. Geol. Paläontologie Abh.* **2016**, *282*, 81–108. [[CrossRef](#)]
283. Zachos, J.; Stott, L.D.; Lohmann, K. Evolution of Early Cenozoic marine temperatures. *Paleoceanography* **1994**, *9*, 353–387. [[CrossRef](#)]
284. Müller, D.; Roest, W.R.; Royer, J.-Y.; Gahagan, L.M.; Sclater, J.G. Digital isochrons of the world's ocean floor. *J. Geophys. Res. Space Phys.* **1997**, *102*, 3211–3214. [[CrossRef](#)]
285. Grossman, E.; Mii, H.-S.; Yancey, T.E. Stable isotopes in Late Pennsylvanian brachiopods from the United States: Implications for Carboniferous paleoceanography. *GSA Bull.* **1993**, *105*, 1284–1296. [[CrossRef](#)]
286. Mazzullo, S.J.; Boardman, D.R.; Grossman, E.; Dimmick-Wells, K. Oxygen-carbon isotope stratigraphy of Upper Carboniferous to Lower Permian marine deposits in Midcontinent U.S.A. (Kansas and ne Oklahoma): Implications for sea water chemistry and depositional cyclicity. *Carbonates Evaporites* **2007**, *22*, 55–72. [[CrossRef](#)]
287. Dennis, K.; Cochran, J.; Landman, N.; Schrag, D. The climate of the Late Cretaceous: New insights from the application of the carbonate clumped isotope thermometer to Western Interior Seaway macrofossil. *Earth Planet. Sci. Lett.* **2013**, *362*, 51–65. [[CrossRef](#)]
288. Alberti, M.; Parent, H.; Garrido, A.C.; Andersen, N.; Garbe-Schönberg, D.; Danise, S. Stable isotopes ($\delta^{13}\text{C}$, $\delta^{18}\text{O}$) and element ratios (Mg/Ca, Sr/Ca) of Jurassic belemnites, bivalves and brachiopods from the Neuquén Basin (Argentina): Challenges and opportunities for palaeoenvironmental reconstructions. *J. Geol. Soc.* **2021**, *178*, 2020–2163. [[CrossRef](#)]
289. Montañez, I.P.; Osleger, D.J.; Chen, J.; Wortham, B.E.; Stamm, R.G.; Nemyrovska, T.I.; Griffin, J.M.; Poletaev, V.I.; Wardlaw, B.R. Carboniferous climate teleconnections archived in coupled bioapatite $\delta^{18}\text{O}_{\text{PO}_4}$ and $^{87}\text{Sr}/^{86}\text{Sr}$ records from the epicontinental Donets Basin, Ukraine. *Earth Planet. Sci. Lett.* **2018**, *492*, 89–101. [[CrossRef](#)]
290. Yin, J.; Werner, W. Reconstruction of palaeosalinity using carbon isotopes and benthic associations: A comparison. *Acta Diabetol.* **1995**, *84*, 223–236. [[CrossRef](#)]
291. Holmden, C.; Hudson, J.D. $^{87}\text{Sr}/^{86}\text{Sr}$ and Sr/Ca Investigation of Jurassic mollusks from Scotland: Implications for paleosalinities and the Sr/Ca ratio of seawater. *GSA Bull.* **2003**, *115*, 1249. [[CrossRef](#)]
292. Wierzbowski, H. Strontium isotope composition of sedimentary rocks and its application to chemostratigraphy and palaeoenvironmental reconstructions. *Ann. Univ. Mariae Curie-Skłodowska Sect. AAA Phys.* **2013**, *68*, 23–37. [[CrossRef](#)]
293. Schouten, S.; Hopmans, E.C.; Schefuß, E.; Damste, J.S. Distributional variations in marine crenarchaeotal membrane lipids: A new tool for reconstructing ancient sea water temperatures? *Earth Planet. Sci. Lett.* **2002**, *204*, 265–274. [[CrossRef](#)]
294. Herbert, T.D. Alkenone paleotemperature determinations. In *Treatise on Geochemistry*; Holland, H.D., Turekian, K.K., Eds.; Elsevier: Oxford, UK, 2003; Volume 6, pp. 391–432.
295. Kim, J.-H.; Schouten, S.; Hopmans, E.C.; Donner, B.; Damste, J.S. Global sediment core-top calibration of the TEX₈₆ paleothermometer in the ocean. *Geochim. Cosmochim. Acta* **2008**, *72*, 1154–1173. [[CrossRef](#)]
296. Kim, J.-H.; van der Meer, J.; Schouten, S.; Helmke, P.; Willmott, V.; Sangiorgi, F.; Koç, N.; Hopmans, E.C.; Damste, J.S. New indices and calibrations derived from the distribution of crenarchaeal isoprenoid tetraether lipids: Implications for past sea surface temperature reconstructions. *Geochim. Cosmochim. Acta* **2010**, *74*, 4639–4654. [[CrossRef](#)]
297. Sachs, J.P.; Pahnke, K.; Smittenberg, R.; Zhang, Z. Biomarker Indicators of Past Climate. In *The Encyclopedia of Quaternary Science*; Elias, S.A., Ed.; Elsevier: Amsterdam, The Netherlands, 2013; Volume 2, pp. 775–782.
298. Holmden, C.; Creaser, R.A.; Muehlenbachs, K.; Leslie, S.A.; Bergström, S.M. Isotopic evidence for geochemical de-coupling between ancient eperic seas and bordering oceans: Implications for secular curves. *Geology* **1998**, *26*, 567–570. [[CrossRef](#)]
299. Dera, G.; Pucéat, E.; Pellenard, P.; Neige, P.; Delsate, D.; Joachimski, M.; Reisberg, L.; Martinez, M. Water mass exchange and variations in seawater temperature in the NW Tethys during the Early Jurassic: Evidence from neodymium and oxygen isotopes of fish teeth and belemnites. *Earth Planet. Sci. Lett.* **2009**, *286*, 198–207. [[CrossRef](#)]
300. Dera, G.; Prunier, J.; Smith, P.L.; Haggart, J.W.; Popov, E.; Guzhov, A.; Rogov, M.; Delsate, D.; Thies, D.; Cuny, G.; et al. Nd isotope constraints on ocean circulation, paleoclimate, and continental drainage during the Jurassic breakup of Pangea. *Gondwana Res.* **2015**, *27*, 1599–1615. [[CrossRef](#)]
301. Moiroud, M.; Pucéat, E.; Donnadiou, Y.; Bayon, G.; Guiraud, M.; Voigt, S.; Deconinck, J.-F.; Monna, F. Evolution of neodymium isotopic signature of seawater during the Late Cretaceous: Implications for intermediate and deep circulation. *Gondwana Res.* **2016**, *36*, 503–522. [[CrossRef](#)]
302. Manca, B.; Burca, M.; Giorgetti, A.; Coatanoean, C.; Garcia, M.-J.; Iona, A. (Sissy) Physical and biochemical averaged vertical profiles in the Mediterranean regions: An important tool to trace the climatology of water masses and to validate incoming data from operational oceanography. *J. Mar. Syst.* **2004**, *48*, 83–116. [[CrossRef](#)]
303. Judd, E.J.; Bhattacharya, T.; Ivany, L.C. A Dynamical Framework for Interpreting Ancient Sea Surface Temperatures. *Geophys. Res. Lett.* **2020**, *47*, e2020GL089044. [[CrossRef](#)]
304. Wierzbowski, H.; Dembicz, K.; Praszkiel, T. Oxygen and carbon isotope composition of Callovian–Lower Oxfordian (Middle–Upper Jurassic) belemnite rostra from central Poland: A record of a Late Callovian global sea-level rise? *Palaeogeogr. Palaeoclim. Palaeoecol.* **2009**, *283*, 182–194. [[CrossRef](#)]

305. Matyja, B.A.; Wierzbowski, A. Sea-bottom relief and bathymetry of Late Jurassic sponge megafacies in Central Poland. In *Advances in Jurassic Research*; Riccardi, A.C., Ed.; Trans Tech Publications: Baech, Switzerland, 1996; pp. 333–340.
306. Pisera, A. Upper Jurassic siliceous sponges from Swabian Alb: Taxonomy and paleoecology. *Paleontol. Pol.* **1997**, *57*, 1–216.
307. Wierzbowski, A.; Matyja, B.A.; Sobieraj, K. Stop 1.4. Julianka, coral colonization of the cyanobacteria-sponge bio-herms at the turn of the Oxfordian and Kimmeridgian. In *Guide Book and Abstracts, Oxfordian and Kimmeridgian Joint Working Groups Meeting, Warszawa and Central Polish Uplands, September 7–12, 1992*; Matyja, B.A., Wierzbowski, A., Radwański, A., Eds.; Verlag nicht ermittelbar: Warszawa, Poland, 1992; pp. 37–40.
308. Matyja, B.A. Płytkowodna platforma węglanowa późnej jury na południowo-zachodnim obrzeżeniu Gór Świętokrzyskich (in Polish). In *Jurassica IX, Małogoszcz, 6–8 września 2011. Materiały Konferencyjne*; Polskie Towarzystwo Geologiczne—Polska Grupa Robocza Systemu Jurajskiego: Kraków, Poland, 2011; pp. 133–151.
309. Wierzbowski, A. The Lower Kimmeridgian of the Wieluń Upland and adjoining regions in central Poland: Lithostratigraphy, ammonite stratigraphy (upper Planula/Platynota to Divisum zones), palaeogeography and climate-controlled cycles. *Vol. Jurass.* **2017**, *15*, 49–120. [[CrossRef](#)]
310. Wierzbowski, A. The Kimmeridgian of the south-western margin of the Holy Cross Mts., central Poland: Stratigraphy and facies development. Part I. From deep-neritic sponge megafacies to shallow water carbonates. *Vol. Jurass.* **2020**, *18*, 161–234. [[CrossRef](#)]
311. Gutowski, J. Field trip B2—Upper Jurassic shallow-water carbonate platform and open shelf facies. Introduction. In *Jurassic of Poland and adjacent Slovakian Carpathians. Field Trip Guidebook 7th International Congress on Jurassic System*; Wierzbowski, A., Aubrecht, R., Golonka, J., Gutowski, J., Krobicki, M., Matyja, B.A., Pieńkowski, G., Uchman, A., Eds.; Polish Geological Institute: Kraków, Poland, 2006; pp. 169–173.
312. Matyja, B.A.; Wierzbowski, A. *Monografia Górnej Jury Pasma Krakowsko-Wieluńskiego. Projekt Badawczy KBN nr 600799101*; 1994; pp. 1–39, (unpublished report).
313. Norris, M.S.; Hallam, A. Facies variations across the Middle-Upper Jurassic boundary in Western Europe and the relationship to sea-level changes. *Palaeogeogr. Palaeoclim. Palaeoecol.* **1995**, *116*, 189–245. [[CrossRef](#)]
314. Hallam, A. A review of the broad pattern of Jurassic sea-level changes and their possible causes in the light of current knowledge. *Palaeogeogr. Palaeoclim. Palaeoecol.* **2001**, *167*, 23–37. [[CrossRef](#)]
315. Dromart, G.; Garcia, J.-P.; Gaumet, F.; Picard, S.; Rousseau, M.; Atrops, F.; Lécuyer, C.; Sheppard, S.M.F. Perturbation of the carbon cycle at the Middle/Late Jurassic transition: Geological and geochemical evidence. *Am. J. Sci.* **2003**, *303*, 667–707. [[CrossRef](#)]
316. Dromart, G.; Garcia, J.-P.; Picard, S.; Atrops, F.; Lecuyer, C.; Sheppard, S. Ice age at the Middle–Late Jurassic transition? *Earth Planet. Sci. Lett.* **2003**, *213*, 205–220. [[CrossRef](#)]
317. Nunn, E.V.; Price, G.; Hart, M.B.; Page, K.N.; Leng, M. Isotopic signals from Callovian–Kimmeridgian (Middle–Upper Jurassic) belemnites and bulk organic carbon, Staffin Bay, Isle of Skye, Scotland. *J. Geol. Soc.* **2009**, *166*, 633–641. [[CrossRef](#)]
318. Dera, G.; Brigaud, B.; Monna, F.; Laffont, R.; Pucéat, E.; Deconinck, J.-F.; Pellenard, P.; Joachimski, M.; Durlet, C. Climatic ups and downs in a disturbed Jurassic world. *Geology* **2011**, *39*, 215–218. [[CrossRef](#)]
319. Price, G.D.; Gröcke, D.R. Strontium-isotope stratigraphy and oxygen- and carbon-isotope variation during the Middle Jurassic–Early Cretaceous of the Falkland Plateau, South Atlantic. *Palaeogeogr. Palaeoclim. Palaeoecol.* **2002**, *183*, 209–222. [[CrossRef](#)]
320. Jenkyns, H.C.; Schouten-Huibers, L.; Schouten, S.; Damsté, J.S.S. Warm Middle Jurassic–Early Cretaceous high-latitude sea-surface temperatures from the Southern Ocean. *Clim. Past* **2012**, *8*, 215–226. [[CrossRef](#)]
321. Dutton, A.; Huber, B.T.; Lohmann, K.; Zinsmeister, W.J. High-resolution stable isotope profiles of a dimitobelid belemnite: Implications for paleodepth habitat and late maastrichtian climate seasonality. *Palaios* **2007**, *22*, 642–650. [[CrossRef](#)]
322. Wierzbowski, H.; Joachimski, M. Stable isotopes, elemental distribution, and growth rings of belemnite rostra: Proxies for belemnite life habitat. *Palaios* **2009**, *24*, 377–386. [[CrossRef](#)]
323. Nützel, A.; Joachimski, M.; Correa, M.L. Seasonal climatic fluctuations in the Late Triassic tropics—High-resolution oxygen isotope records from aragonitic bivalve shells (Cassian Formation, Northern Italy). *Palaeogeogr. Palaeoclim. Palaeoecol.* **2010**, *285*, 194–204. [[CrossRef](#)]
324. Stevens, G.R.; Clayton, R.N. Oxygen isotope studies on Jurassic and Cretaceous belemnites from New Zealand and their biogeographic significance. *N. Z. J. Geol. Geophys.* **1971**, *14*, 829–897. [[CrossRef](#)]
325. Ullmann, C.; Frei, R.; Korte, C.; Hesselbo, S. Chemical and isotopic architecture of the belemnite rostrum. *Geochim. Cosmochim. Acta* **2015**, *159*, 231–243. [[CrossRef](#)]
326. Wierzbowski, H. Life span and growth rate of Middle Jurassic mesohibolitid belemnites deduced from rostrum microincrements. *Vol. Jurass.* **2013**, *11*, 1–18.
327. Rexfort, A.; Mutterlose, J. Stable isotope records from *Sepia officinalis*—a key to understanding the ecology of belemnites? *Earth Planet. Sci. Lett.* **2006**, *247*, 212–221. [[CrossRef](#)]
328. Bettencourt, V.; Guerra, A. Carbon- and oxygen-isotope composition of the cuttlebone of *Sepia officinalis*: A tool for predicting ecological information? *Mar. Biol.* **1999**, *133*, 651–657. [[CrossRef](#)]
329. Rollion-Bard, C.; Erez, J.; Zilberman, T. Intra-shell oxygen isotope ratios in the benthic foraminifera genus *Amphistegina* and the influence of seawater carbonate chemistry and temperature on this ratio. *Geochim. Cosmochim. Acta* **2008**, *72*, 6006–6014. [[CrossRef](#)]

330. Valley, J.W.; Kita, N.T. In situ oxygen isotope geochemistry by ion microprobe. In *Secondary Ion Mass Spectrometry in the Earth Sciences: Gleaning the Big Picture from a Small Spot*; Fayek, M., Ed.; Mineralogical Association of Canada Short Course 41: Toronto, ON, Canada, 2009; pp. 19–63.
331. Žigaitė, Ž.; Whitehouse, M. Stable oxygen isotopes of dental biomineral: Differentiation at the intra- and inter-tissue level of modern shark teeth. *GFF* **2014**, *136*, 337–340. [[CrossRef](#)]
332. Narkiewicz, M.; Narkiewicz, K.; Krzeminska, E.; Kruczek, S.A. Oxygen isotopic composition of conodont apatite in the equatorial epeiric Belarussian basin (Eifelian)—Relationship to fluctuating seawater salinity and temperature. *Palaios* **2017**, *32*, 439–447. [[CrossRef](#)]
333. Kozdon, R.; Ushikubo, T.; Kita, N.; Spicuzza, M.; Valley, J. Intratest oxygen isotope variability in the planktonic foraminifer *N. pachyderma*: Real vs. apparent vital effects by ion microprobe. *Chem. Geol.* **2009**, *258*, 327–337. [[CrossRef](#)]
334. Kozdon, R.; Kelly, D.C.; Kitajima, K.; Strickland, A.; Fournelle, J.H.; Valley, J.W. In situ $\delta^{18}\text{O}$ and Mg/Ca analyses of diagenetic and planktic foraminiferal calcite preserved in a deep-sea record of the Paleocene-Eocene thermal maximum. *Paleoceanography* **2013**, *28*, 517–528. [[CrossRef](#)]
335. Wycech, J.B.; Kelly, C.; Kitajima, K.; Kozdon, R.; Orland, I.J.; Valley, J.W. Combined effects of gametogenic calcification and dissolution on $\delta^{18}\text{O}$ measurements of the planktic foraminifer *Trilobatus sacculifer*. *Geochem. Geophys. Geosyst.* **2018**, *19*, 4487–4501. [[CrossRef](#)]
336. Wycech, J.B.; Kelly, D.C.; Kozdon, R.; Orland, I.J.; Spero, H.J.; Valley, J.W. Comparison of $\delta^{18}\text{O}$ analyses on individual planktic foraminifer (*Orbulina universa*) shells by SIMS and gas-source mass spectrometry. *Chem. Geol.* **2018**, *483*, 119–130. [[CrossRef](#)]
337. Kilburn, M.R.; Wacey, D. NanoSIMS as an analytical tool in the geosciences. In *Principles and Practice of Analytical Techniques in Geosciences, Royal Society of Chemistry Special Volume*; Grice, K., Ed.; Royal Society of Chemistry: London, UK, 2015; pp. 1–34. [[CrossRef](#)]
338. Rollion-Bard, C.; Mangin, D.; Champenois, M. Development and application of oxygen and carbon isotopic measurements of biogenic carbonates by ion microprobe. *Geostand. Geoanal. Res.* **2007**, *31*, 39–50. [[CrossRef](#)]
339. Helser, T.E.; Kastle, C.R.; McKay, J.L.; Orland, I.J.; Kozdon, R.; Valley, J. Evaluation of micromilling/conventional isotope ratio mass spectrometry and secondary ion mass spectrometry of $\delta^{18}\text{O}$ values in fish otoliths for sclerochronology. *Rapid Commun. Mass Spectrom.* **2018**, *32*, 1781–1790. [[CrossRef](#)] [[PubMed](#)]
340. Balestra, B.; Orland, I.J.; Fessenden-Rahn, J.; Gorski, G.; Franks, R.; Rahn, T.; Paytan, A. Paired analyses of oxygen isotope and elemental ratios within individual shells of benthic foraminifera genus *Uvigerina*. *Chem. Geol.* **2020**, *533*, 119377. [[CrossRef](#)]
341. Rollion-Bard, C.; Marin-Carbonne, J. Determination of SIMS matrix effects on oxygen isotopic compositions in carbonates. *J. Anal. At. Spectrom.* **2011**, *26*, 1285–1289. [[CrossRef](#)]
342. Trotter, J.A.; Williams, I.S.; Barnes, C.R.; Lécuyer, C.; Nicoll, R.S. Did cooling oceans trigger Ordovician biodiversification? Evidence from Conodont Thermometry. *Science* **2008**, *321*, 550–554. [[CrossRef](#)] [[PubMed](#)]
343. Li, Y.; Tang, G.-Q.; Liu, Y.; He, S.; Chen, B.; Li, Q.-L.; Li, X.-H. Revisiting apatite SIMS oxygen isotope analysis and Qinghu-AP reference material. *Chem. Geol.* **2021**, *582*, 120445. [[CrossRef](#)]
344. Trotter, J.; Williams, I.; Nicora, A.; Mazza, M.; Rigo, M. Long-term cycles of Triassic climate change: A new $\delta^{18}\text{O}$ record from conodont apatite. *Earth Planet. Sci. Lett.* **2015**, *415*, 165–174. [[CrossRef](#)]
345. Pietzner, H.; Vahl, J.; Werner, H.; Ziegler, W. Zur chemischen Zusammensetzung und Mikromorphologie der Conodonten. *Palaeontogr. Abt. A* **1968**, *128*, 115–152.
346. Vennemann, T.; Hegner, E.; Cliff, G.; Benz, G. Isotopic composition of recent shark teeth as a proxy for environmental conditions. *Geochim. Cosmochim. Acta* **2001**, *65*, 1583–1599. [[CrossRef](#)]
347. Aubert, M.; Williams, I.S.; Boljkovac, K.; Moffat, I.; Moncel, M.-H.; Dufour, E.; Grün, R. In situ oxygen isotope micro-analysis of faunal material and human teeth using a SHRIMP II: A new tool for palaeo-ecology and archaeology. *J. Archaeol. Sci.* **2012**, *39*, 3184–3194. [[CrossRef](#)]
348. Wheeley, J.; Jardine, P.E.; Raine, R.; Boomer, I.; Smith, M.P. Paleoeologic and paleoceanographic interpretation of $\delta^{18}\text{O}$ variability in Lower Ordovician conodont species. *Geology* **2018**, *46*, 467–470. [[CrossRef](#)]
349. Ghosh, P.; Adkins, J.; Affek, H.; Balta, B.; Guo, W.; Schauble, E.A.; Schrag, D.; Eiler, J.M. ^{13}C - ^{18}O bonds in carbonate minerals: A new kind of paleothermometer. *Geochim. Cosmochim. Acta* **2006**, *70*, 1439–1456. [[CrossRef](#)]
350. Eiler, J.M. Paleoclimate reconstruction using carbonate clumped isotope thermometry. *Quat. Sci. Rev.* **2011**, *30*, 3575–3588. [[CrossRef](#)]
351. Passey, B.H.; Henkes, G.A. Carbonate clumped isotope bond reordering and geospeedometry. *Earth Planet. Sci. Lett.* **2012**, *351*–352, 223–236. [[CrossRef](#)]
352. Henkes, G.A.; Passey, B.; Grossman, E.; Shenton, B.J.; Pérez-Huerta, A.; Yancey, T.E. Temperature limits for preservation of primary calcite clumped isotope paleotemperatures. *Geochim. Cosmochim. Acta* **2014**, *139*, 362–382. [[CrossRef](#)]
353. Stolper, D.A.; Eiler, J.M. The kinetics of solid-state isotope-exchange reactions for clumped isotopes: A study of inorganic calcites and apatites from natural and experimental samples. *Am. J. Sci.* **2015**, *315*, 363–411. [[CrossRef](#)]
354. Spencer, C.; Kim, S.-T. Carbonate clumped isotope paleothermometry: A review of recent advances in CO_2 gas evolution, purification, measurement and standardization techniques. *Geosci. J.* **2015**, *19*, 357–374. [[CrossRef](#)]
355. Tripathi, A.; Eagle, R.; Thiagarajan, N.; Gagnon, A.C.; Bauch, H.; Halloran, P.; Eiler, J.M. ^{13}C - ^{18}O isotope signatures and ‘clumped isotope’ thermometry in foraminifera and coccoliths. *Geochim. Cosmochim. Acta* **2010**, *74*, 5697–5717. [[CrossRef](#)]

356. Thiagarajan, N.; Adkins, J.; Eiler, J. Carbonate clumped isotope thermometry of deep-sea corals and implications for vital effects. *Geochim. Cosmochim. Acta* **2011**, *75*, 4416–4425. [[CrossRef](#)]
357. Grauel, A.-L.; Schmid, T.W.; Hu, B.; Bergami, C.; Capotondi, L.; Zhou, L.; Bernasconi, S. Calibration and application of the ‘clumped isotope’ thermometer to foraminifera for high-resolution climate reconstructions. *Geochim. Cosmochim. Acta* **2013**, *108*, 125–140. [[CrossRef](#)]
358. Henkes, G.A.; Passey, B.; Wanamaker, A.; Grossman, E.; Ambrose, W.G.; Carroll, M.L. Carbonate clumped isotope compositions of modern marine mollusk and brachiopod shells. *Geochim. Cosmochim. Acta* **2013**, *106*, 307–325. [[CrossRef](#)]
359. Eagle, R.A.; Eiler, J.M.; Tripathi, A.K.; Ries, J.B.; Freitas, P.S.; Hiebenthal, C.; Wanamaker, A.D.; Taviani, M.; Elliot, M.; Marensi, S.; et al. The influence of temperature and seawater carbonate saturation state on ^{13}C – ^{18}O bond ordering in bivalve mollusks. *Biogeosciences* **2013**, *10*, 4591–4606. [[CrossRef](#)]
360. Zaarur, S.; Affek, H.P.; Brandon, M.T. A revised calibration of the clumped isotope thermometer. *Earth Planet. Sci. Lett.* **2013**, *382*, 47–57. [[CrossRef](#)]
361. Wacker, U.; Fiebig, J.; Tödter, J.; Schöne, B.R.; Bahr, A.; Friedrich, O.; Tütken, T.; Gischler, E.; Joachimski, M. Empirical calibration of the clumped isotope paleothermometer using calcites of various origins. *Geochim. Cosmochim. Acta* **2014**, *141*, 127–144. [[CrossRef](#)]
362. Kele, S.; Breitenbach, S.F.; Capezzuoli, E.; Meckler, A.N.; Ziegler, M.; Millan, I.M.; Kluge, T.; Deák, J.; Hanselmann, K.; John, C.; et al. Temperature dependence of oxygen- and clumped isotope fractionation in carbonates: A study of travertines and tufas in the 6–95°C temperature range. *Geochim. Cosmochim. Acta* **2015**, *168*, 172–192. [[CrossRef](#)]
363. Bonifacie, M.; Calmels, D.; Eiler, J.M.; Horita, J.; Chaduteau, C.; Vasconcelos, C.; Agrinier, P.; Katz, A.; Passey, B.H.; Ferry, J.M.; et al. Calibration of the dolomite clumped isotope thermometer from 25 to 350 °C, and implications for a universal calibration for all (Ca, Mg, Fe)CO₃ carbonates. *Geochim. Cosmochim. Acta* **2017**, *200*, 255–279. [[CrossRef](#)]
364. Kelson, J.R.; Huntington, K.W.; Schauer, A.; Saenger, C.; Lechler, A.R. Toward a universal carbonate clumped isotope calibration: Diverse synthesis and preparatory methods suggest a single temperature relationship. *Geochim. Cosmochim. Acta* **2017**, *197*, 104–131. [[CrossRef](#)]
365. Bernasconi, S.M.; Müller, I.A.; Bergmann, K.D.; Breitenbach, S.F.M.; Fernandez, A.; Hodell, D.A.; Jaggi, M.; Meckler, A.N.; Millan, I.; Ziegler, M. Reducing uncertainties in carbonate clumped isotope analysis through consistent carbonate-based standardization. *Geochem. Geophys. Geosyst.* **2018**, *19*, 2895–2914. [[CrossRef](#)]
366. Petersen, S.V.; Defliese, W.F.; Saenger, C.; Daëron, M.; Huntington, K.W.; John, C.M.; Kelson, J.R.; Bernasconi, S.M.; Colman, A.S.; Kluge, T.; et al. Effects of Improved ^{17}O Correction on Interlaboratory Agreement in Clumped Isotope Calibrations, Estimates of Mineral-Specific Offsets, and Temperature Dependence of Acid Digestion Fractionation. *Geochem. Geophys. Geosyst.* **2019**, *20*, 3495–3519. [[CrossRef](#)]
367. Bajnai, D.; Guo, W.; Spötl, C.; Coplen, T.B.; Methner, K.; Löffler, N.; Krsnik, E.; Gischler, E.; Hansen, M.; Henkel, D.; et al. Dual clumped isotope thermometry resolves kinetic biases in carbonate formation temperatures. *Nat. Commun.* **2020**, *11*, 4005. [[CrossRef](#)]
368. Meinicke, N.; Ho, S.; Hannisdal, B.; Nürnberg, D.; Tripathi, A.; Schiebel, R.; Meckler, A.N. A robust calibration of the clumped isotopes to temperature relationship for foraminifers. *Geochim. Cosmochim. Acta* **2020**, *270*, 160–183. [[CrossRef](#)]
369. Staudigel, P.; Swart, P. Isotopic behavior during the aragonite-calcite transition: Implications for sample preparation and proxy interpretation. *Chem. Geol.* **2016**, *442*, 130–138. [[CrossRef](#)]
370. Ritter, A.; Mavromatis, V.; Dietzel, M.; Kwiecien, O.; Wiethoff, F.; Griesshaber, E.; Casella, L.A.; Schmahl, W.W.; Koelen, J.; Neuser, R.D.; et al. Exploring the impact of diagenesis on (isotope) geochemical and microstructural alteration features in biogenic aragonite. *Sedimentology* **2017**, *64*, 1354–1380. [[CrossRef](#)]
371. Leutert, T.J.; Sexton, P.F.; Tripathi, A.; Piasecki, A.; Ho, S.L.; Meckler, A.N. Sensitivity of clumped isotope temperatures in fossil benthic and planktic foraminifera to diagenetic alteration. *Geochim. Cosmochim. Acta* **2019**, *257*, 354–372. [[CrossRef](#)]
372. Pepper, A.S.; Corvi, P.J. Simple kinetic models of petroleum formation. Part I: Oil and gas generation from kerogen. *Mar. Pet. Geol.* **1995**, *12*, 291–319. [[CrossRef](#)]
373. Finnegan, S.; Bergmann, K.; Eiler, J.M.; Jones, D.S.; Fike, D.A.; Eisenman, I.; Hughes, N.C.; Tripathi, A.K.; Fischer, W.W. The magnitude and duration of Late Ordovician–Early Silurian glaciation. *Science* **2011**, *331*, 903–906. [[CrossRef](#)]
374. Petersen, S.; Tabor, C.R.; Lohmann, K.C.; Poulsen, C.; Meyer, K.W.; Carpenter, S.J.; Erickson, J.M.; Matsunaga, K.K.; Smith, S.; Sheldon, N. Temperature and salinity of the Late Cretaceous Western Interior Seaway. *Geology* **2016**, *44*, 903–906. [[CrossRef](#)]
375. Saenger, C.; Affek, H.P.; Felis, T.; Thiagarajan, N.; Lough, J.M.; Holcomb, M. Carbonate clumped isotope variability in shallow water corals: Temperature dependence and growth-related vital effects. *Geochim. Cosmochim. Acta* **2012**, *99*, 224–242. [[CrossRef](#)]
376. Tripathi, A.K.; Hill, P.S.; Eagle, R.A.; Mosenfelder, J.L.; Tang, J.; Schauble, E.A.; Eiler, J.M.; Zeebe, R.E.; Uchikawa, J.; Coplen, T.B.; et al. Beyond temperature: Clumped isotope signatures in dissolved inorganic carbon species and the influence of solution chemistry on carbonate mineral composition. *Geochim. Cosmochim. Acta* **2015**, *166*, 344–371. [[CrossRef](#)]
377. Kimball, J.; Eagle, R.; Dunbar, R. Carbonate “clumped” isotope signatures in aragonitic scleractinian and calcitic gorgonian deep-sea corals. *Biogeosciences* **2016**, *13*, 6487–6505. [[CrossRef](#)]
378. Price, G.; Passey, B. Dynamic polar climates in a greenhouse world: Evidence from clumped isotope thermometry of Early Cretaceous belemnites. *Geology* **2013**, *41*, 923–926. [[CrossRef](#)]

379. Tobin, T.S.; Wilson, G.P.; Eiler, J.M.; Hartman, J.H. Environmental change across a terrestrial Cretaceous–Paleogene boundary section in eastern Montana, USA, constrained by carbonate clumped isotope paleothermometry. *Geology* **2014**, *42*, 351–354. [[CrossRef](#)]
380. Evans, D.; Sagoo, N.; Renema, W.; Cotton, L.J.; Müller, W.; Todd, J.A.; Saraswati, P.K.; Stassen, P.; Ziegler, M.; Pearson, P.N.; et al. Eocene greenhouse climate revealed by coupled clumped isotope–Mg/Ca thermometry. *Proc. Natl. Acad. Sci. USA* **2018**, *115*, 1174–1179. [[CrossRef](#)] [[PubMed](#)]
381. Price, G.D.; Bajnai, D.; Fiebig, J. Carbonate clumped isotope evidence for latitudinal seawater temperature gradients and the oxygen isotope composition of Early Cretaceous seas. *Palaeogeogr. Palaeoclim. Palaeoecol.* **2020**, *552*, 109777. [[CrossRef](#)]
382. Tesakova, E. Late Callovian and Early Oxfordian ostracods from the Dubki section (Saratov area, Russia): Implications for stratigraphy, paleoecology, eustatic cycles and palaeobiogeography. *Neues Jahrb. Geol. Paläontologie Abh.* **2008**, *249*, 25–45. [[CrossRef](#)]
383. Głowniak, E.; Kiselev, D.N.; Rogov, M.; Wierzbowski, A.; Wright, J.K. The Middle Oxfordian to lowermost Kimmeridgian ammonite succession at Mikhalenino (Kostroma District) of the Russian Platform, and its stratigraphical and palaeobiogeographical importance. *Vol. Jurass.* **2010**, *8*, 5–48.
384. Tesakova, E.M.; Demidov, S.M.; Guzhov, A.V.; Rogov, M.; Kiselev, D. Middle Oxfordian—Lower Kimmeridgian ostracod zones from the Mikhalenino section (Kostroma region) and their comparison with synchronous strata of the Eastern and Western Europe. *Neues Jahrb. Geol. Paläontologie Abh.* **2012**, *266*, 239–249. [[CrossRef](#)]
385. Ustinova, M.A. Foraminifers and stratigraphy of Middle Oxfordian—Lower Kimmeridgian of Kostroma Region (Mikhalenino section). *Bull. Moscow Soc. Nat.* **2012**, *87*, 43–52. (In Russian)
386. Colpaert, C.; Nikitenko, B.; Khafaeva, S.; Wall, A.F. The evolution of Late Callovian to Early Kimmeridgian foraminiferal associations from the central part of the Russian Sea (Makar'yev section, Volga River Basin, Russia). *Palaeogeogr. Palaeoclim. Palaeoecol.* **2016**, *451*, 97–109. [[CrossRef](#)]
387. Donnadieu, Y.; Dromart, G.; Goddérès, Y.; Pucéat, E.; Brigaud, B.; Dera, G.; Dumas, C.; Olivier, N. A mechanism for brief glacial episodes in the Mesozoic greenhouse. *Paleoceanography* **2011**, *26*, 3212. [[CrossRef](#)]
388. Wierzbowski, H.; Rogov, M. Reconstructing the palaeoenvironment of the Middle Russian Sea during the Middle–Late Jurassic transition using stable isotope ratios of cephalopod shells and variations in faunal assemblages. *Palaeogeogr. Palaeoclim. Palaeoecol.* **2011**, *299*, 250–264. [[CrossRef](#)]